J. Astrophys. Astr. (1990) **11**, 323–410

A Synthesis Map of the Sky at 34.5 MHz

K. S. Dwarakanath & N. Udaya Shankar *Raman Research Institute, Bangalore 560080*

Received 1990 March 17; accepted 1990 May 29

Abstract. This paper describes a wide-field survey made at 34.5 MHz using GEETEE,[1] the low frequency telescope at Gauribidanur (latitude 13°36′12″ N). This telescope was used in the transit mode and by performing 1-D synthesis along the north-south direction the entire observable sky was mapped in a single day. This minimized the problems that hinder wide-field low-frequency mapping. This survey covers the declination range of −50° to +70° (−33° to +61° without aliasing) and the complete 24 hours of right ascension. The synthesized beam has a resolution of 26′ × 42′ sec ($\delta - 14°.1$). The sensitivity of the survey is 5 Jy/beam (1σ). Special care has been taken to ensure that the antenna responds to all angular scale structures and is suitable for studies of both point sources and extended objects.

Key words: radio continuum—synthesis mapping—wide-field—low-frequency.

1. Introduction

There have been many attempts to map large regions of the sky at decametric wavelengths. As early as 1960, Shain, Komesaroff & Higgins (1961) mapped a part of the Galactic plane at 19.7 MHz with 1°.4 resolution using a Mills Cross antenna. Soon afterwards, Williams, Kenderdine & Baldwin (1966) at Cambridge used the aperture synthesis technique to map the northern sky at 38 MHz with a resolution of 0°.7. In Table 1, we have summarized some of the mapping observations made at low frequencies. These surveys revealed several interesting phenomena, such as the turnovers in the spectra of supernova remnants due to absorption of the radiation in the intervening gas (Kassim 1989), and H II regions appearing in absorption against the more intense Galactic nonthermal background (Jones & Finlay 1974). Analyses of these observations have been rewarding and complement the studies made at metric and decimetric wavelengths. Such studies have thrown light on the distribution of thermal gas in the Galactic plane, the haloes around galaxies, *etc.* In addition, they played a vital role in the discovery of the first millisecond pulsar, which can be traced to the discovery of a very-steep-spectrum point source at low frequencies (Erickson 1983).

Notwithstanding these efforts, there is a need for a wide-field survey such as we present here. A low-frequency map of the Galactic background combined with a

[1] This telescope is jointly operated by the Indian Institute of Astrophysics, Bangalore and the Raman Research Institute, Bangalore.

Table 1. Some of the mapping observations made at low frequencies.

Freq. (MHz)	Size	Observatory	Resol. (deg.)	Coverage	Reference
19.7	'+' Array 1.6 km EW 1.6 km NS	C.S.I.R.O.	1.4	$224° < l < 16°$ $-6° < b < +6°$	Shain, Komesaroff & Higgins (1961)
38	Array 1 km EW Movable NS	Cambridge	0.75	$-10° < \delta < +90°$ 24 Hr in RA	Williams, Kenderdine & Baldwin (1966)
29.9	Array 1 km EW Movable NS	Fleurs, NSW	0.8	$225° < l < 30°$ $-10° < b < +10°$	Jones & Finlay (1974)
10	'T' Array 1.2 km EW 0.7 km NS	Penticton	2.0	$-5° < \delta < +71°$ 24 Hr in RA	Caswell (1976)
30.9	'T' Array 3 km EW 1.8 km NS	Clark Lake	0.2	$350° < l < 250°$ $-3° < b < +3°$	Kassim (1988)
30	Single dish 210 ft.	Parkes	11	$-90° < \delta < 0°$ 24 Hr in RA	Mathewson, Broten and Cole (1965)
38	Single dish 250 ft.	Jodrell	8	$-25° < \delta < +70°$ 24 Hr in RA	Milogradov-Turin and Smith (1973)

higher-frequency survey of comparable resolution, such as that at 408 MHz by Haslam *et al.* (1982), can yield useful spectral information. A detailed map of the sky can reveal not only the well-studied H II regions in the Galactic plane, but also those at higher latitudes. It is of interest to study these in the light of the results from the Infra-Red Astronomical Satellite (IRAS). The present low-frequency survey with its wide, uniform coverage is also a useful data base to investigate a number of problems pertaining to the distribution of extragalactic sources. In addition, it can be used to look for very-steep-spectrum sources which could represent millisecond pulsars.

Some of the problems that have plagued wide-field low-frequency mapping are those involved in the construction and maintenance of the large arrays needed to achieve even moderate resolutions, compounded with difficulties due to the ionosphere and terrestrial interference. In the present survey an attempt has been made to minimise these problems by choosing an appropriate time and mode for the observations.

In this paper, Section 2 describes the observations, along with the main features of the telescope. The methods of data analysis and calibration are described in Section 3, which also contains a discussion of the flux-density scale at 34.5 MHz. The final section contains the results of the survey in the form of contour maps covering almost the entire sky observable from Gauribidanur. This section also discusses the noise in these maps.

2. Observations

A detailed description of the telescope used for the observations is to be found in Udaya Shankar (1986) and Dwarakanath (1989), as well in Udaya Shankar &

Ravishankar (1990; UR). Below, we outline some of the salient features of the antenna, receiver system and observations.

The telescope (GEETEE) is situated near Gauribidanur (longitude 77°26′07″ E; latitude 13°36′12″ N), about 80 km north of Bangalore, India. The antenna system is in the shape of the letter T and consists of 1000 dipoles with a 1.4-km long East-West (EW) arm and a 0.45-km long South (S) arm. The dipoles are aligned East-West and spaced 8.6 m apart in this direction. They accept linear polarization. The East-West array consists of four rows of dipoles spaced 5 m apart in the north-south direction and has a collecting area of $\approx 12{,}000\ m^2$. The south array consists of 90 rows, each containing four dipoles, placed 5 m apart along the NS direction. It has a collecting area of $\approx 7000\ m^2$. Since the spacing between the rows of the S array is 5 m, while the wavelength of operation is 8.7 m, the array has a grating response for zenith angles greater than $\pm 47°$, which becomes equal to the main beam response at a zenith angle of $\pm 60°$.

The receiver system consists of 32 front ends with a 128-channel one-bit digital correlator. One-bit correlators measure the normalized correlation coefficient. The advantage of this system is that the measured visibilities are not critically dependent on the gains of the S-array amplifiers but are only affected by their bandshapes and noise temperatures. While the amplifier gains can vary with time (*e.g.* diurnal effects), the bandshapes and noise temperatures are more stable.

A novel method has been employed to obtain the amplitude information (UR) using a hardware scheme similar to that used in the one-bit correlators. However, here a threshold detector is used instead of a zero-cross detector. A suitable threshold value is that which is sensitive to the change in the area of the probability density function of the input signal. If ρ_a and ρ_c are the analog correlation and the normalised one-bit correlation coefficient respectively, then,

$$\rho_a = \sigma_1 \sigma_2 \operatorname{Sin}\left(\frac{\pi}{2}\rho_c\right) \tag{1}$$

where, σ_1 and σ_2 are the r.m.s. values of the signals being multiplied. In our case, these signals correspond to those from the EW array and from any row of the S array. Their amplitudes were continuously recorded to obtain σ_1 and σ_2.

The continuum observations made with GEETEE were meridian transit observations. When making the sky survey, we used only one of the four dipole rows in the EW array. Rows I and IV (numbering from the north) were considered inappropriate since they see a more asymmetric environment (see UR for a schematic of the array) and either rows II or III were better suited for our observations. In fact, the observations were carried out using dipole-row III in the EW array and the 88 southernmost rows in the S-array. The 88 visibilities corresponding to the various baselines which row III of the EW array forms with the individual rows of the S-array were measured. Time-division multiplexing with a cycle time of 1 s was adopted and at any instant only one out of each adjacent four rows in the S array was active. This meant that the same transmission line and front end could be used for each set of four rows in the S-array. The 88 complex visibilities were recorded continuously, except for an interval of 1 min in each hour when the output from a noise diode in the field replaced the EW antenna. The recording from the noise diode monitored the gain variations of the last stage amplifiers in the front end and the subsequent sections of the antenna system in the EW array both of which affect the measurement of σ_1. These variations were found to

be <0.6 per cent. A similar recording was made to keep track of the factors affecting the measurement of σ_2. In addition, at the beginning of each 24-hour observation, the output from the noise diode in the EW array was recorded for about 15–30 min. Since the rows of the S-array were contributing the sky noise at this time, which is uncorrelated with the noise diode output, the measured correlation coefficient gives the receiver offsets caused by biases in the zero-cross detectors, etc.

An important objective of the present survey was to map the Galactic background radiation and give the brightness temperature unambiguously at each point in the sky. This is possible if the antenna system responds to all angular-scale structures (larger than its resolution) in the sky. With this in view, we have included all spacings in our observations and, in particular, the zero spacing (UR). The visibility resulting from the multiplication of the signals from row III of the EW array with the S-array row in line with it (S_3) corresponds to the zero spacing. The noise due to the F.E.T. amplifier in S_3, which is common to both the EW array and S_3, contributes ≈ 500 K to the signal from the sky in this spacing. Since the brightness temperature of the sky near 30 MHz is $\gtrsim 10{,}000$ K, this leads to a small, correctable offset in the estimated brightness temperatures of the sky.

Observing conditions at Gauribidanur depend critically on solar activity. Non-solar astronomy is best performed during a solar minimum. The present observations were made during a period (last 15 days of January 1987) when the ionospheric disturbances were at a minimum and the interference was remarkably low. In principle, any single day is sufficient to produce an all-sky map. By observing for 15 days, it was possible tc make a detailed check of the repeatability of the measurements.

Observations of strong point sources are the most sensitive way of judging both telescope performance and observing conditions. We used the following five sources as routine checks of the system: 3C144 (Tau A), 3C218 (Hydra A), 3C274 (Virgo A), 3C405 (Cygnus A) and 3C461 (Cas A). All of these are unresolved by GEETEE and are sufficiently strong to measure the visibility for each baseline. They cover a wide range of R.A. and Dec. and give an overall picture of telescope performance. The results of the checks made on these point sources imply the following:

(a) the amplitudes of the illumination patterns of the S-array rows repeat with an r.m.s. of 1 per cent as estimated from the same source on two different days and with an r.m.s. of 6 per cent as estimated from two different sources on the same day.

(b) the instrumental phases repeat with an r.m.s. of 1° from day to day as determined from the same source and with an r.m.s. of 6° from source to source.

(c) the amplitude and phase distributions over the EW aperture show r.m.s. deviations of 0.6 dB and 8° respectively.

3. Data analysis and calibration

3.1 *Producing the CLEANed Map*

The brightness distribution $B(l, m)$ of the sky is related to the visibility $V(u, v)$ through the Fourier transform relation:

$$B(l, m) = \iint V(u, v)\, e^{-j2\pi(ul+vm)}\, du dv. \qquad (2)$$

The raw or dirty map $B'(l_0, m_0)$ at any celestial position l_0, m_0 is the convolution of the brightness distribution with the antenna response $P(l, m)$:

$$B'(l_0, m_0) = \iint P(l-l_0, m-m_0) B(l, m)\, \mathrm{d}\Omega \tag{3}$$

(Christiansen & Högbom 1985). A single row of the EW array and each row of the S-array have primary beams which look at essentially the whole sky along the meridian—their far-field voltage pattern (E) in the plane perpendicular to the axis of the dipole is expected to be:

$$E(\theta) = \sin\left(\frac{2\pi}{\lambda} H \cos(\theta)\right) \tag{4}$$

where θ is the zenith angle, H is the height of the centre of the dipole above the reflecting screen and λ is the wavelength of observation. By Fourier transforming the visibilities along v, the instantaneous brightness distribution of the sky along NS can be obtained. Thus, in a single sidereal day, the entire observable sky was mapped. Hermitian symmetry was assumed for the visibilities (see the discussion about 'Tee' and 'Cross' arrays in Christiansen & Högbom 1985). The procedure for obtaining a raw or dirty map is outlined in Fig. 1.

Interference of short duration is easily detected by its appearance on the raw map. There were only about half a dozen occasions when such interference could be seen, each corrupting only 1 or 2 samples of data. An 8th-order polynomial was fitted to the adjacent data stretches and used to fill in these gaps.

To obtain the final brightness distribution, the dirty map has to be deconvolved. The conventional CLEAN algorithm (Högbom 1974) proceeds by locating successive maxima in the dirty map and subtracting the dirty beam from each such position. The height of the dirty beam subtracted is usually chosen to be a fraction of the maximum. This loop gain is often chosen to be 0.2. The implicit assumption here is that the sky is empty except for the discrete sources. This is not the case for our maps which contain both point sources and a varying Galactic background. A discussion of the unsuitability of CLEAN under such circumstances and of some possible solutions can be found in Thompson, Moran & Swenson (1986). The present method of deconvolution uses the two-dimensional point spread function (PSF) or the two-dimensional response of the antenna, and a modified version of the conventional CLEAN.

The PSF was generated from the dirty map around the strong source Cygnus A. The extent of the PSF was ± 1 hour in R.A. and the full extent in declination. The modified CLEAN algorithm adopts a 'local maximum' rather than a 'global maximum' criterion. Thus, the 'maxima' are heights above the local background and not absolute values in the dirty map. The details of generating the PSF and of the modified CLEAN are discussed in an accompanying paper (Dwarakanath, Deshpande & Udaya Shankar 1990; DDU). For the present purpose, we will just state the results—this method deconvolves only the sources of similar size to the beam, leaving the extended emission unaltered. In our case, this converges much faster than the conventional CLEAN. It was possible to CLEAN the whole map down to an almost uniform level of 5σ, where σ is the r.m.s. fluctuation in the dirty map. To estimate the σ, the dirty map was divided into many $5° \times 5°$ regions. The r.m.s. fluctuation in each region was estimated through an iterative scheme in which all values beyond 5σ were excluded. The σ in the dirty map was estimated by averaging these r.m.s. fluctuations. The CLEAN components were convolved with a Gaussian beam of the same full-width-at-

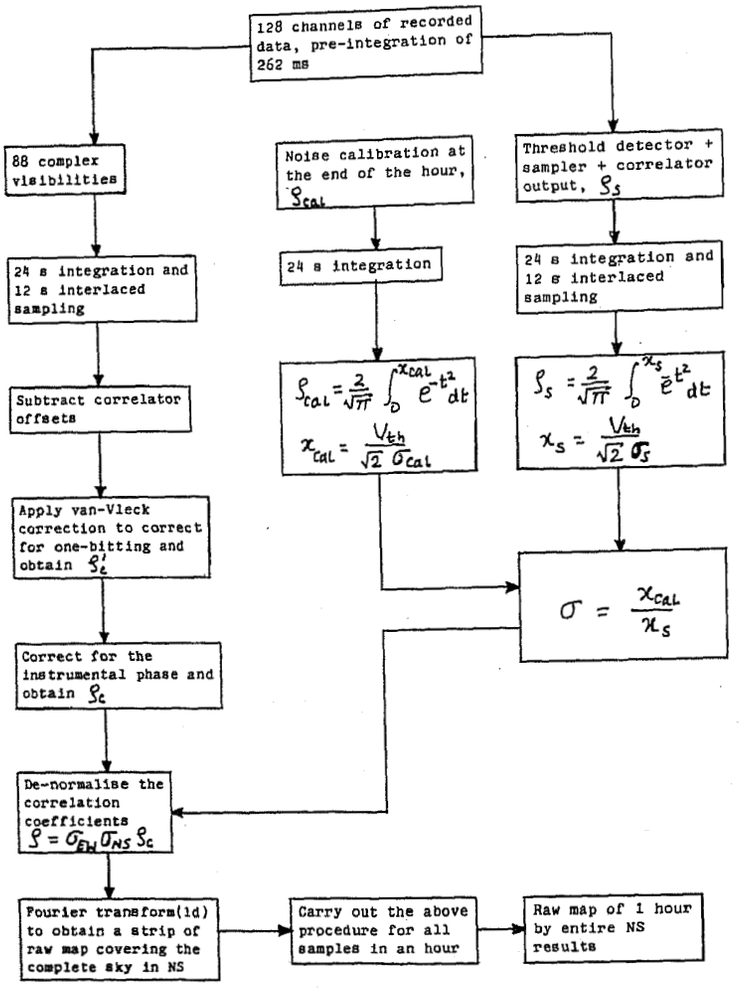

Figure 1. A flow chart of the procedure used to obtain the raw maps.

half-maximum and area (full-beam area) as the dirty beam and added to the map of the residuals to produce the final maps (Fig. 2).

The final maps showed several features which were suspected of being non-astronomical artefacts. These were of the size of the synthesized beam in NS but continued for hours in EW. With a view to understanding their origin and correcting for it, the following analysis was made. The residual map from the CLEANing of one hour by the full extent in declination was averaged along time and the resultant profile Fourier transformed to give the amplitude of correlations as a function of baseline. This showed values higher than expected from noise in the short spacings (< 50 m) due to the contribution from the celestial background. However, many of the longer baselines also showed unexpectedly high values. In addition, the pattern in the longer baselines repeated when this analysis was performed on the residuals at different sidereal times. This was a clear indication of an instrumental origin. These offsets were subtracted for the longer (> 50 m) baselines, although this could not be done for the shorter baselines due to the contribution from the sky background.

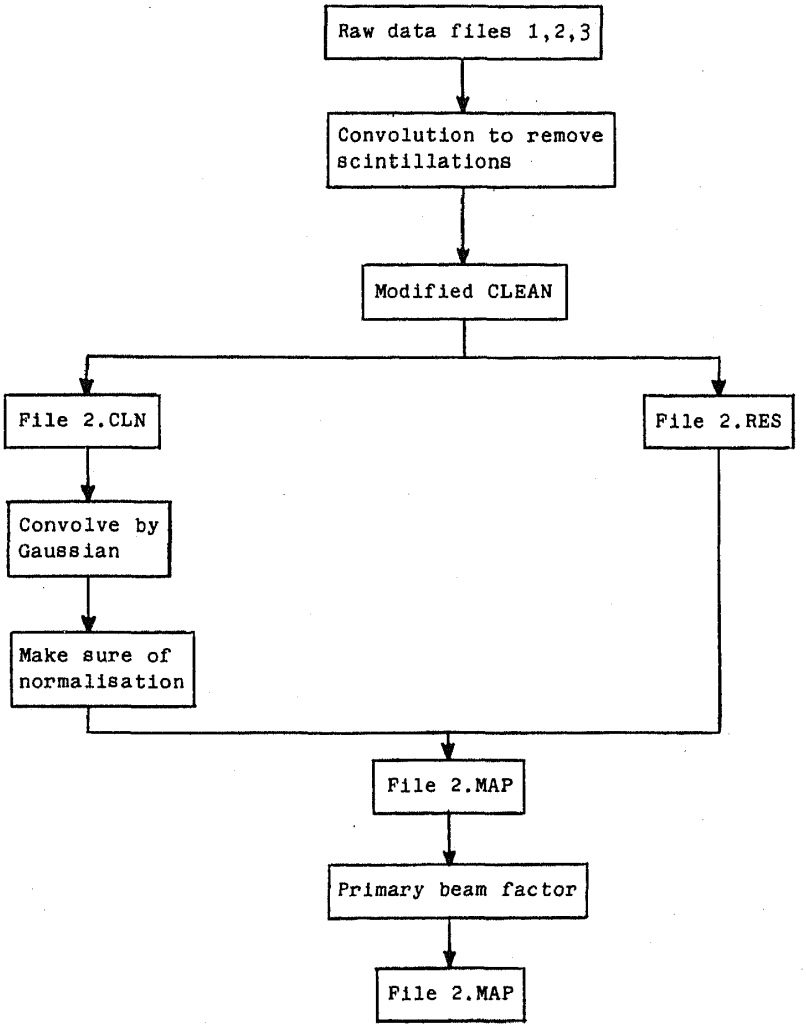

Figure 2. Overall scheme to produce the final maps from the raw maps.

3.2 *Calibration*

For further use, the CLEANed maps can be expressed in units of Jy/beam or, equivalently, in brightness temperature. Cygnus A was chosen as the calibrator for this purpose. Absolute flux density measurements of Cyg A are available from 10 MHz to 22 GHz (Baars *et al.* 1977). At frequencies around 30 MHz its absolute flux density is known to within 5 per cent, and has been calculated to be 25396 Jy at 34.5 MHz from the spectral fit given by Baars *et al.* To associate a brightness temperature with the Galactic background emission, we have to obtain the solid angle of the antenna response. This can be done by integrating the PSF that was used for CLEANing the maps.

It is important to check that the flux density scale so obtained is

(a) independent of the strength of the source
(b) does not have any systematic pattern as a function of R.A. or Dec. and,
(c) is repeatable with time.

For this purpose, the results from the survey at 38 MHz by Williams, Kenderdine & Baldwin (1966) were used. Kellermann, Pauliny-Toth & Williams (1969) list 38-MHz flux densities for most 3C sources. Their list contains 21 sources whose estimated standard error is 5 per cent (called 'A' sources) and 118 sources with estimated standard errors between 5 and 15 per cent (called 'B' sources). We have estimated the 34.5-MHz flux densities of these sources from our maps. A function of the form shown in Fig. 3 was convolved with the map in both the R.A. and Dec. directions. This essentially filters out all the background variations with angular scales larger than the separation between the negative delta functions. The resultant map can simply be summed within the size of the source to obtain the integrated flux density of the source. A percentage difference between the two flux densities was obtained as follows:

$$\% \text{ error} = \frac{\text{flux density at 38 MHz} - \text{flux density at 34.5 MHz}}{\text{flux density at 38 MHz}} \times 100. \qquad (5)$$

Fig. 4 shows this % error plotted against declination for the (B) sources. We omitted the (B) sources which are weak ($\lesssim$30 Jy) or at high declinations ($\gtrsim$70°), or which fall beyond 3σ of the distribution. A sloping trend is clearly seen. It is extremely unlikely that any of our antenna-based effects are monotonic in declination from $-2°$ to $+60°$ when the instrumental zenith is at $+14°.1$. A clue to understanding this pattern comes from the fact that the 38-MHz survey consists of two surveys—one centered at $+7°$ and the other centered at $+52°$, with the FWHM of the NS antenna patterns being $+47°$. Thus, the source list at 38 MHz is made up of two sets of sources with

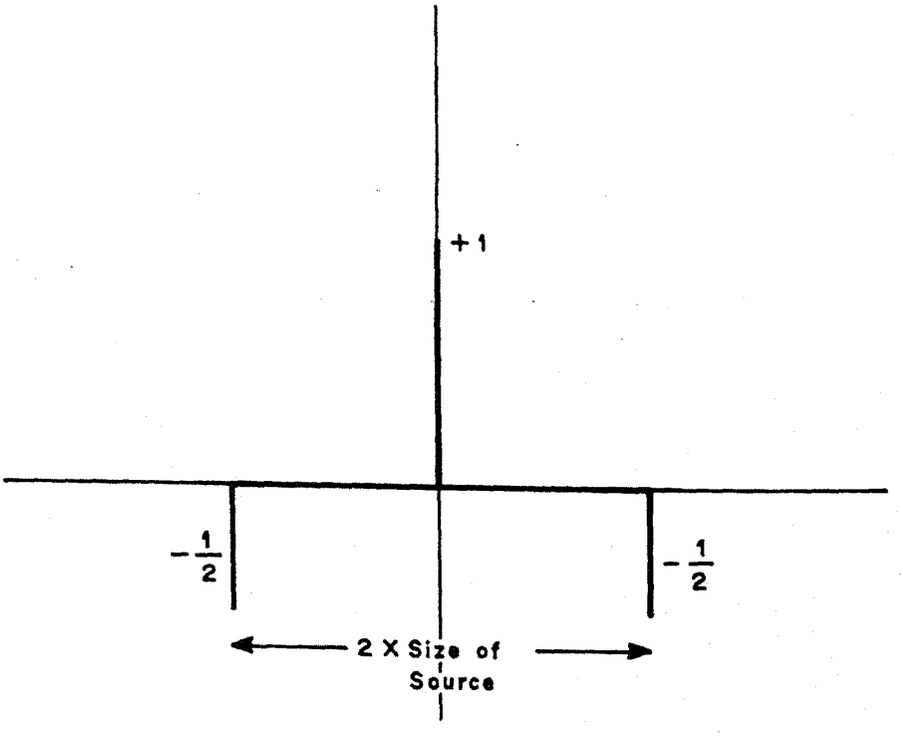

Figure 3. Convolving function used to filter the background. A special case of this has been used by Williams, Kenderdine & Baldwin (1966) to obtain flux densities of point sources in their survey.

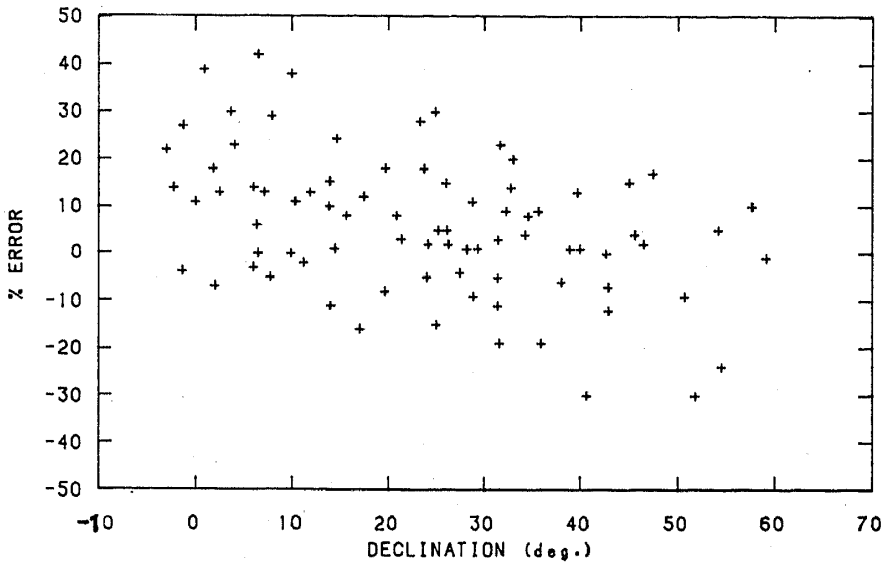

Figure 4. Percentage differences between the flux densities of some 3C sources at 34.5 and 38 MHz plotted as a function of the declination of the sources. The slope is probably due to the difference in the flux density calibration of the 3C sources at 38 MHz depending on whether they are above or below $+30°$ declination.

declinations greater or less than $+30°$. We have calculated the average and r.m.s. value of the % error in the two zones $-\leqslant+30°$ and $>+30°$. The results are as follows:

	avg.	r.m.s.	error on the mean	
If Dec. is $\leqslant+30°$, % error =	9.5	±18	2.5	(52)
$>+30°$, % error =	-0.5	±14	2.6	(30)

where the numbers in the brackets indicate the number of sources in the two zones. The averages are different at the 4σ level. Fig. 5 shows the same plot as Fig. 4 but with the offset subtracted for dec. $\leqslant+30°$. The slope is much less apparent. Similar plots of the % error *vs* R.A. and source flux density indicate that there are no systematic patterns against either parameter. Taking an average value for the r.m.s. of the % error between the flux densities at 38 and 34.5 MHz to be 16 per cent, and the r.m.s. value of the % error in the 38 MHz flux densities to be 10 per cent, an r.m.s. value of 12 per cent is implied to the flux densities of the (B) sources at 34.5 MHz.

For the (A) sources the results are as follows:

	avg.	r.m.s.	error on the mean	
If Dec. is $\leqslant+30°$, % error =	0.63	±4	1.4	(8)
$>+30°$, % error =	5.4	±8	2.5	(10)

Due to the small numbers involved, it is difficult to comment on the statistical significance of the difference in the averages. However, the average of the two r.m.s. values of 6 per cent implies an r.m.s. of <5 per cent for the flux densities of the (A) sources at 34.5 MHz.

In obtaining the % error from Equation (5) we have not corrected the source flux densities for their spectra. However, this does not change the difference between the

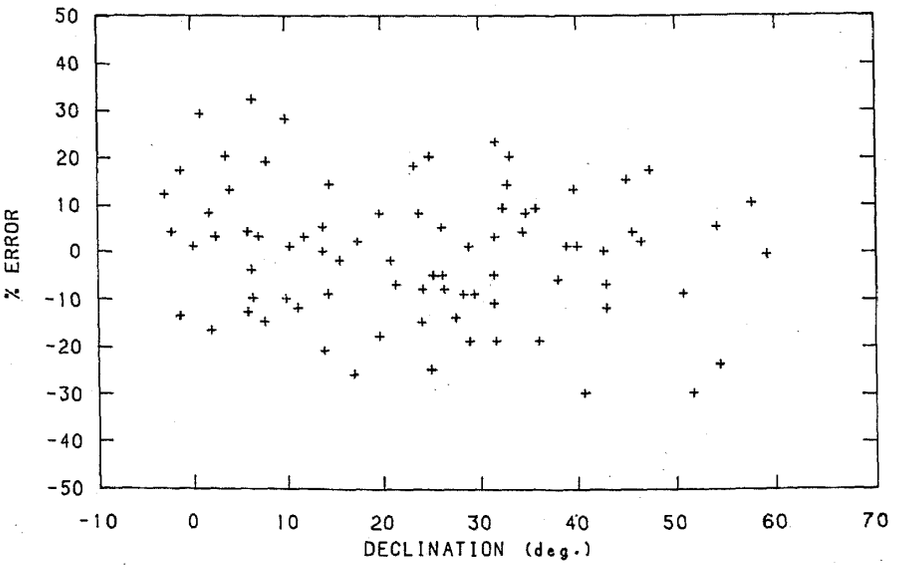

Figure 5. Percentage difference between the flux densities as in Fig. 4 but with the average calibration difference in the flux densities at 38 MHz between the sources above and below $+30°$ dec. subtracted. The systematic pattern seen in Fig. 4 is much less apparent here.

two averages (for declination greater or less than $+30°$) significantly. With a view of comparing the flux density scales at 38 and 34.5 MHz we did the following—(a) the flux density scale at 38 MHz was brought to that Baars *et al.* (1977) by using a factor 1.1 as implied by the flux density measurements on Cygnus A at 38 MHz (Williams, Kenderdine & Baldwin 1966), and (b) the 38 MHz flux densities were then extrapolated to 34.5 MHz with a mean spectral index of -0.75 (Kellermann, Pauliny-Toth & Williams 1969). These two corrections bring down the two averages for the (B) sources to $+7$ and -3 per cent respectively. Thus, the corrected flux density scale at 38 MHz and that at 34.5 MHz agree to within 5% as implied by the flux density estimates made on ≈ 100 (B) sources.

3.3 *Repeatability*

It was important to check the repeatability of the 34.5-MHz observations as interference, the ionosphere and system variations could have affected the data. With this in mind, the flux densities of all the (B) sources were estimated from another day's observation, and the flux density differences between the two days computed. They agreed to within 8 per cent (r.m.s.).

3.4 *Bandwidth Decorrelation*

For a bandwidth of 400 kHz and a zenith angle of 50°, there is an average of 8 per cent decorrelation between the signals from the rows of the EW and S-arrays. Since this is a small percentage, it does not seriously degrade the signal-to-noise ratio. In addition, as we sum over the source size or the beam size (whichever is the larger) when estimating flux densities of the sources, these flux densities are unaffected by the bandwidth decorrelation.

4. The maps

ıe results of the survey are given in the form of contour maps in equatorial ordinates. We have used the NOD2 program library to prepare the contour maps. ıe maps have the same format as those of the 408 MHz all-sky survey (Haslam *et al.* 82) and are precessed to 1950. Arrows on the contours which point clockwise enclose ıima while those that point anti-clockwise enclose maxima. In Fig. 6 we present a w-resolution (2°) map from the present survey of the entire region of the sky that is ıt aliased (all 24 hr of R.A. for $-36° \leqslant$ Dec. $\leqslant +64°$; Although the unaliased region ould strictly be $-33° \leqslant$ Dec. $\leqslant +61°$, due to the effect of the primary beam, aliasing < 10 per cent at zenith angles of $\pm 50°$, and we have set our declination limits by is). These low-resolution maps give an overall impression of the sky at 34.5 MHz. ıe numbers on the contours are in units of 5722 K (full-beam brightness temperure) above absolute zero. The absolute levels of the contours are accurate to within per cent—the accuracy to which the flux density of Cygnus A, our calibrator, is ıown. The steps in the contour levels are as follows:

1 to 5 every 0.25 units, labelled every 1 unit,
5 to 10 every 0.5 units, labelled every 2 units,
10 to 20 every 1.0 units, labelled every 4 units,
20 to 32 every 1.5 units, labelled every 6 units.

ɔr the purpose of comparison, we present the 408-MHz map of Haslam *et al.* (1982), so convolved to 2° (Fig. 7). In this figure, the labels on the contours are in units of) K. The steps in the contour level are as given above.

Some of the large-scale features that have been recognised earlier (Large, Quigley & aslam 1962; Quigley & Haslam 1965; Berkhuijsen, Haslam & Salter 1971; ɛrkhuijsen 1971 and Milogradov-Turin & Smith 1973) and which can be seen clearly the 408-MHz map are listed in Table 2. A comparison between Figs 6 and 7 shows

Table 2. Some large scale features that can be seen on both the 34.5 and 408 MHz maps and their temperature spectral indices (β) where temperature $\propto$ frequency$^{\beta}$. The error in β is 0.03 (1σ).

	Position (α, δ) (hour, deg.)	Temperature spectral index between 34.5 MHz and 408 MHz
Loop II (Cetus Arc)	2.5, +30 to 21, −5	Varies from −2.6 to −2.8 as one moves from $2^h.5$, +30° to 21^h, −5°
Loop III	3, +45	−2.55
Spur 185−	5, +15	−2.55
Loop III	5, +60	−2.5; more pronounced at 5^h, +50°
	8, +15	not seen clearly
Loop I (North Polar Spur)	17, +10	Base of the spur is at more like 18^h, 0°. Spectral index varies from −2.7 at the base to −2.4 at the tip (13^h, +15°)
Loop III	19, +55	not seen clearly
Spur 80−	22, +20	−2.7
Loop III	22.5, +40	−2.7

that all but two of these are seen in the 34.5-MHz map. Some interesting features towards the Galactic centre can also be seen at 34.5 MHz. These are (a) the $l=0°$ feature which is an arc of emission starting at 17^h20^m, $-25°$ and extending up to 16^h, $-22°$ (see Sofue *et al.* 1988 for a 408 MHz map), (b) the $l=355°$ feature which is an arc starting at 16^h40^m, $-25°$ and going towards 16^h, $-30°$, and (c) the $l=345°$ feature between 15^h40^m, $-25°$ and 15^h, $-30°$.

4.1 *Some Spurious Features*

The above inter-comparisons between the various maps give us some confidence in interpreting the large-scale features seen on our maps. However, there are some features which we believe to be spurious.

The areas of extended emission centred around $\alpha=17^h40^m$, $\delta=+42°$ and at $\alpha=17^h$, $\delta=+30°$, as well as the adjacent minimum ($\alpha=17^h40^m$, $\delta=+60°$) are unlikely to be of astronomical origin. For one thing they are not present in the 38-MHz map made with a single dish (Milogradov-Turin & Smith 1973). Further, they are aligned in R.A. with the brightest portion of the Galactic plane. These regions are $\approx 10°$ in extent and have an average brightness of ≈ 25 Jy/beam at full resolution.

Another feature we believe to be spurious is the ridge of emission at $-15°$ declination which extends from 20^h to 5^h.

From the geometry of these spurious features, and as they repeat at the same sidereal times we conclude that they are not due to interference, even from a satellite. Since they are also present in the raw maps, they could not be artefacts introduced in the CLEANing procedure. The common aspect of all these features is their large angular size. This immediately suggests an explanation in terms of the measured visibilities in the short baselines. As detailed in Section 3.1, we have not removed any offsets present in the short-spacing (<50 m) visibilities since it was impossible to separate these from the contribution of the large-scale sky background in these baselines. The ridge of emission at declination $-15°$ running parallel to constant declination may be due to this. However, it is unlikely that this explains other features, which may be due to the peculiarities in the illumination pattern of the short-spacing S-array elements which may also be a function of the zenith angle. Interaction between the short spacing S-array elements and the EW antenna could lead to such effects, as noted previously by Jones and Finlay (1974) in their 29.9-MHz survey. If such peculiarities are indeed present, then given the intense broad emission region near the Galactic centre, one would expect to see its 'sidelobes'. An attempt was made to correct for this by using several strong point sources at different zenith angles (such as Cyg A, Cas A, Tau A, Vir A and Hyd A) but without success. Since there is no strong source at similar declination to the Galactic centre, we cannot test this hypothesis. Nevertheless, we believe this to be the most plausible explanation. It should be pointed out that the spurious features under discussion are at the level of ≈ 5 per cent of the intensity of the Galactic centre region. Hence, if the above explanation is correct we do not expect to see similar features elsewhere since there are no other extended regions comparable in brightness to the Galactic centre.

In addition, we wish to point out that the features seen in the maps between $20^h32^m <$ R.A. $< 20^h36^m$ and at almost all the declinations are due to interference which was not excised.

4.2 *The Full-Resolution Maps*

In this section, we present the full-resolution 34.5-MHz maps obtained from our survey. The numbers on the contours are in units of 5722 K (full-beam brightness temperature). The steps in the contour levels are as follows:

1 to 5 every 0.5 units, labelled every 1 unit,
5 to 10 every 1 unit, labelled every 2 units,
10 to 20 every 2 units, labelled every 4 units,
20 to 32 every 3 units, labelled every 6 units,
32 to Max. every 4 units, labelled every 8 units.

The convention for indicating maxima and minima are as described earlier in this section.

It is important to discuss the noise in the maps. There are two factors which are expected to contribute to the random fluctuations (over the size of the beam) in the map: *system noise* and *confusion.*

At decametric wavelengths, the system temperature is almost entirely determined by the sky noise. A typical antenna temperature encountered at 34.5 MHz is $\approx$ 10,000 K. In comparison, the first-stage amplifiers of the receiver have noise temperatures of only 500 K. Given a bandwidth of 400 kHz and an integration time of 24 s, the system noise is equivalent to a brightness of 3.5 Jy/beam (remembering that for this survey we have used only one EW row and adopted time multiplexing). However, the raw maps of the present survey were convolved along the EW direction with a sin $(x)/x$ function. The half power width of this function was that of the EW antenna along the EW direction ($\approx$ 100 s) so that astronomical spatial frequencies remained unaffected. This effectively increases the integration time by a factor of 4, bringing down the system noise to 1.8 Jy/beam.

It is possible to obtain a reasonable estimate of the system noise from the maps themselves. If the raw maps are convolved with a sin $(x)/x$ function whose resolution corresponds that of the antenna, then all spatial variations smaller than the resolution will be smoothed out. A subtraction of the convolved map from the raw map leaves only the contribution of the system noise in the frequency range between $1/(2t_{\rm res})$ and $1/t_{\rm int}$ Hz. As discussed above, before CLEANing, the raw maps were smoothed in time with a sin $(x)/x$ function of resolution $(=t_{\rm res})$ 84 s (corresponding to EW resolution of the EW antenna at 0° dec.). So, the system noise in the final maps is band-limited to $1/(2\times 84)$ Hz. This can be estimated by extrapolating the contribution obtained between $1/(2t_{\rm res})$ and $1/t_{\rm int}$ Hz. The value so obtained indeed agrees with our estimate made above.

The contribution from confusion is expected to be as important as the system noise in determining the sensitivity of the GEETEE for point source detection. One source per main beam of the GEETEE implies $\approx$4300 sources per steradian at the zenith. An estimate based on the $\log(N)$ *vs* $\log(S)$ plot at 408 MHz (Shaver & Pierre 1989), and assuming a spectral index of -0.8, gives the confusion limit at 34.5 MHz as 3.2 Jy/beam. Since this is almost twice the system noise, it follows that our maps are effectively confusion limited (at least in those regions where the antenna temperature is $\lesssim$10,000 K).

To estimate the confusion from the maps, we can find the difference between each point on the map and the average value of the map one resolution element away. The

r.m.s. value of this difference over the region of interest will then provide an estimate which includes both confusion and system noise. Since these two sources of noise are uncorrelated we can write $\sigma^2=\sigma_s^2+\sigma_c^2$ (where σ is the r.m.s. fluctuation on the map, σ_s the contribution from system noise and σ_c that due to confusion). Using the value of σ_s obtained from the difference map (as described above), σ_c can now be estimated. Such an analysis was made for regions of low and high intensity. The region of sky in the range $12^h\,30^m \leqslant$ R.A. $\leqslant 13^h\,30^m$, and $-36° \leqslant$ Dec. $\leqslant +64°$ was divided into $5° \times 5°$ areas and, for each, σ_s and σ were determined. The average values of $\sigma_s=1.8$ Jy/beam and $\sigma=4.9$ Jy/beam gave $\sigma_c=4.6$ Jy/beam. A similar analysis made for $17^h\,30^m \leqslant$ R.A. $\leqslant 18^h\,30^m$, $-36° \leqslant$ Dec. $\leqslant +64°$ gave values of $\sigma_s=3.9$ Jy/beam and $\sigma=6.0$ Jy/beam implying $\sigma_c=4.6$ Jy/beam. These numbers appear reasonable. The increase of system noise from 1.8 Jy/beam in the colder region to 3.9 Jy/beam in the hotter region is expected as the antenna temperatures of both the EW and the S array rows increase by a factor of 2 in going from the one to the other (the system noise will increase in proportion to the system temperature, T_{SYS}, all other parameters being equal. In a correlation telescope, $T_{SYS}=\sqrt{T_{SYS1} \times T_{SYS2}}$ where the subscripts 1 and 2 refer to the two telescopes whose outputs are multiplied—in our case the EW antenna and a given row of the S-array). Thus, the variations of the total noise in the map are very small—varying from 4.9 Jy/beam in colder regions to 6.0 Jy/beam towards hotter regions.

4.3 *Dynamic Range of the Maps*

The dynamic range can be defined as the ratio of the flux densities of the strongest and the weakest sources detected in a given region. Clearly, this will depend upon how close or far away one is from a strong source. In addition, in the present case it also depends upon the 'direction'. In the R.A. and Dec. directions, for example, the residual sidelobe levels of a point source are 0.2 to 0.5 per cent of the peak value, implying a 5σ dynamic range of 20 to 16 dB. The 'diagonal' directions are much cleaner. Except around Cyg A and Cas A, the noise in the diagonal direction is essentially the noise inherent to the map and is not relevant to the discussion of the dynamic range of the map.

Since we have chosen Cygnus A to generate the PSF, the region around Cygnus A has the maximum apparent dynamic range. In the CLEANed map this is $\approx$27 dB.

Due to a variety of problems (*e.g.* curved R.A. sidelobes, sidelobes beyond ± 1 hr, differences between the true PSF and the Cygnus PSF used for CLEANing, strength of the source, etc.), CLEANing the region around Cas A posed more problems and this could not be cleaned down to the 5σ noise level. Consequently, the dynamic range near Cas A is poorer than around Cyg A. The kind of dynamic range obtained around Cyg A is attainable only beyond 20° in declination and $\approx$30 min in R.A. from Cas A.

In general, one should be very cautious in identifying any sources at the same R.A. or Dec. as strong sources. We have deliberately left the residual sidelobes in the map to give the user a proper feeling for their strength, thus aiding their interpretation. In addition, beyond the declination ranges of $-33°$ to $+61°$ care should be exercised as these regions are affected by the grating response of the antenna.

4.4 *Survey Parameters*

Summarizing the main parameters of the survey:

Telescope	GEETEE—Gauribidanur Radio Telescope located at 13°36′12″ N
Instrumental zenith	+14°.1
Coverage	$-50° < \text{Dec.} < +70°$ ($-33° < \text{Dec.} < +61°$ without aliasing), and the full R.A. range.
Operating frequency	34.5 MHz
FWHM	$26' \times 42'\text{sec}\,(\delta - 14°.1)$
Telescope Configuration	One row of EW array and 88 rows of S-array. 1-D synthesis along NS
Collecting area	EW array, 1 row: 3000 m^2 S-array: 7000 m^2
Bandwidth	400 kHz
Integration time	24 s; this is effectively decreased by a factor of 4 due to the switching but increased by a factor of 4 due to filtering of the raw data during analysis.
Systen noise	1.8 to 3.9 Jy/beam (1σ)
Confusion	5 Jy/beam (1σ)
Absolute accuracy	5 per cent

Acknowledgements

We thank A. A. Deshpande, R. Nityananda, V. Radhakrishnan, T. S. Ravishankar, Ch. V. Sastry and G. Srinivasan for their contributions at various stages of the survey and for the many useful discussions we had with them. We also thank H. A. Ashwathappa, G. Jayakumar, C. N. Nanje Gowda and G. N. Rajasekhar for their help and co-operation during the observations. We thank C. G. T. Haslam and C. J. Salter for providing us the NOD2 library and the 408 MHz all-sky survey data. We also thank C. J. Salter for his valuable suggestions which have helped to improve the clarity and readability of this paper.

References

Baars, J. W. M., Genzel, R., Pauliny-Toth, I. I. K., Witzel, A. 1977, *Astr. Astrophys.*, **61,** 99.
Berkhuijsen, E. M. 1971, *Astr. Astrophys.*, **14,** 359.
Berkhuijsen, E. M., Haslam, C. G. T., Salter, C. J. 1971, *Astr. Astrophys.*, **14,** 252.
Caswell, J. L. 1976, *Mon. Not. R. astr. Soc.*, **177,** 601.
Christiansen, W. N., Högbom, J. A. 1985, *Radiotelescopes*, Cambridge University Press.
Dwarakanath, K. S. 1989, *PhD Thesis*, Dept. of Physics, Indian Institute of Science, Bangalore.
Dwarakanath, K. S., Deshpande, A. A., Udaya Shankar, N. 1990, *J. Astrophys. Astr.*, **11,** 311 (DDU).
Erickson, W. C. 1983, *Astrophys. J.*, **264,** L13.
Haslam, C. G. T., Salter, C. J., Stoffel, H., Wilson, W. E. 1982, *Astr. Astrophys. Suppl.*, **47,** 1.
Högbom, J. A. 1974, *Astr. Astrophys. Suppl.*, **15,** 417.

Jones, B. B., Finlay, E. A. 1974, *Aust. J. Phys.*, **27**, 687.
Kassim, N. E. 1988, *Astrophys. J. Suppl.*, **68**, 715.
Kassim, N. E. 1989, *Astrophys. J.*, **347**, 915.
Kellermann, K. I., Pauliny-Toth, I. I. K., Williams, P. J. S. 1969, *Astrophys. J.*, **157**, 1.
Large, M. I., Quigley, M. J. S., Haslam, C. G. T. 1962, *Mon. Not. R. astr. Soc.*, **124**, 405.
Mathewson, D. S., Broten, N. W., Cole, D. J. 1965, *Aust. J. Phys.*, **18**, 665.
Milogradov-Turin, J., Smith, F. G. 1973, *Mon. Not. R. astr. Soc.*, **161**, 269.
Quigley, M. J. S., Haslam, C. G. T. 1965, *Nature*, **208**, 741.
Shain, C. A., Komesaroff, M. M., Higgins, C. S. 1961, *Aust. J. Phys.*, **14**, 508.
Shaver, P. A., Pierre, M. 1989, *Astr. Astrophys.*, **220**, 35.
Sofue, Y., Reich, W., Reich, P. 1988, NRO Preprint no. 196.
Thompson, A. R., Moran, J. M., Swenson Jr., G. W. 1986, *Interferometry and Synthesis in Radio Astronomy*, John Wiley & Sons.
Udaya Shankar, N. 1986, *PhD Thesis*, Dept. of Physics, Bangalore Univ.
Udaya Shankar, N., Ravi Shankar, T. S. 1990, *J. Astrophys. Astr.*, **11**, 297 (UR).
Williams, P. J. S., Kenderdine, S., Baldwin, J. E. 1966, *Mem. R. astr. Soc.*, **70**, 53.

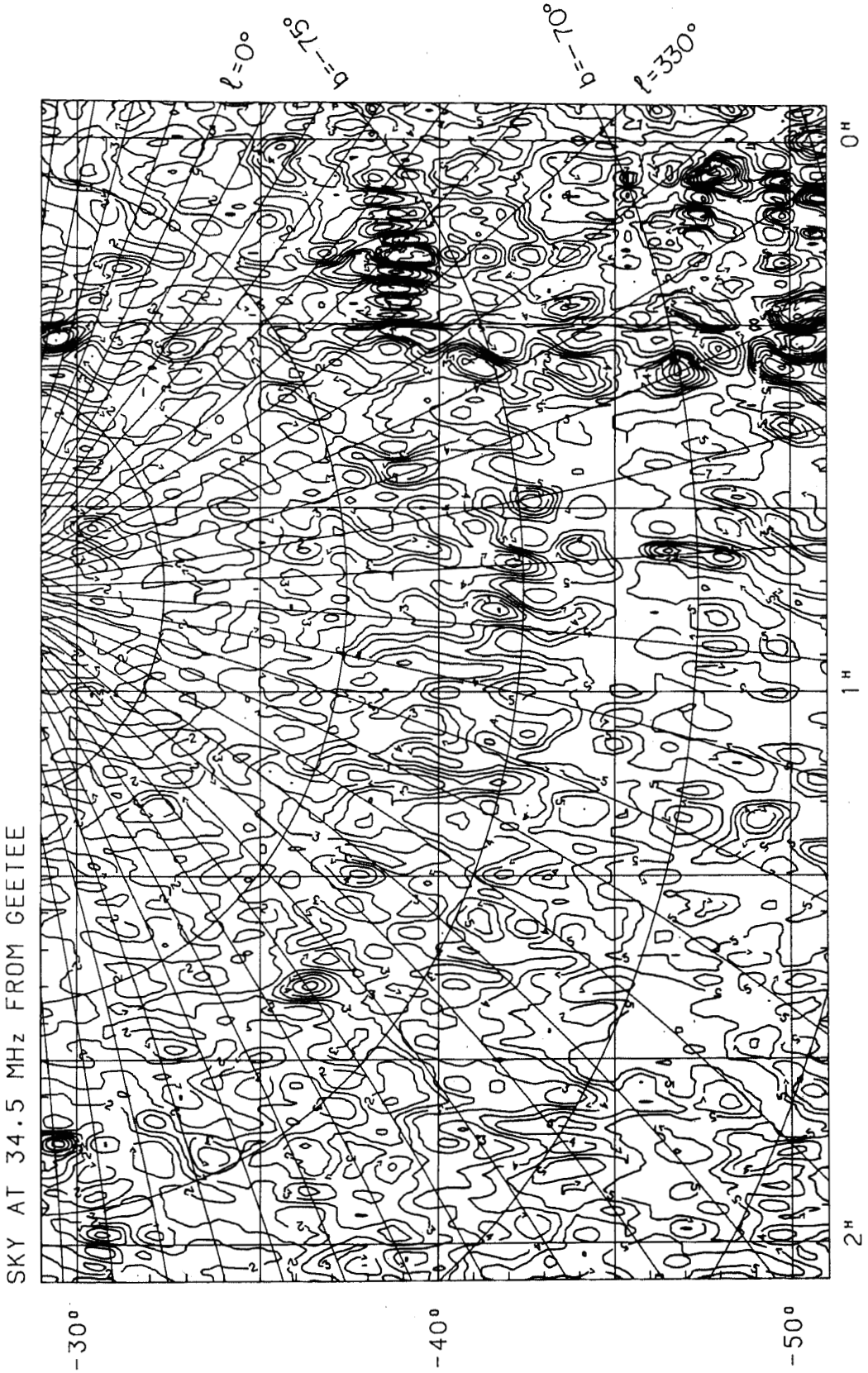
SKY AT 34.5 MHz FROM GEETEE
l=0°
b=-75°
b=-70°
l=330°
0H
1H
2H
-30°
-40°
-50°

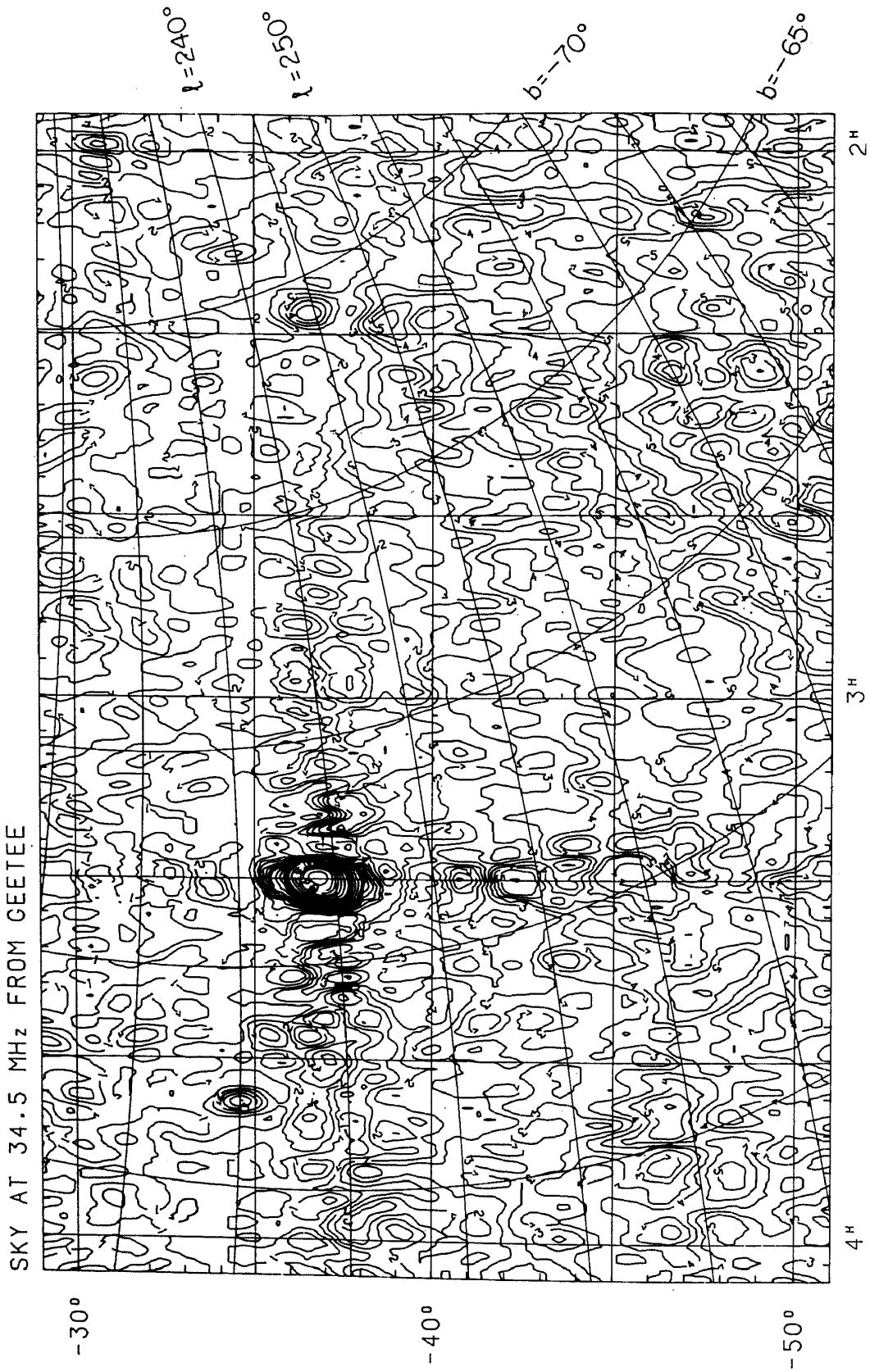
l=240°
l=250°
b=−70°
b=−65°
2H
3H
4H
SKY AT 34.5 MHz FROM GEETEE
−30°
−40°
−50°

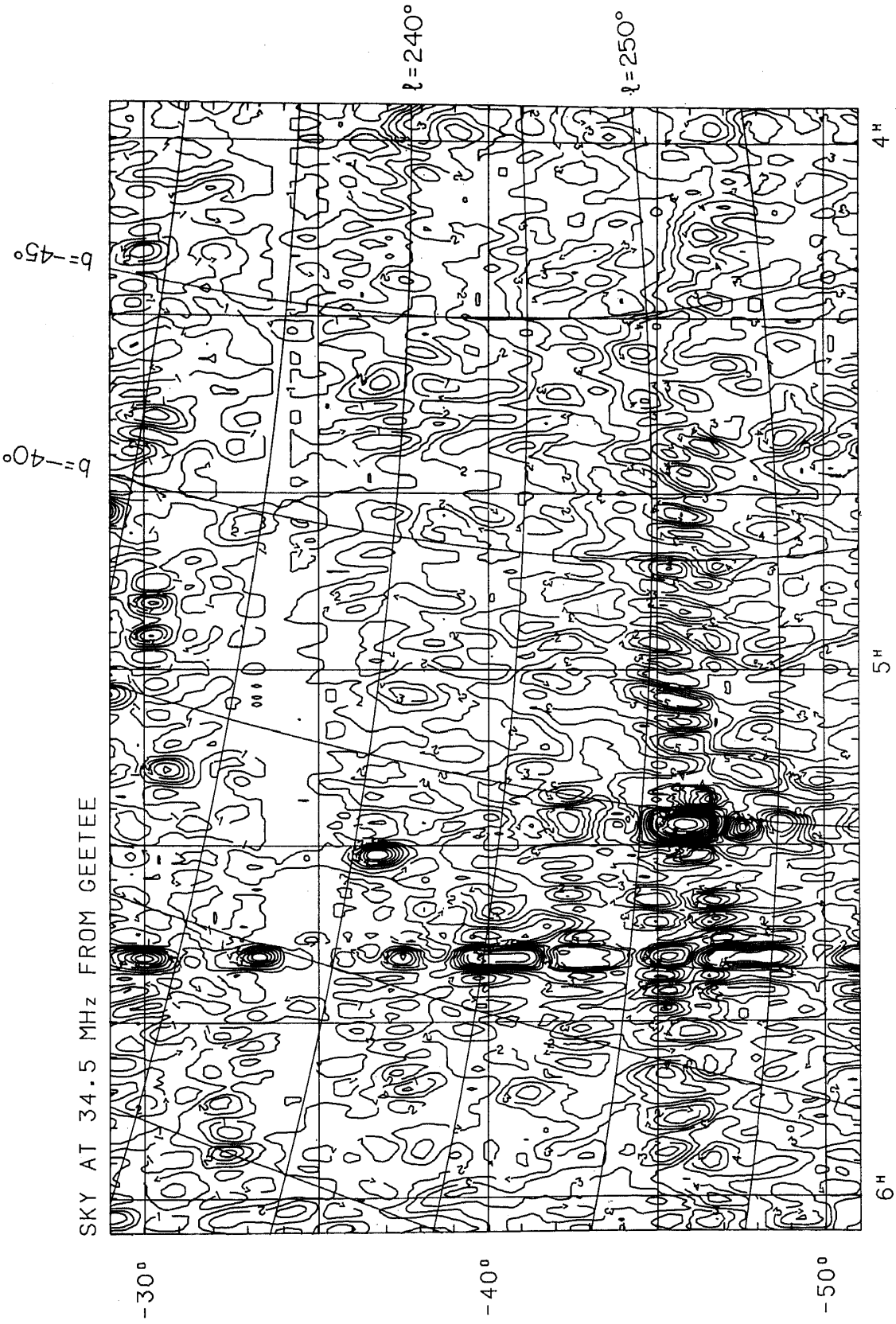
SKY AT 34.5 MHz FROM GEETEE
l=240°
l=250°
b=-45°
b=-40°
4H
5H
6H
-30°
-40°
-50°

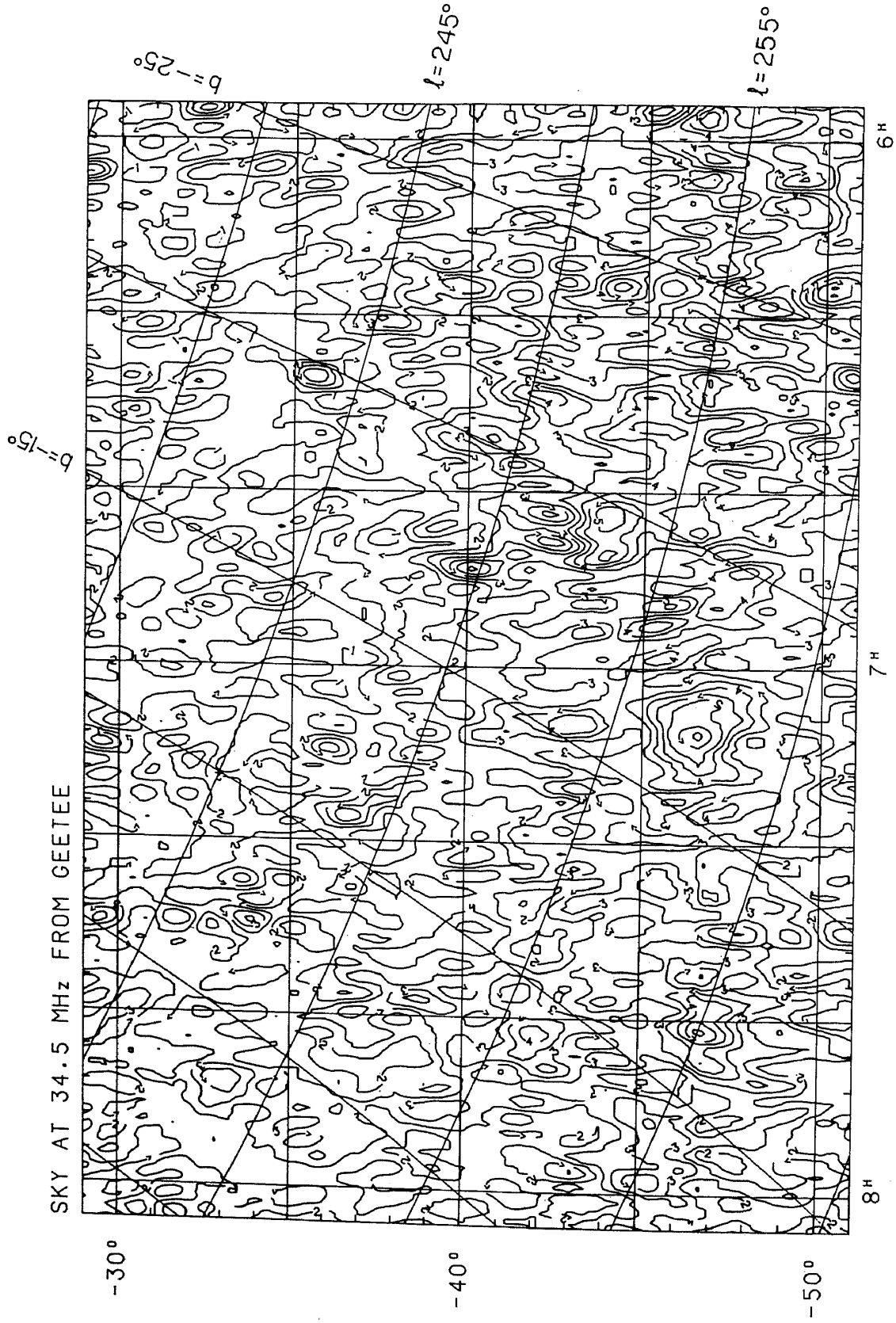
SKY AT 34.5 MHz FROM GEETEE
b=-25°
b=-15°
l=245°
l=255°
6H
7H
8H
-30°
-40°
-50°

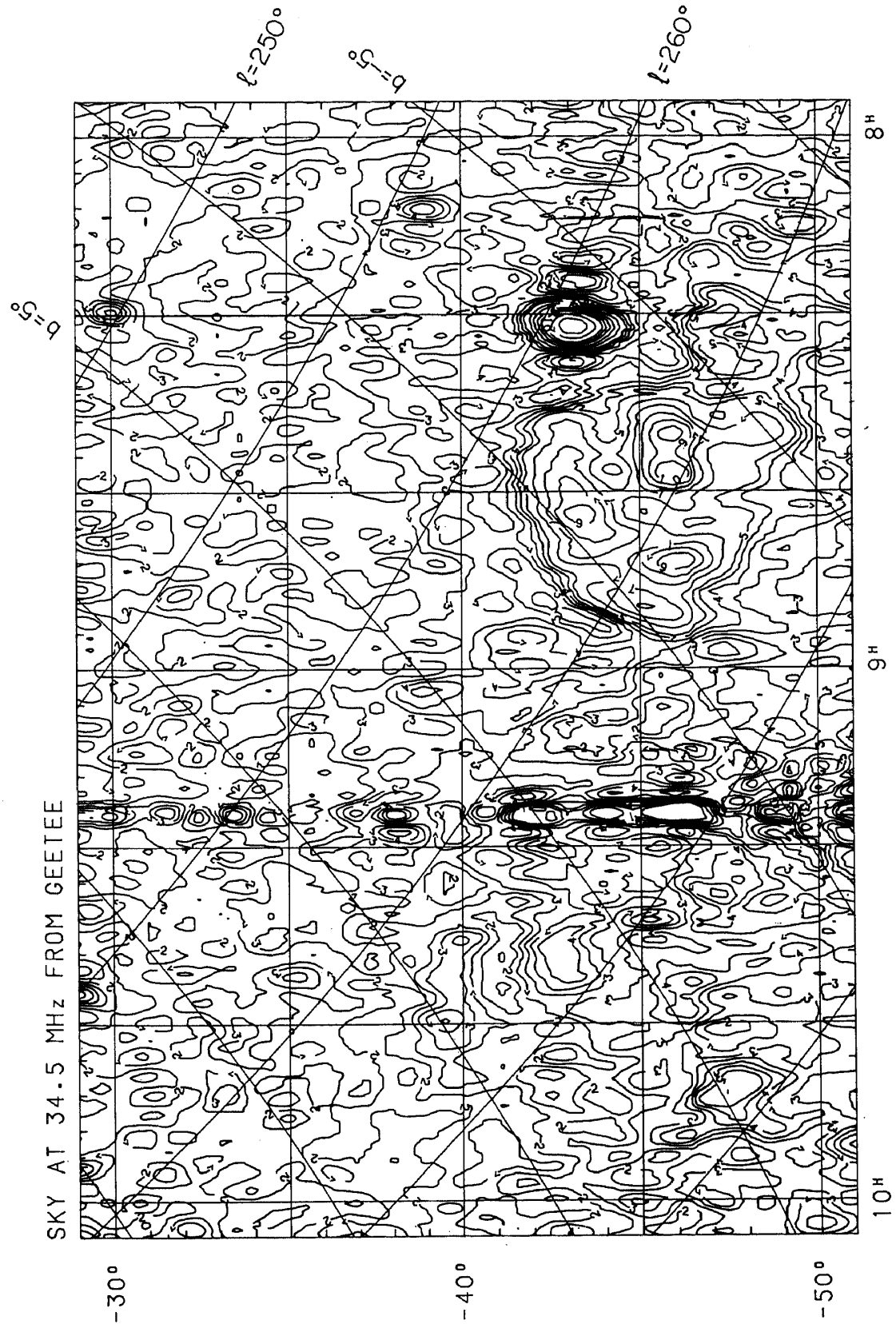
SKY AT 34.5 MHz FROM GEETEE
l=250°
l=260°
δ=0
δ=-5
-30°
-40°
-50°
8H
9H
10H

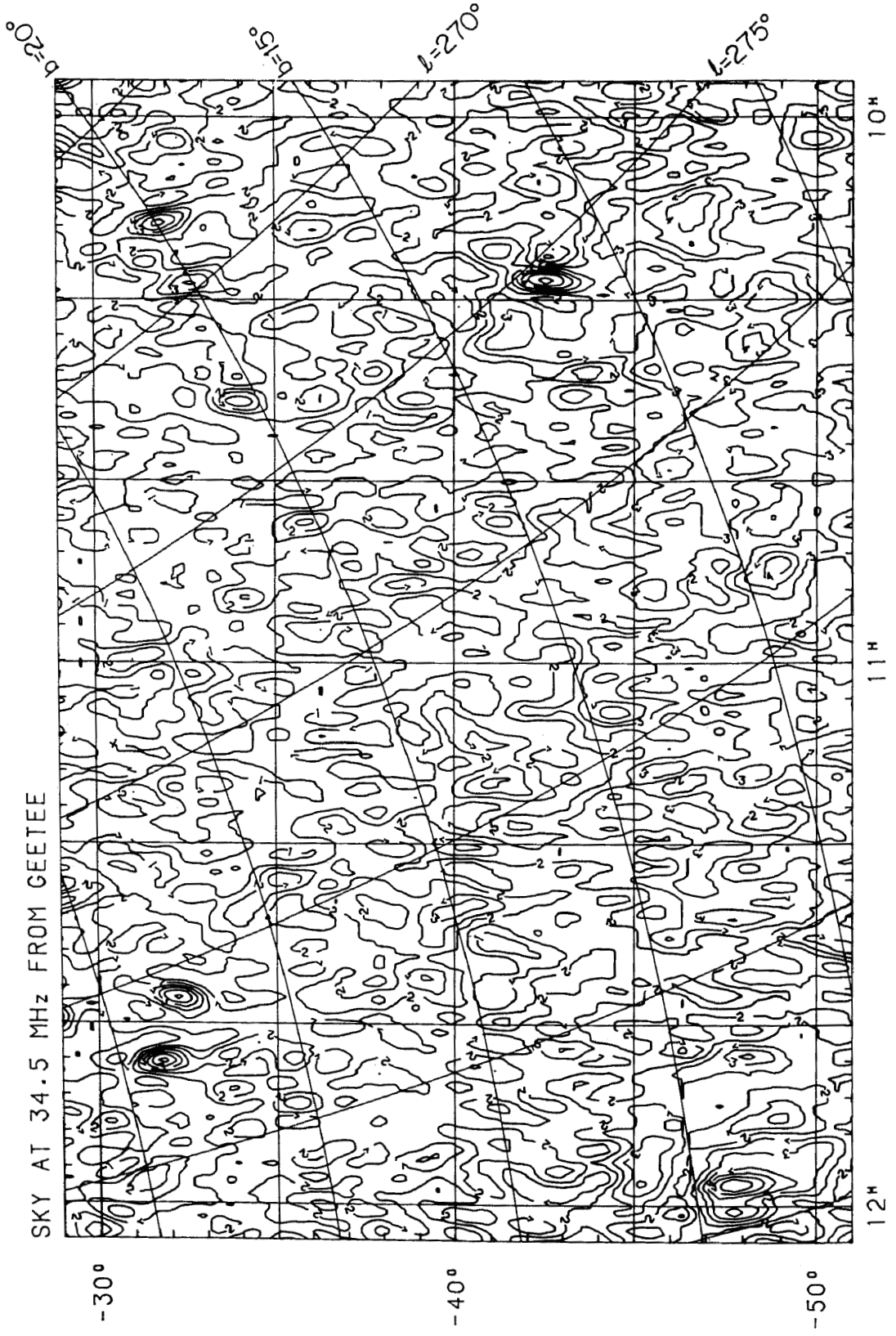
SKY AT 34.5 MHz FROM GEETEE
b=0°
b=15°
l=270°
l=275°
10ʰ
11ʰ
12ʰ
-30°
-40°
-50°

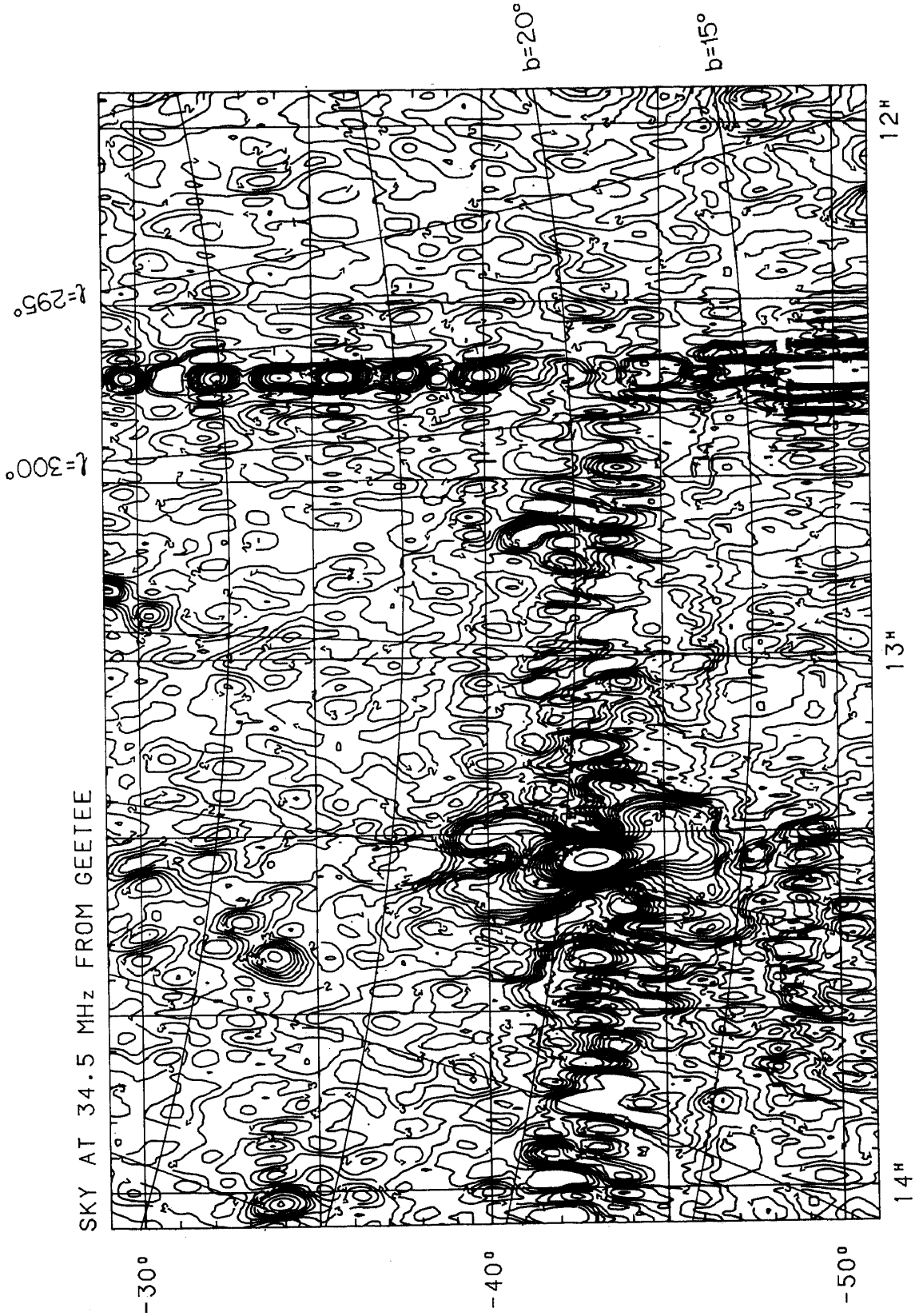
b=20°
b=15°
12ʰ
13ʰ
14ʰ
l=295°
l=300°
-30°
-40°
-50°
SKY AT 34.5 MHz FROM GEETEE

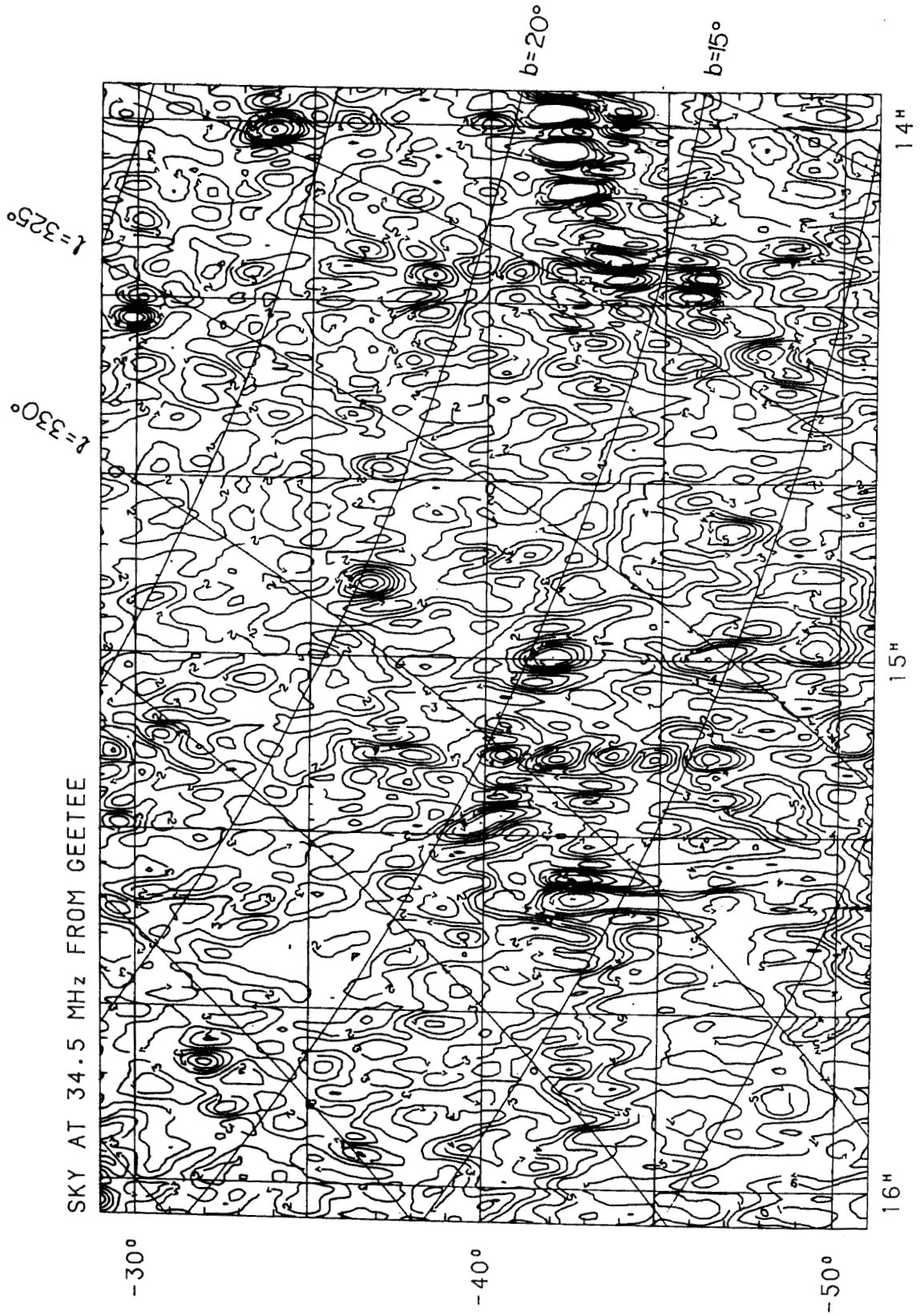
SKY AT 34.5 MHz FROM GEETEE
b=20°
b=15°
14H
15H
16H
-30°
-40°
-50°
l=325°
l=330°

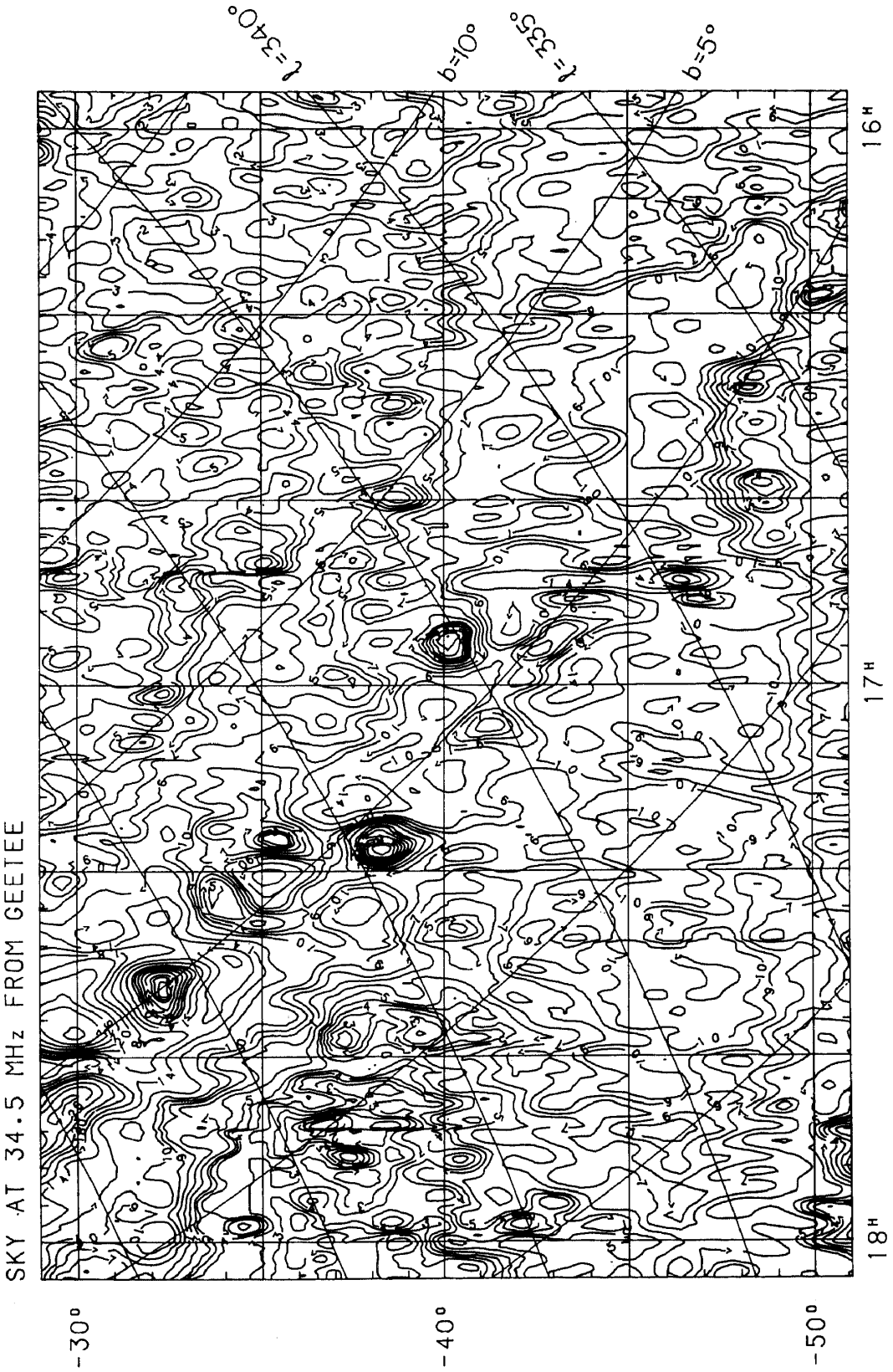
SKY AT 34.5 MHz FROM GEETEE
l=340°
b=10°
l=335°
b=5°
16H
17H
18H
-30°
-40°
-50°

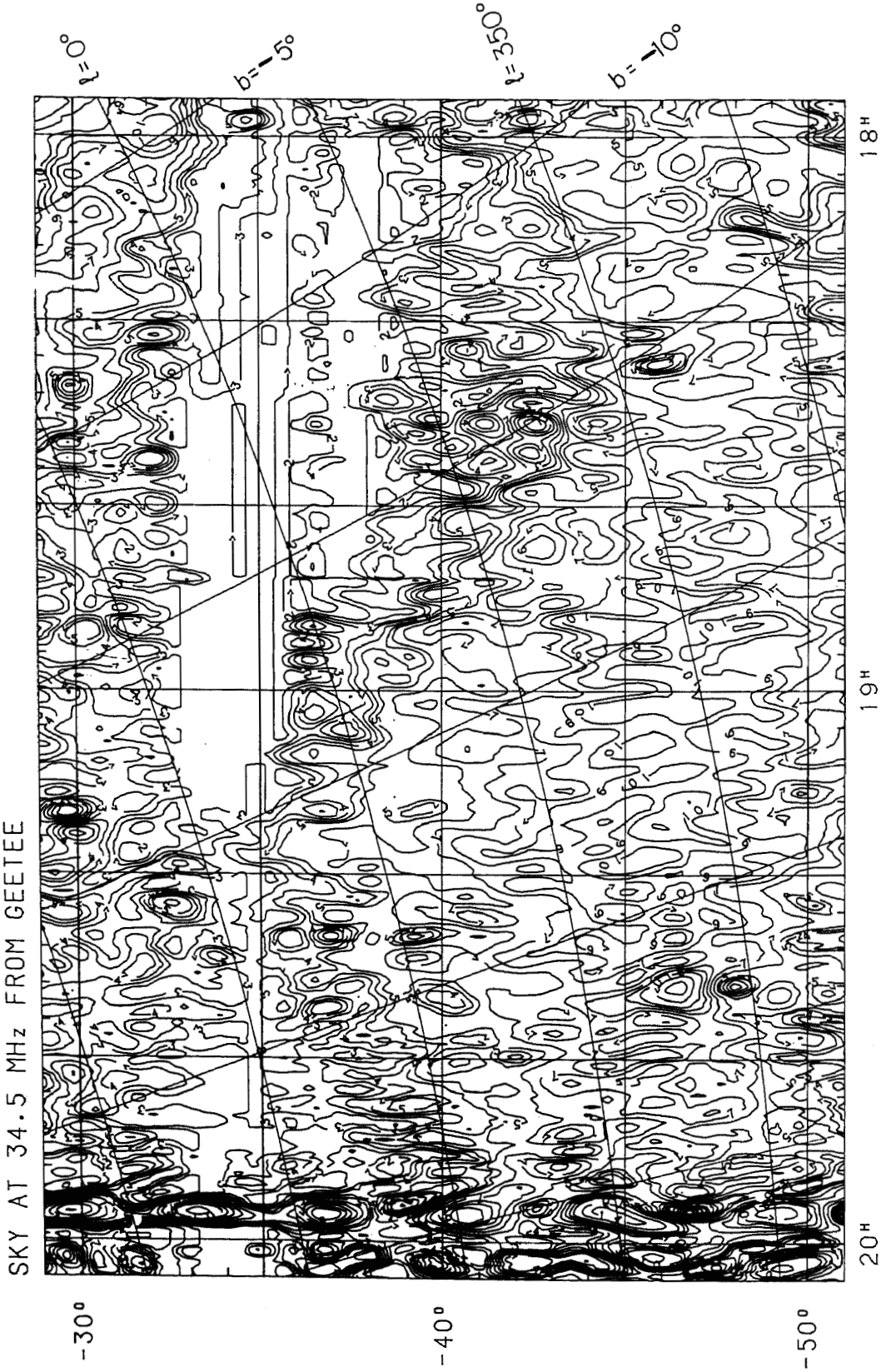
SKY AT 34.5 MHz FROM GEETEE
l=0°
b=-5°
l=350°
b=-10°
18H
19H
20H
-30°
-40°
-50°

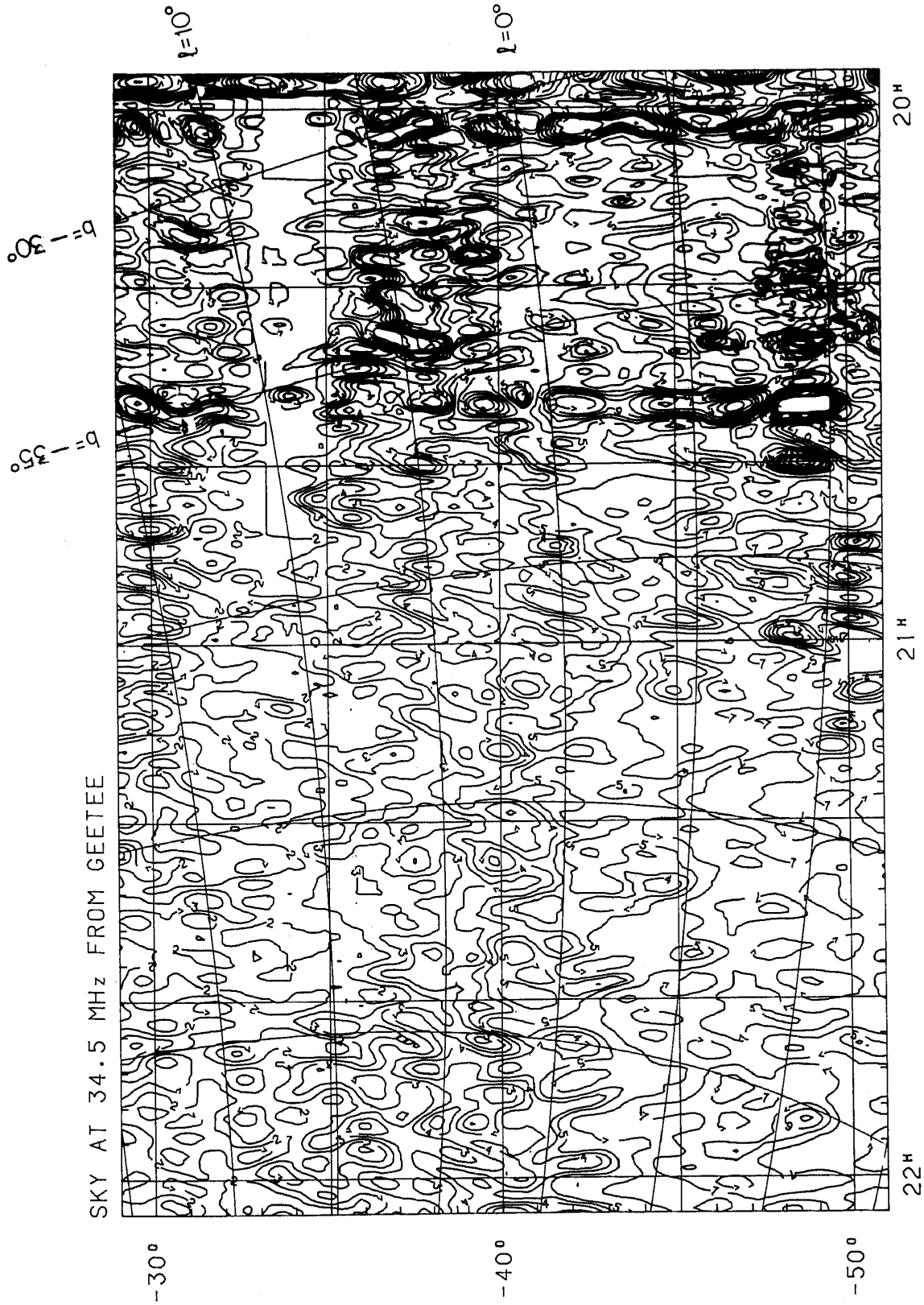
SKY AT 34.5 MHz FROM GEETEE
l=10°
l=0°
b=-30°
b=-35°
20ʰ
21ʰ
22ʰ
-30°
-40°
-50°

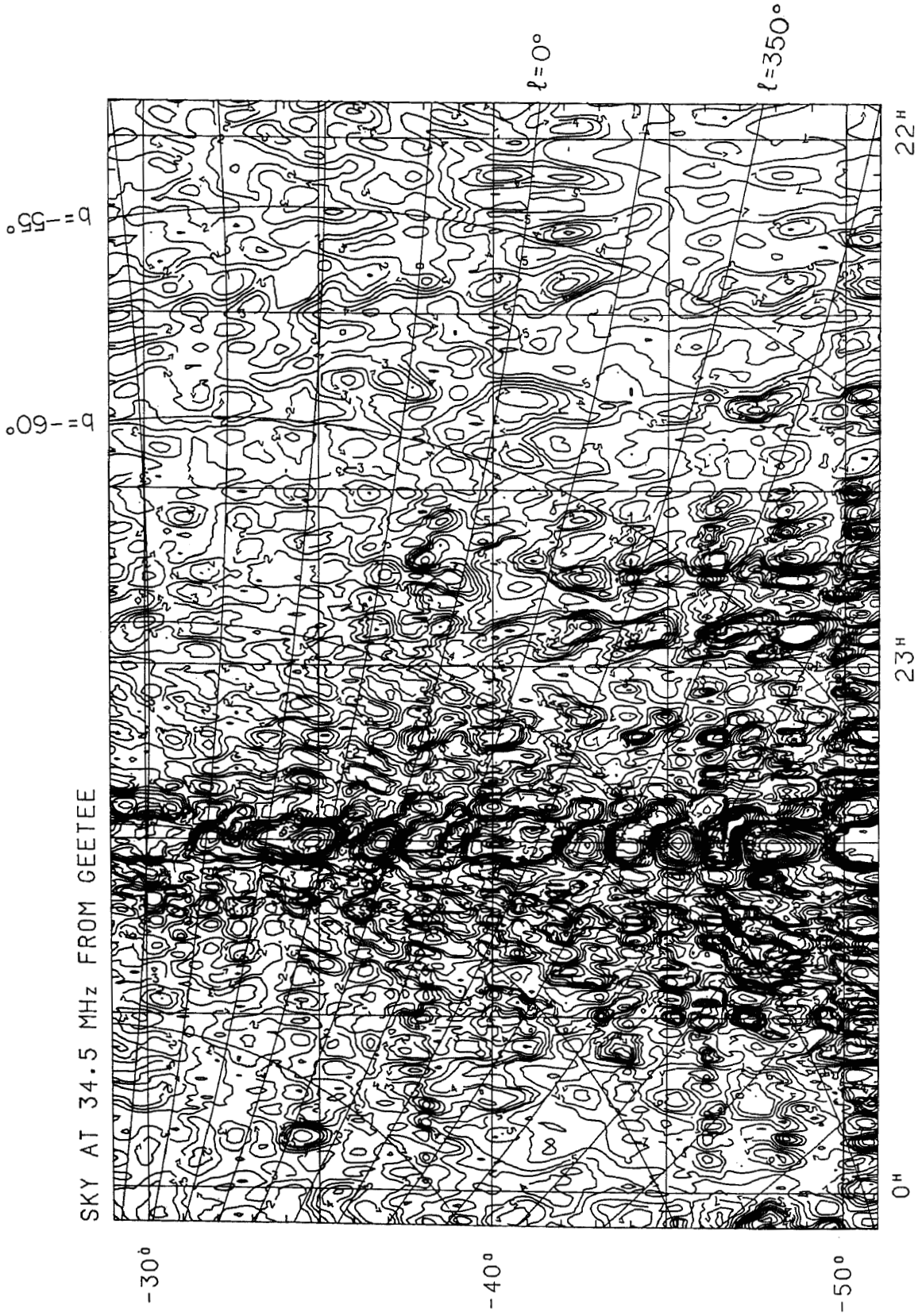
SKY AT 34.5 MHz FROM GEETEE
b = −55°
b = −60°
ℓ = 0°
ℓ = 350°
22H
23H
0H
-30°
-40°
-50°

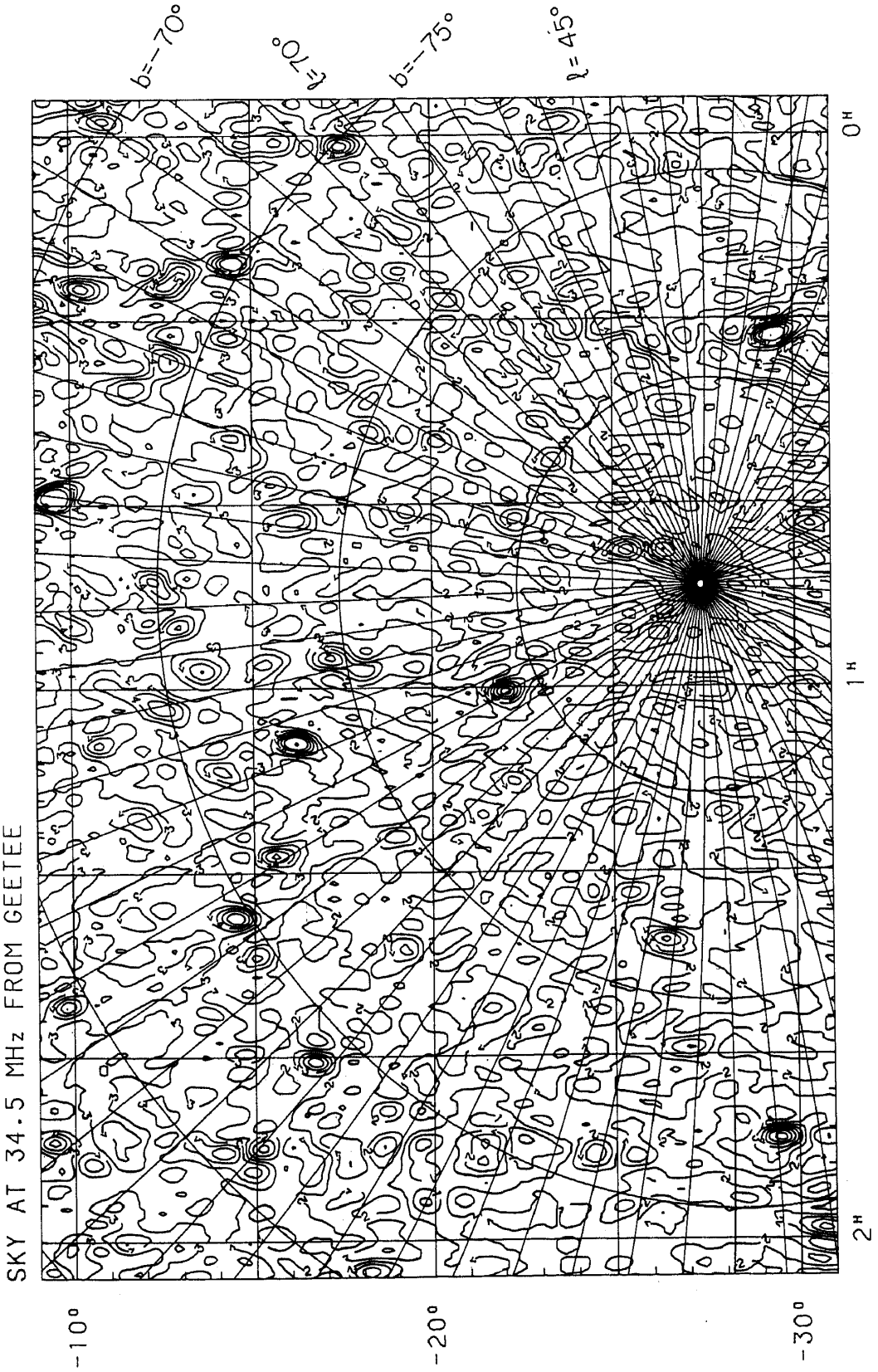
b=−70°
b=−70°
b=−75°
l = 45°
0ʰ
1ʰ
2ʰ
−10°
−20°
−30°
SKY AT 34.5 MHz FROM GEETEE

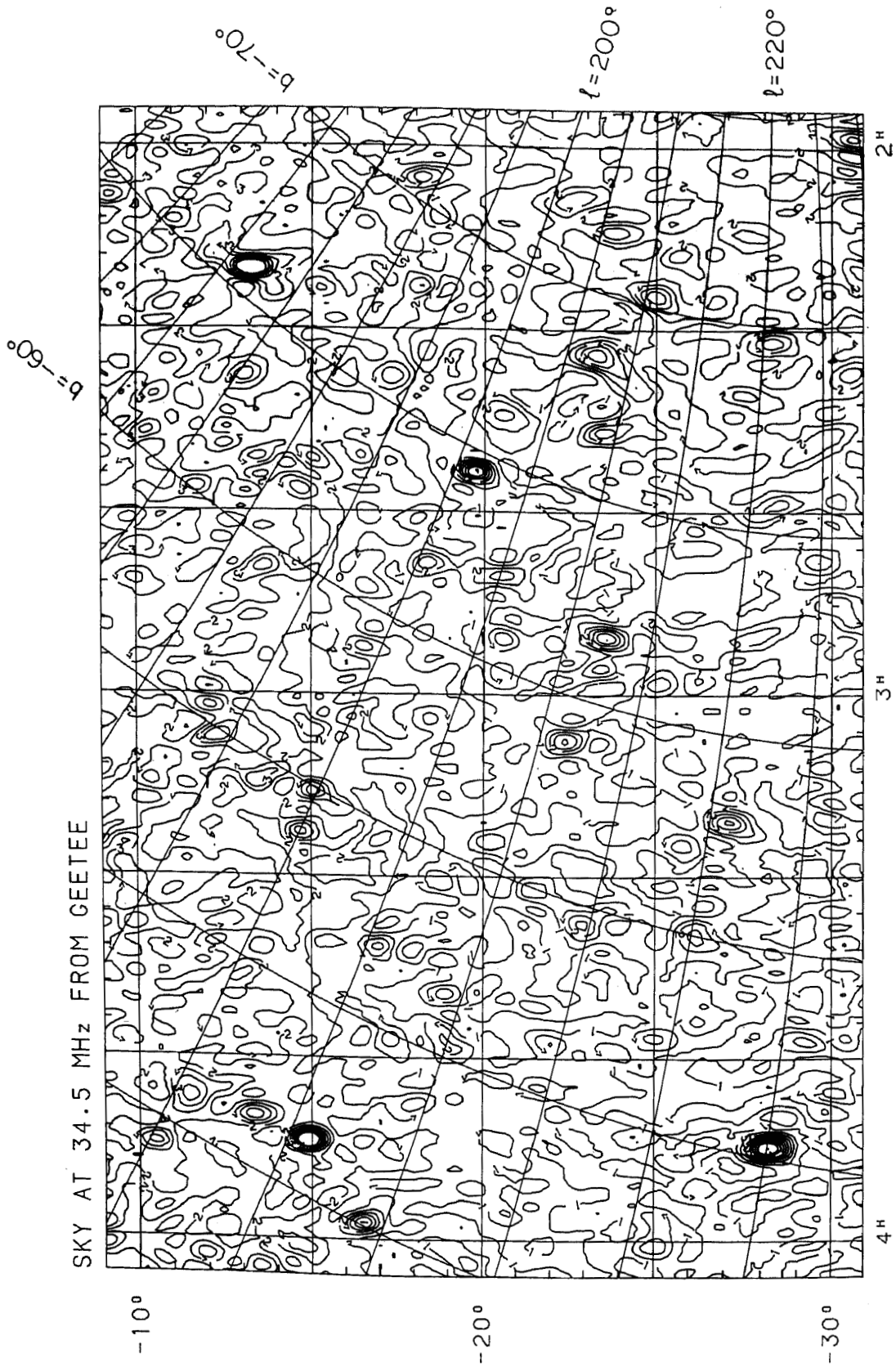
SKY AT 34.5 MHz FROM GEETEE
b=-60°
b=-70°
l=200°
l=220°
2H
3H
4H
-10°
-20°
-30°

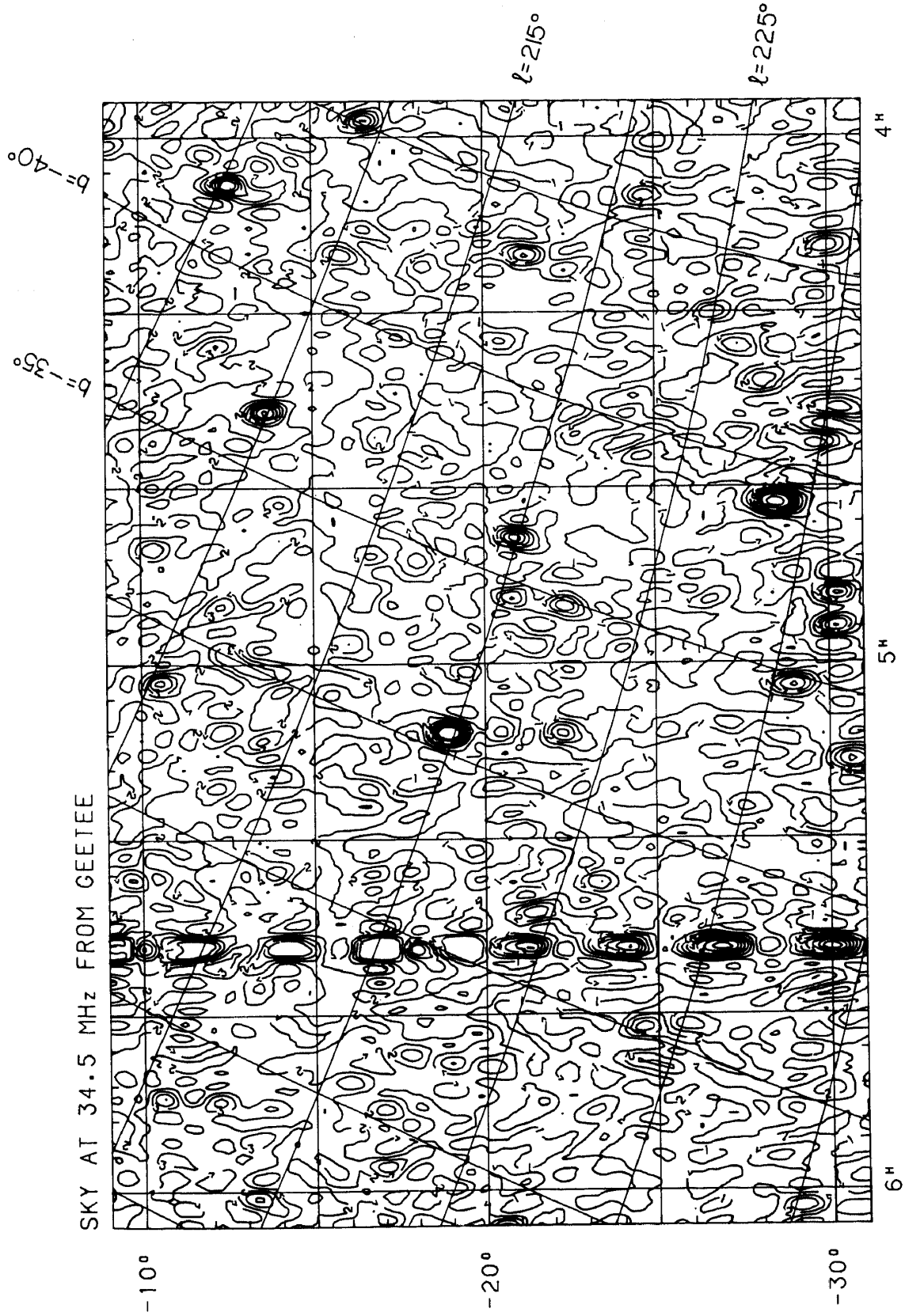
SKY AT 34.5 MHz FROM GEETEE
l=215°
l=225°
b=-40°
b=-35°
4H
5H
6H
-10°
-20°
-30°

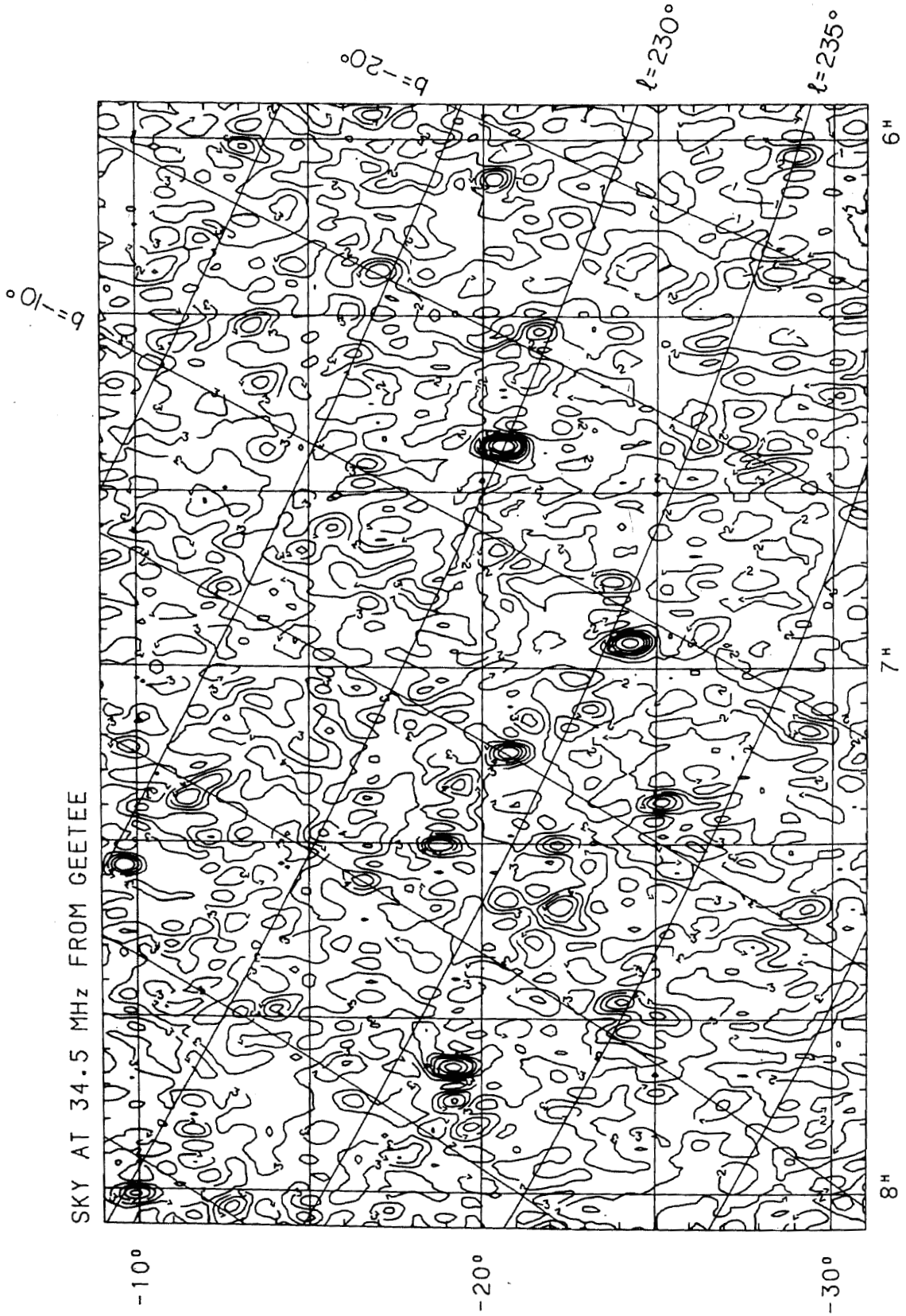
SKY AT 34.5 MHz FROM GEETEE
b=-10°
b=-20°
l=230°
l=235°
6H
7H
8H
-10°
-20°
-30°

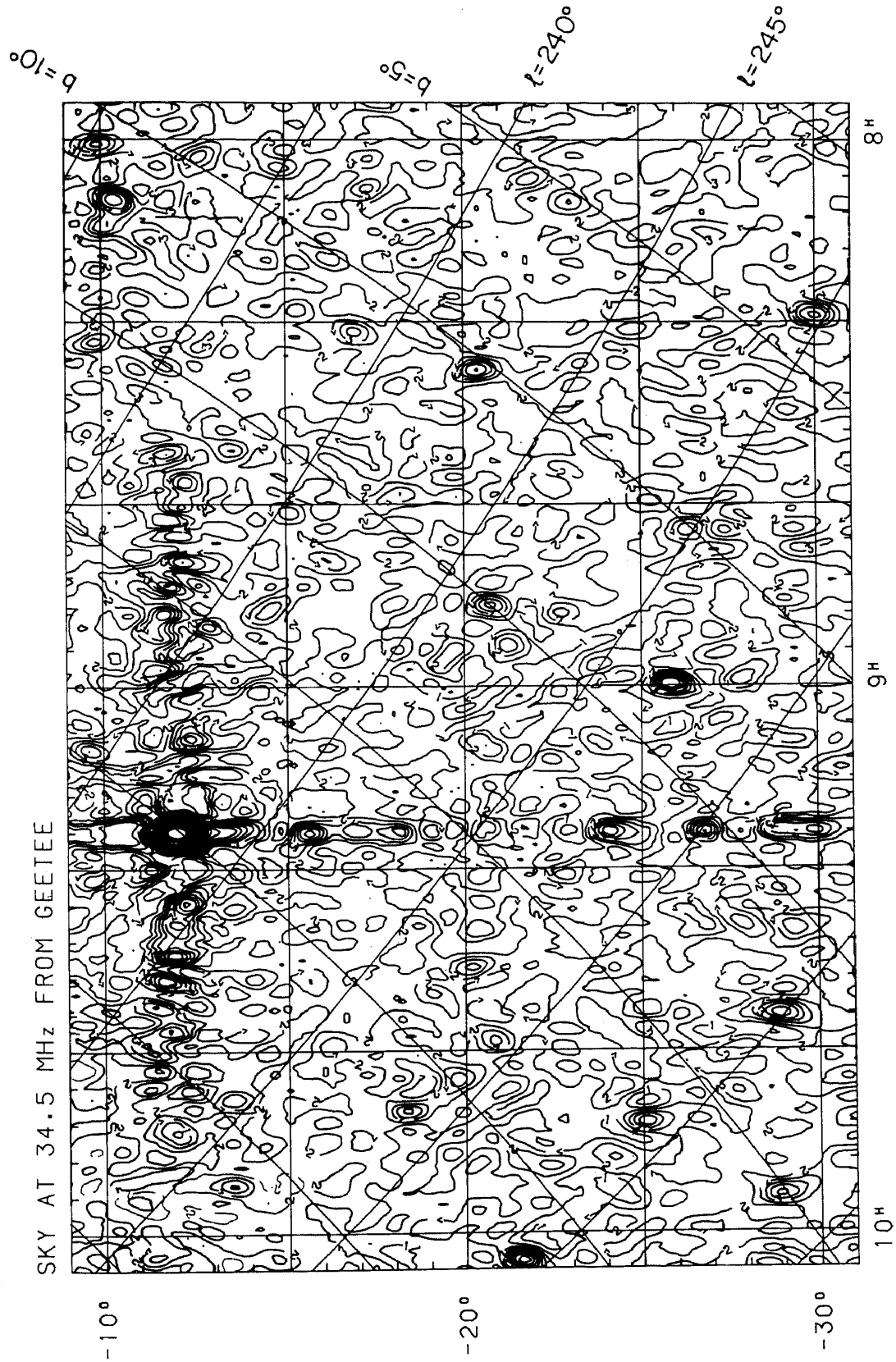
b=10°
b=5°
l=240°
l=245°
8H
9H
10H
-10°
-20°
-30°
SKY AT 34.5 MHz FROM GEETEE

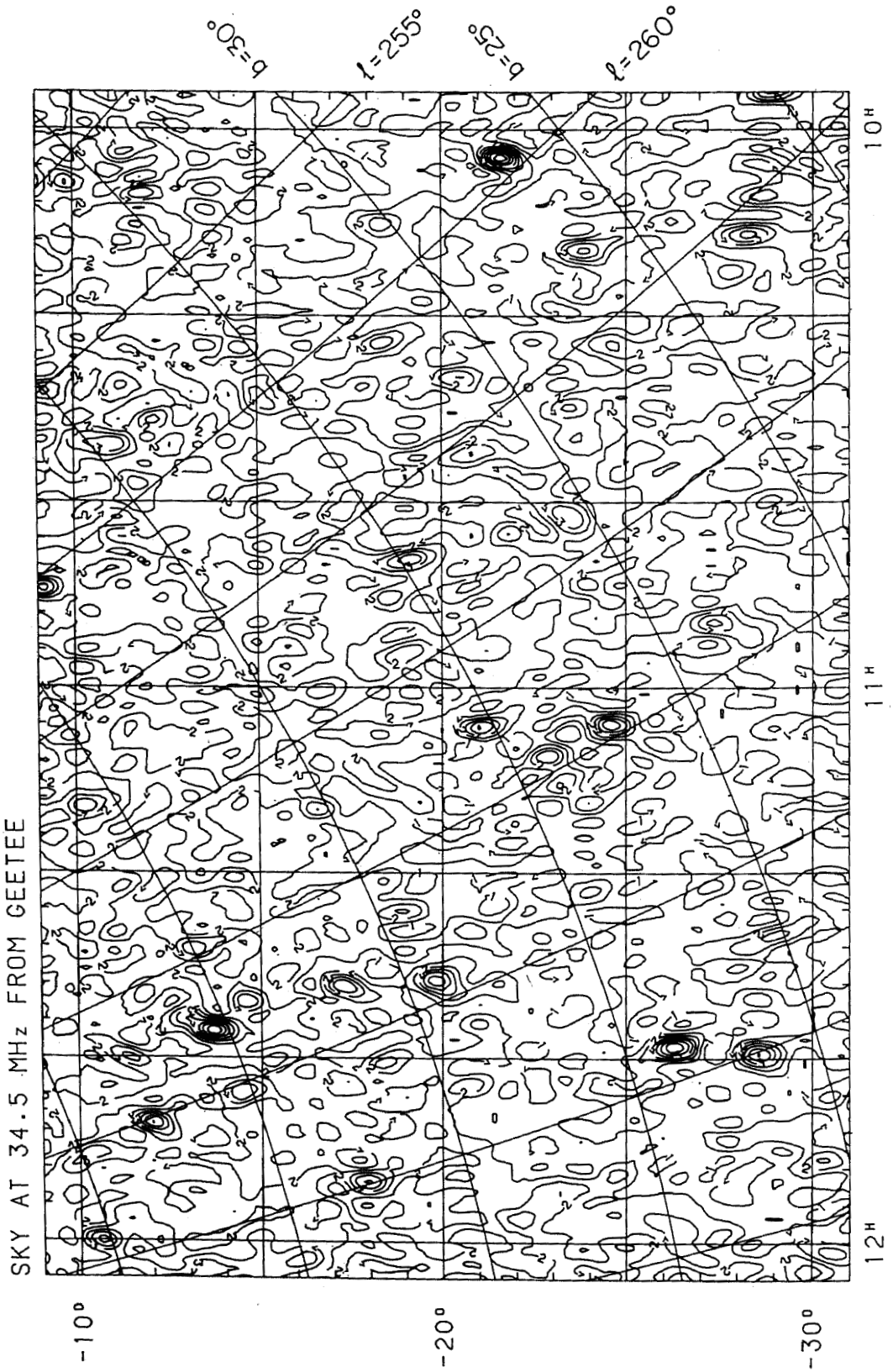
b=30°
l=255°
b=25°
l=260°
10H
11H
12H
-10°
-20°
-30°
SKY AT 34.5 MHz FROM GEETEE

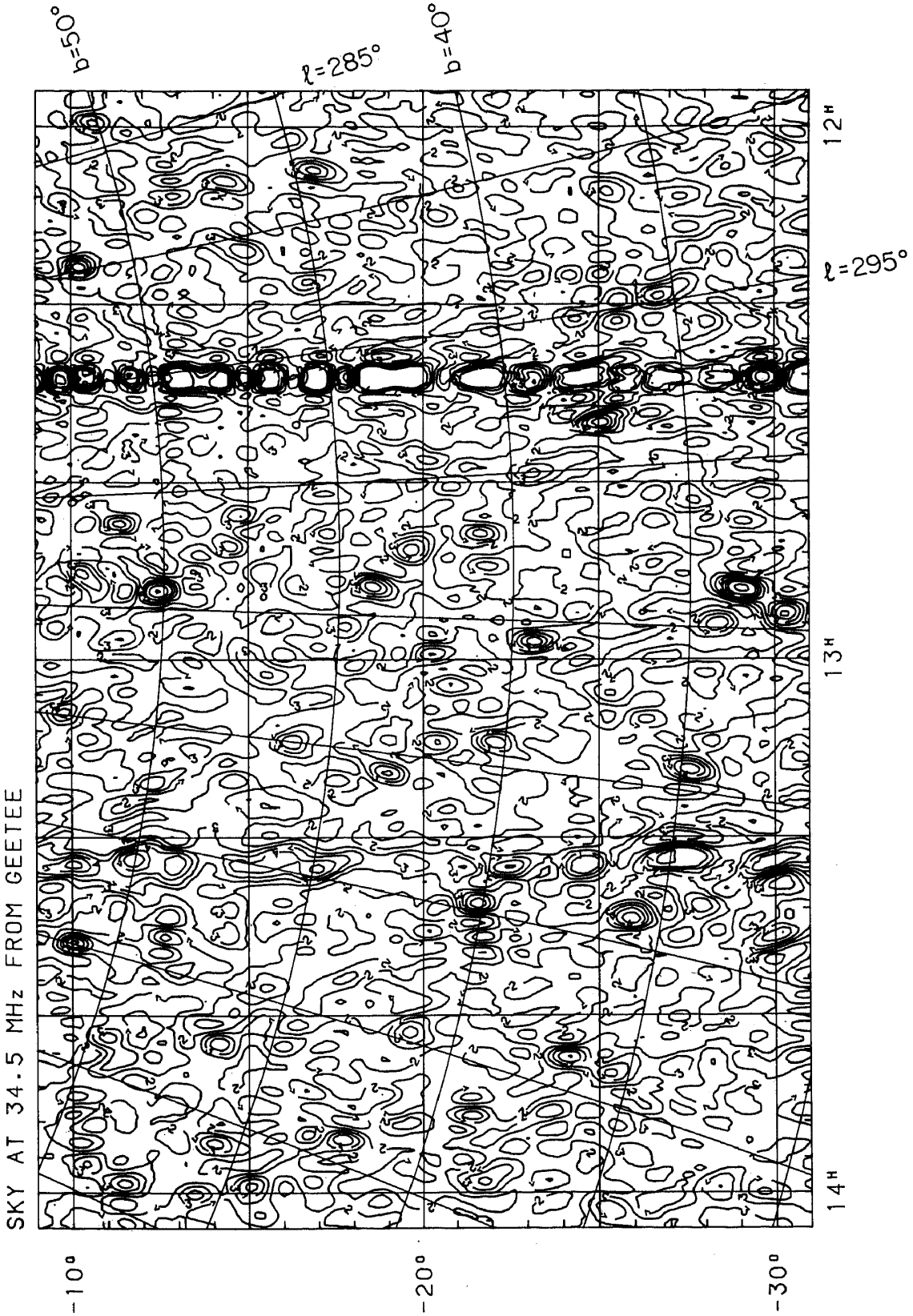
b=50°
ℓ=285°
b=40°
12ᴴ
ℓ=295°
13ᴴ
14ᴴ
-10°
-20°
-30°
SKY AT 34.5 MHz FROM GEETEE

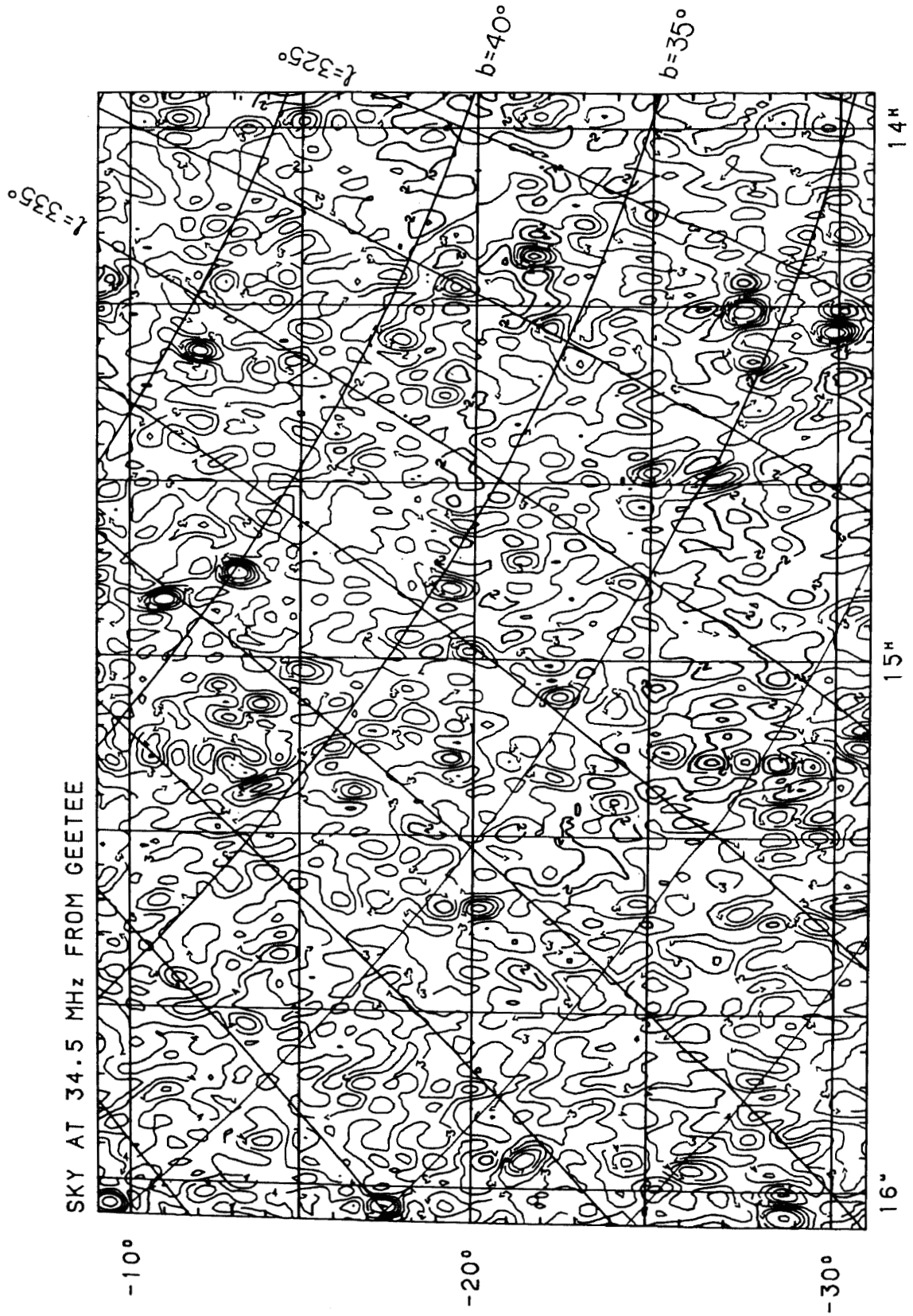
SKY AT 34.5 MHz FROM GEETEE
l=335°
l=325°
b=40°
b=35°
14H
15H
16H
-10°
-20°
-30°

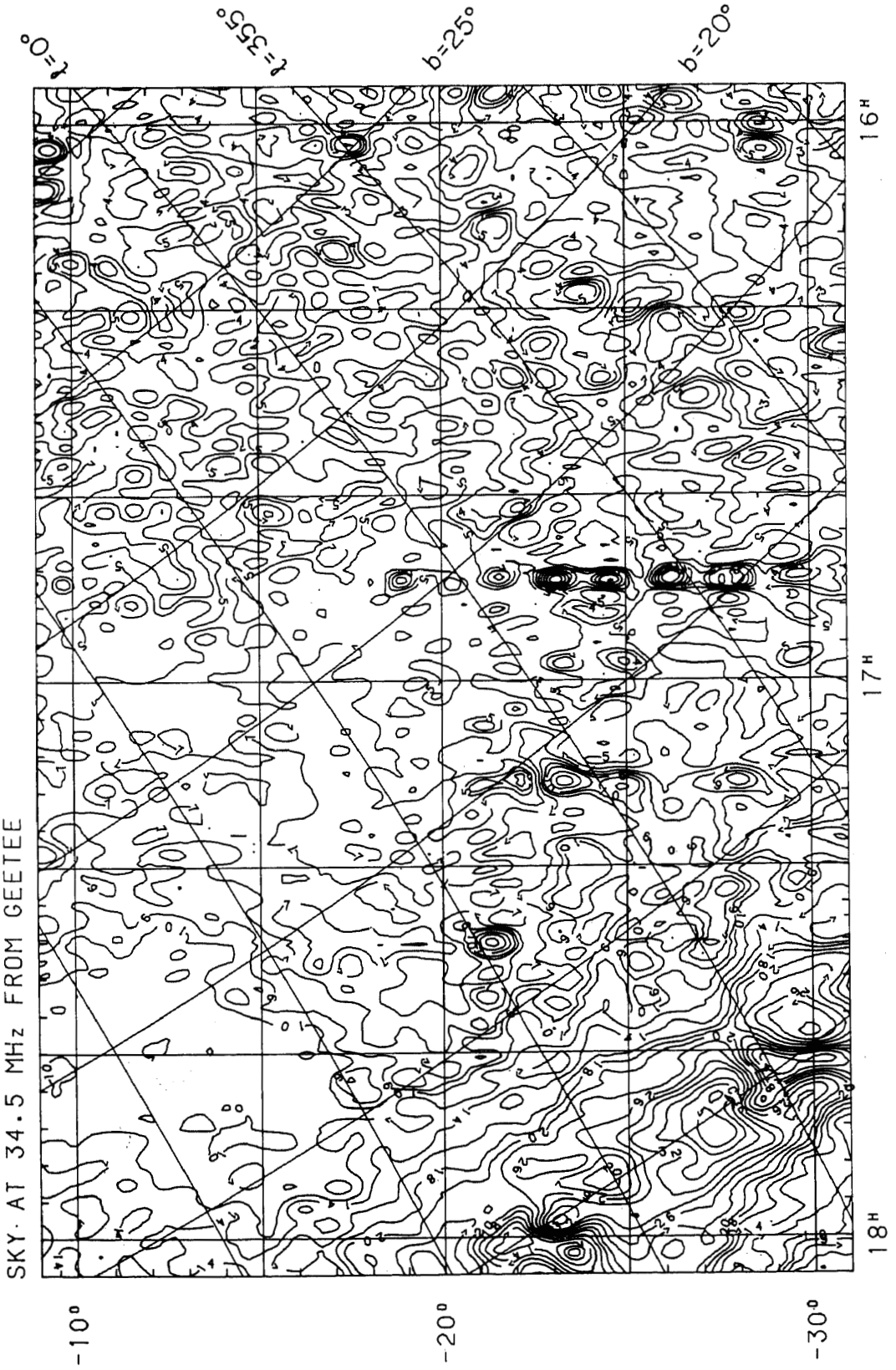
SKY AT 34.5 MHz FROM GEETEE
l=0°
l=355°
b=25°
b=20°
16H
17H
18H
-10°
-20°
-30°

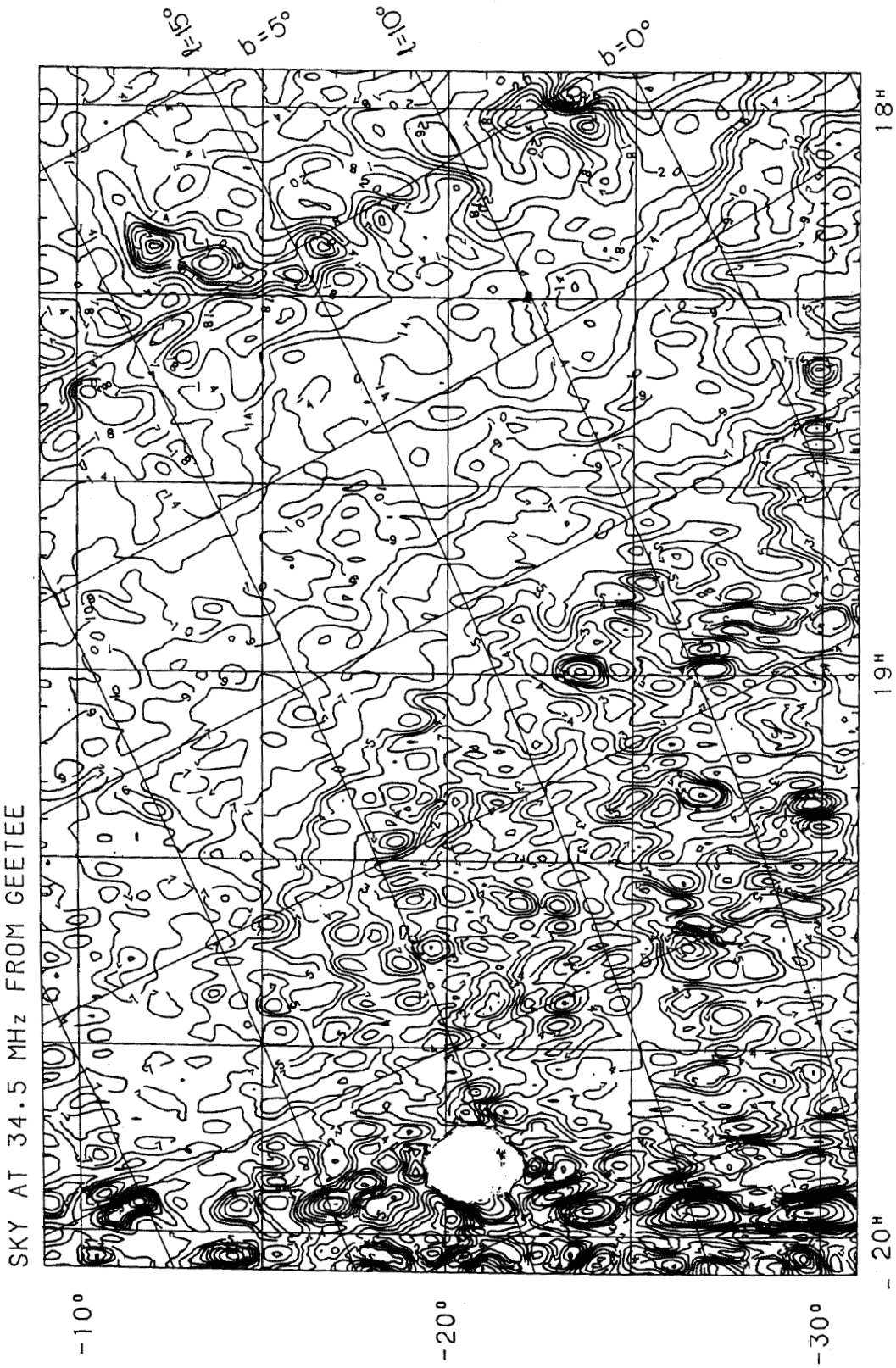
b=15°
b=5°
b=10°
b=0°
18H
19H
20H
-10°
-20°
-30°
SKY AT 34.5 MHz FROM GEETEE

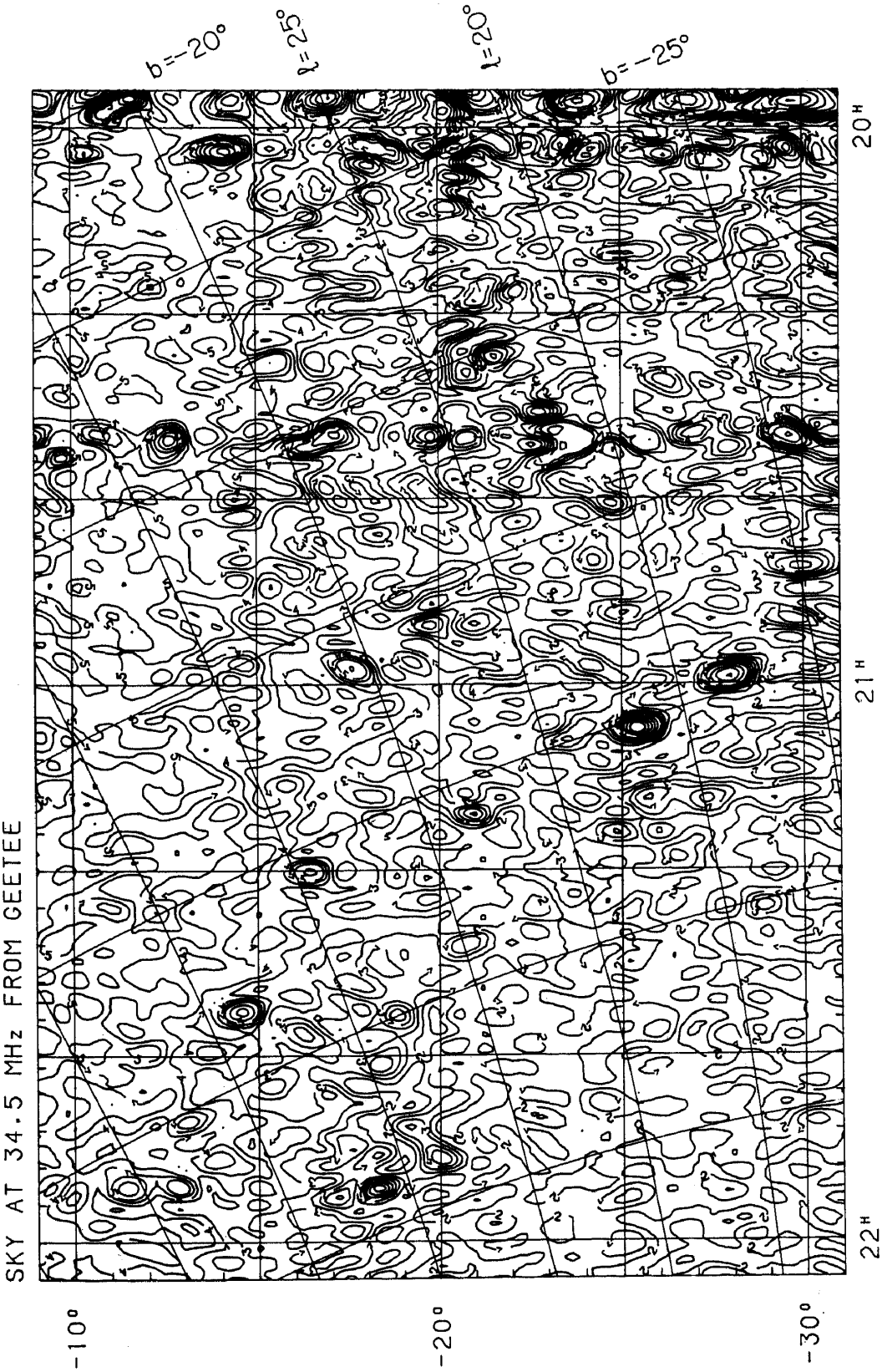
b=-20°
l=25°
l=20°
b=-25°
20H
21H
22H
-10°
-20°
-30°
SKY AT 34.5 MHz FROM GEETEE

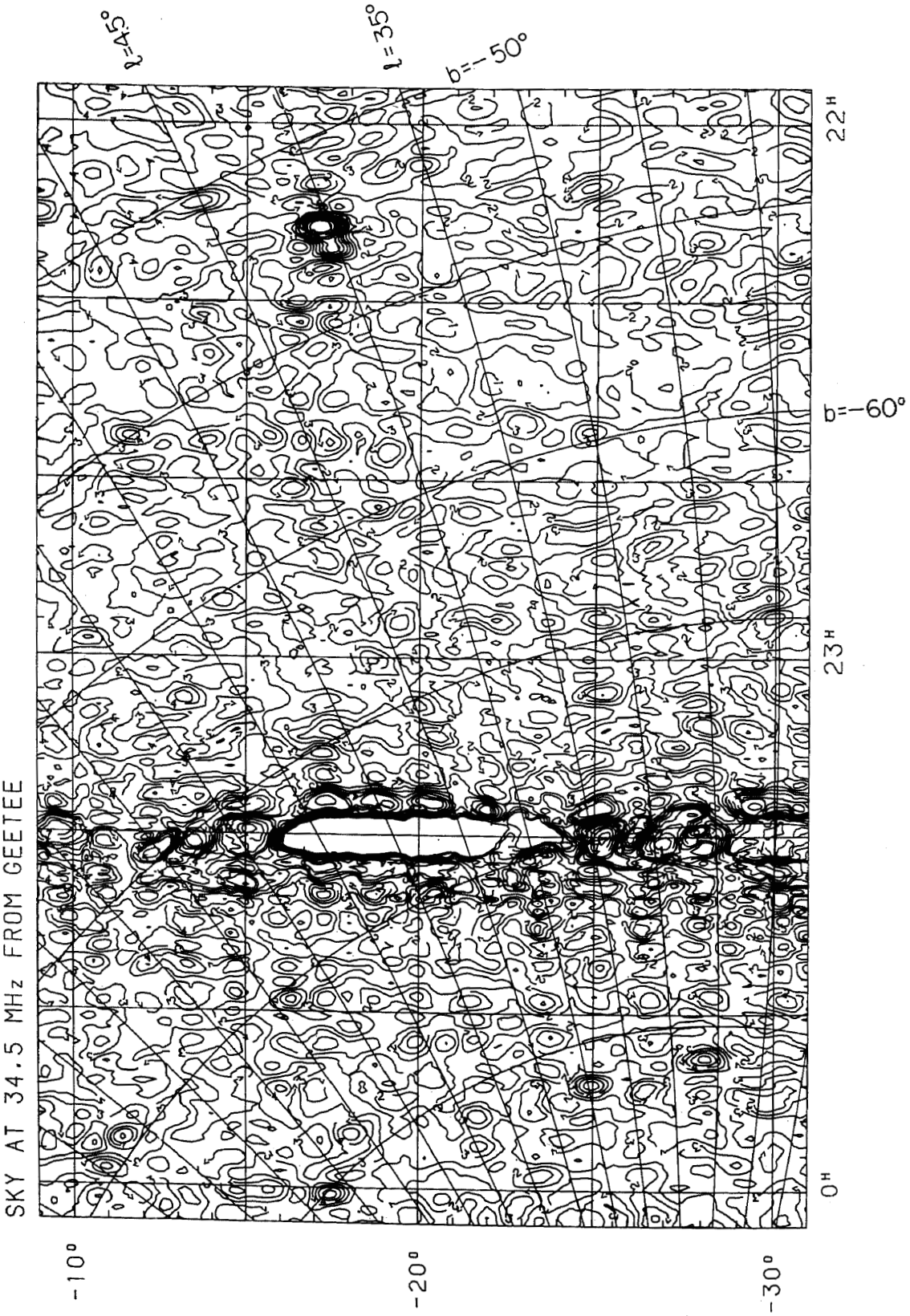
l=45°
l=25°
b=-50°
22H
b=-60°
23H
0H
-10°
-20°
-30°
SKY AT 34.5 MHz FROM GEETEE

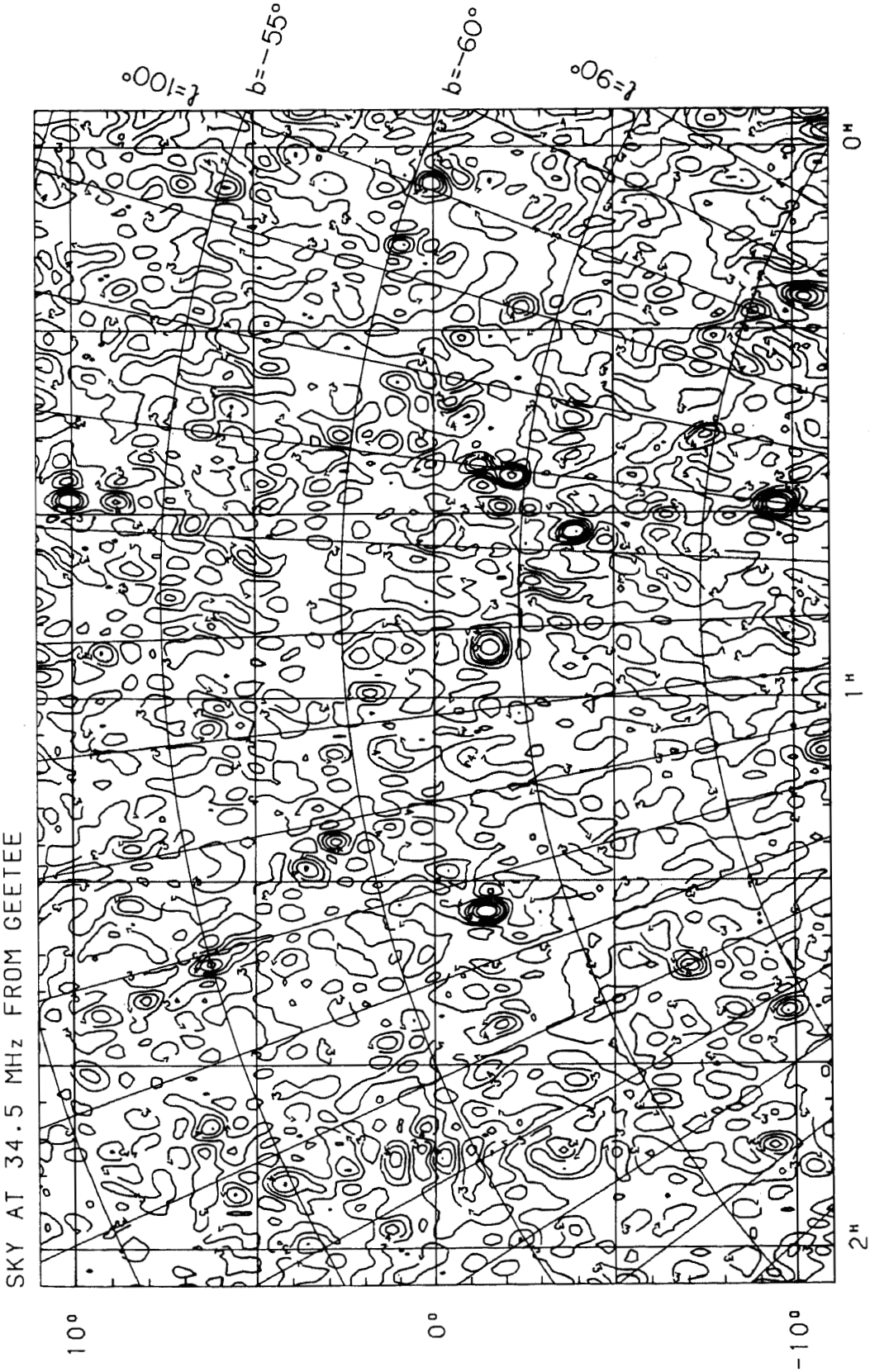
SKY AT 34.5 MHz FROM GEETEE
l=100°
b=−55°
b=−60°
l=90°
0H
1H
2H
10°
0°
−10°

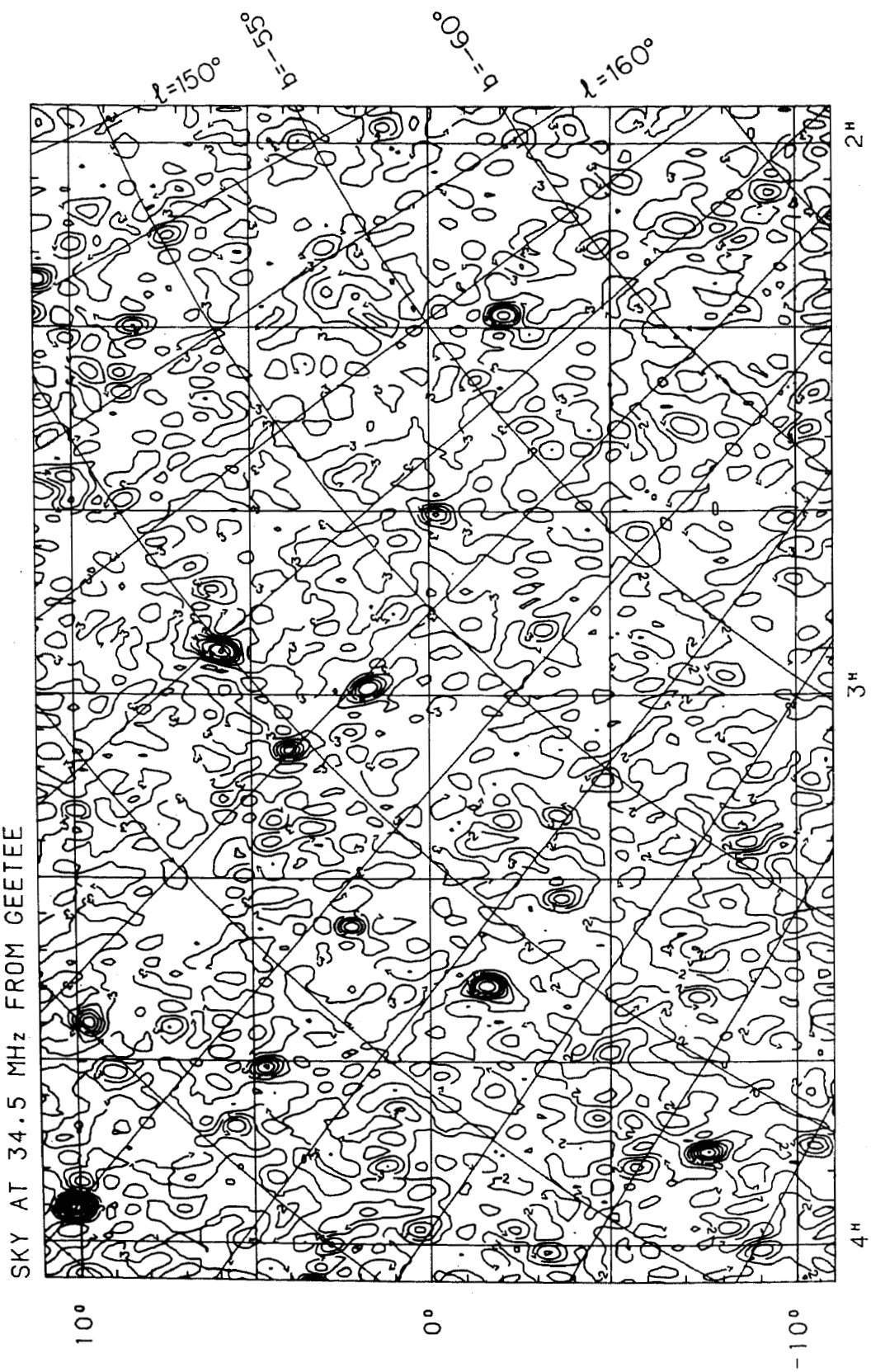
SKY AT 34.5 MHz FROM GEETEE
l=150°
b=-55°
b=-60°
l=160°
2H
3H
4H
10°
0°
-10°

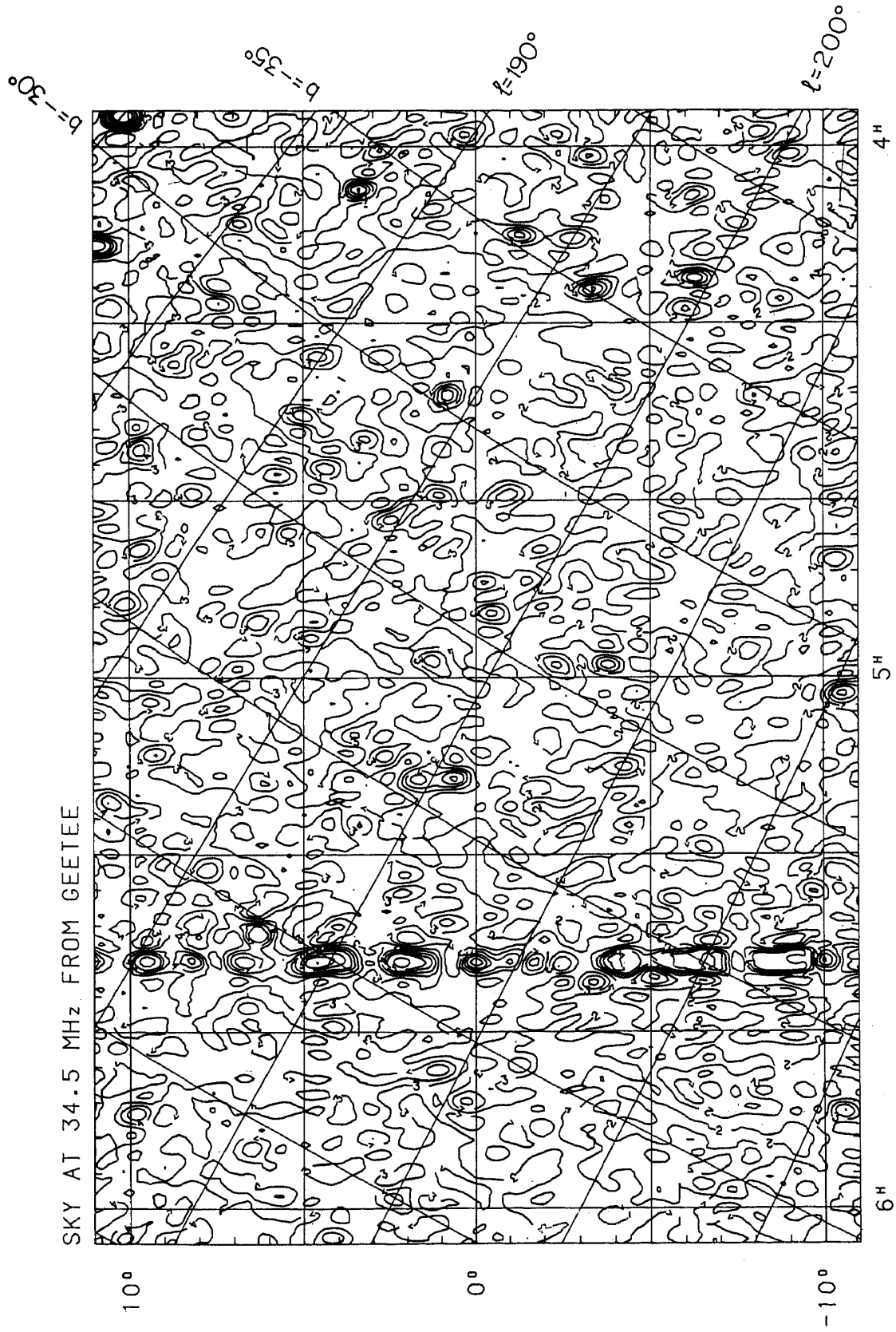
SKY AT 34.5 MHz FROM GEETEE
b=-30°
b=-35°
ℓ=190°
ℓ=200°
4H
5H
6H
10°
0°
-10°

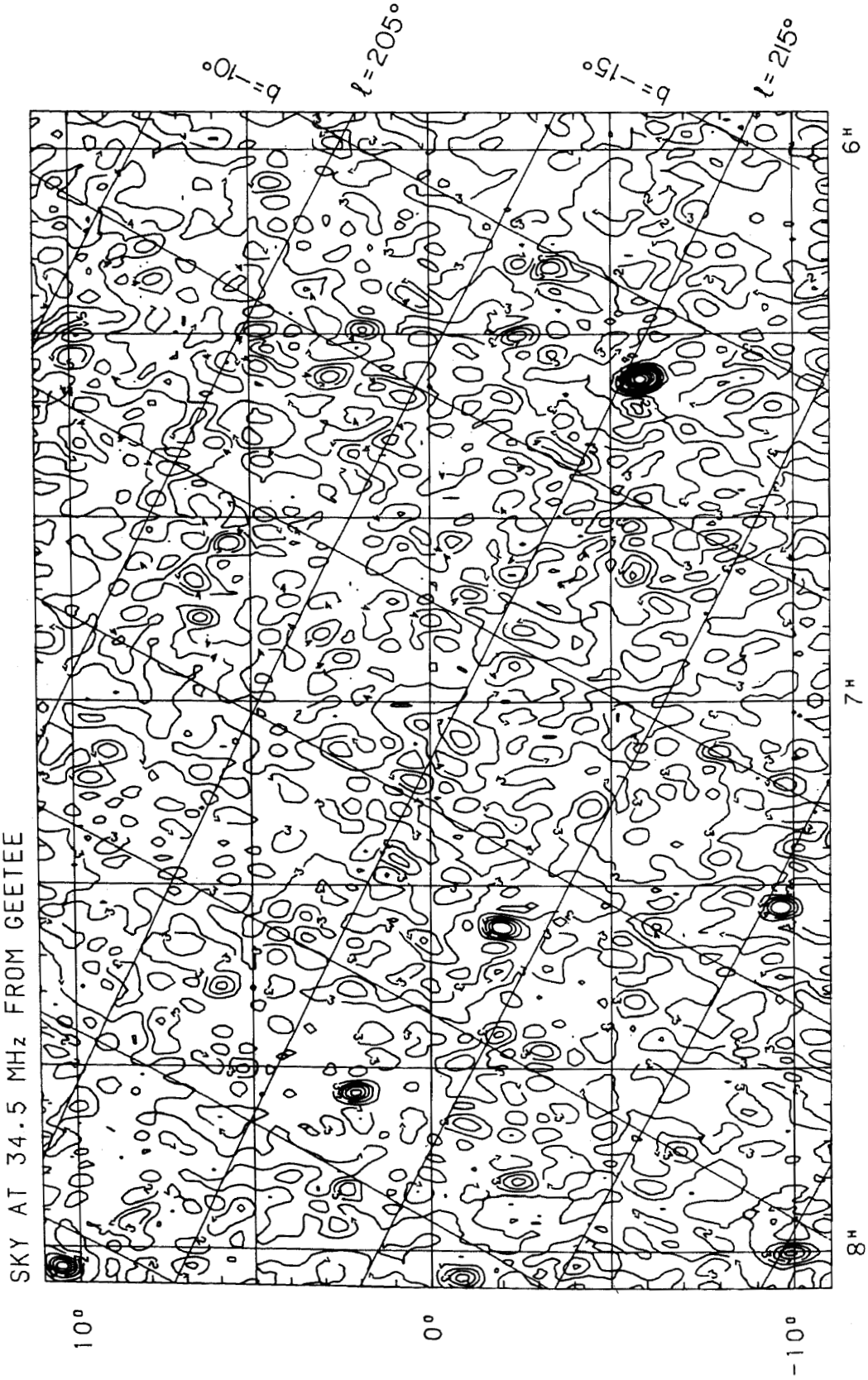
SKY AT 34.5 MHz FROM GEETEE
b=-10°
l=205°
b=-15°
l=215°
6H
7H
8H
10°
0°
-10°

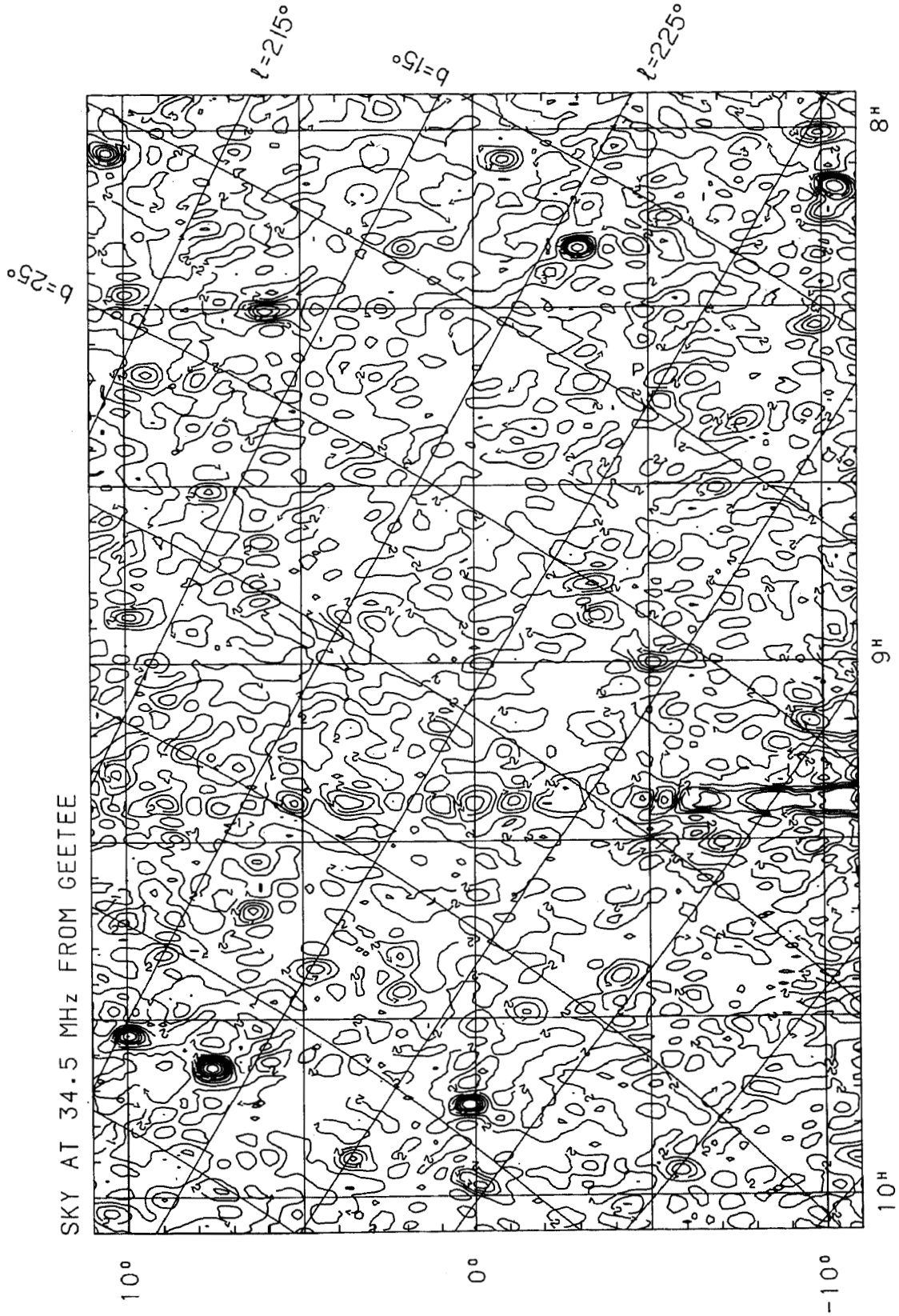
SKY AT 34.5 MHz FROM GEETEE
l=215°
b=15°
l=225°
b=25°
8H
9H
10H
10°
0°
-10°

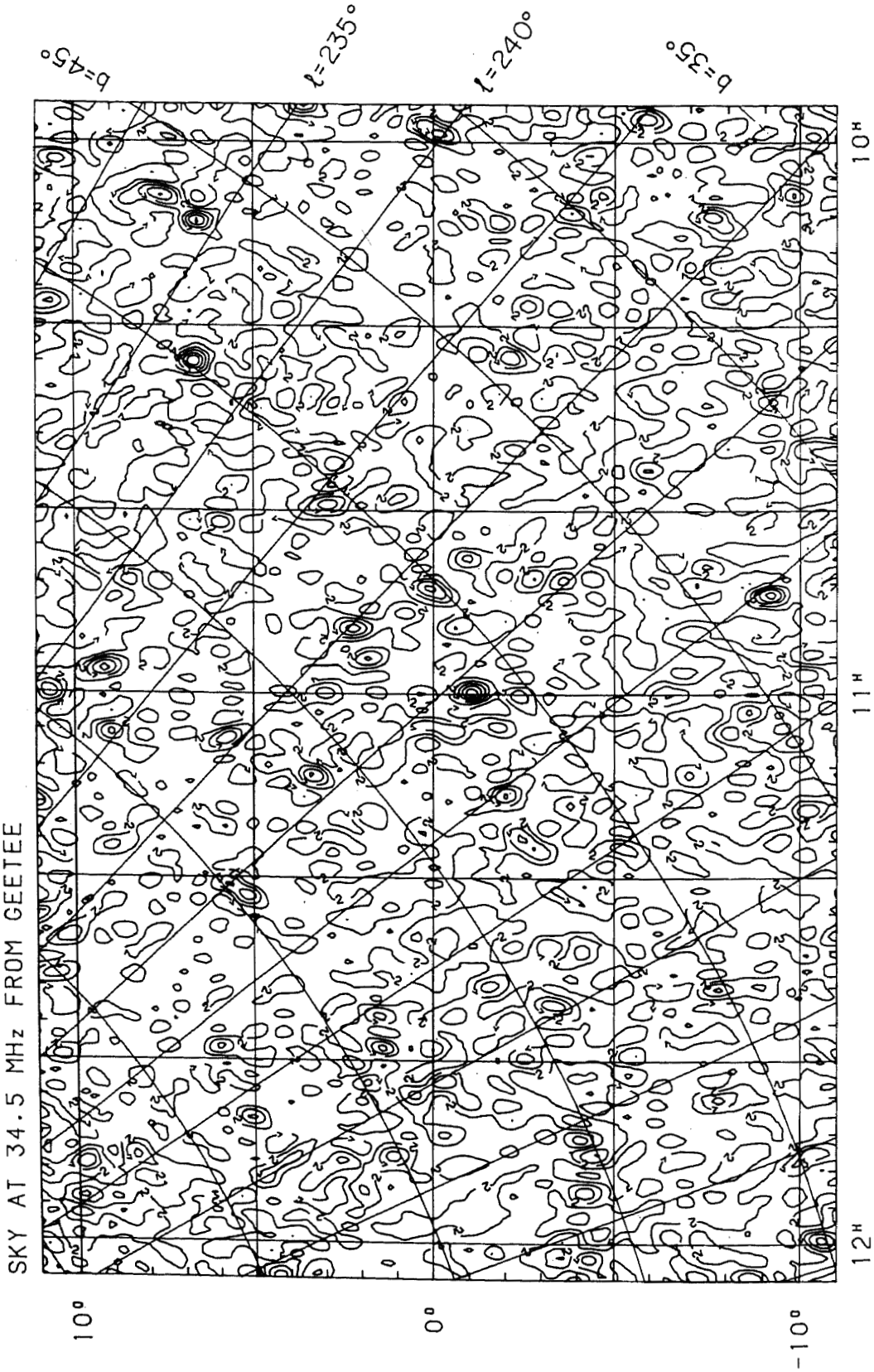
SKY AT 34.5 MHz FROM GEETEE
b=45°
ℓ=235°
ℓ=240°
b=35°
10ʰ
11ʰ
12ʰ
10°
0°
-10°

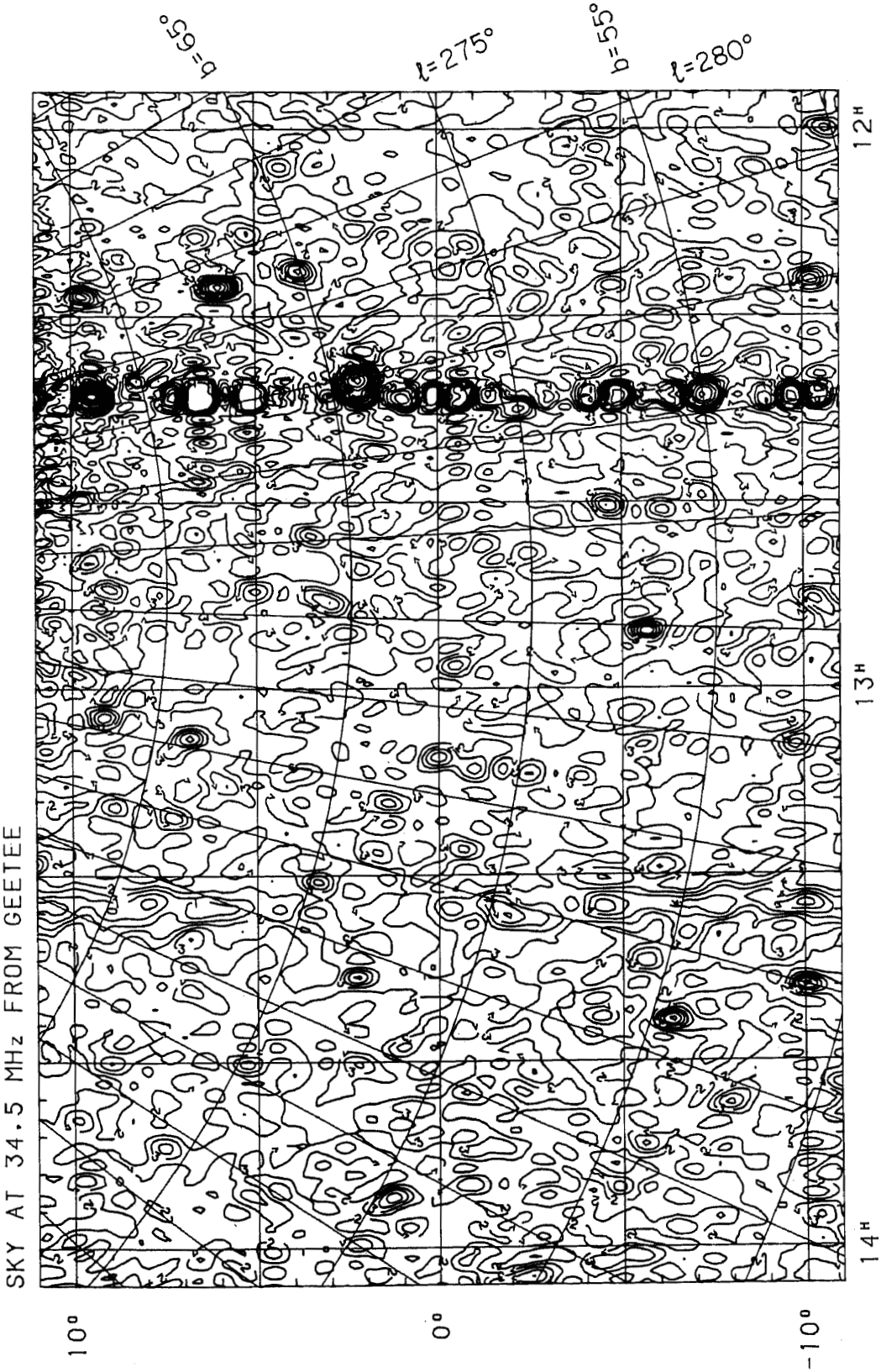
b=65°
l=275°
b=55°
l=280°
12H
13H
14H
10°
0°
-10°
SKY AT 34.5 MHz FROM GEETEE

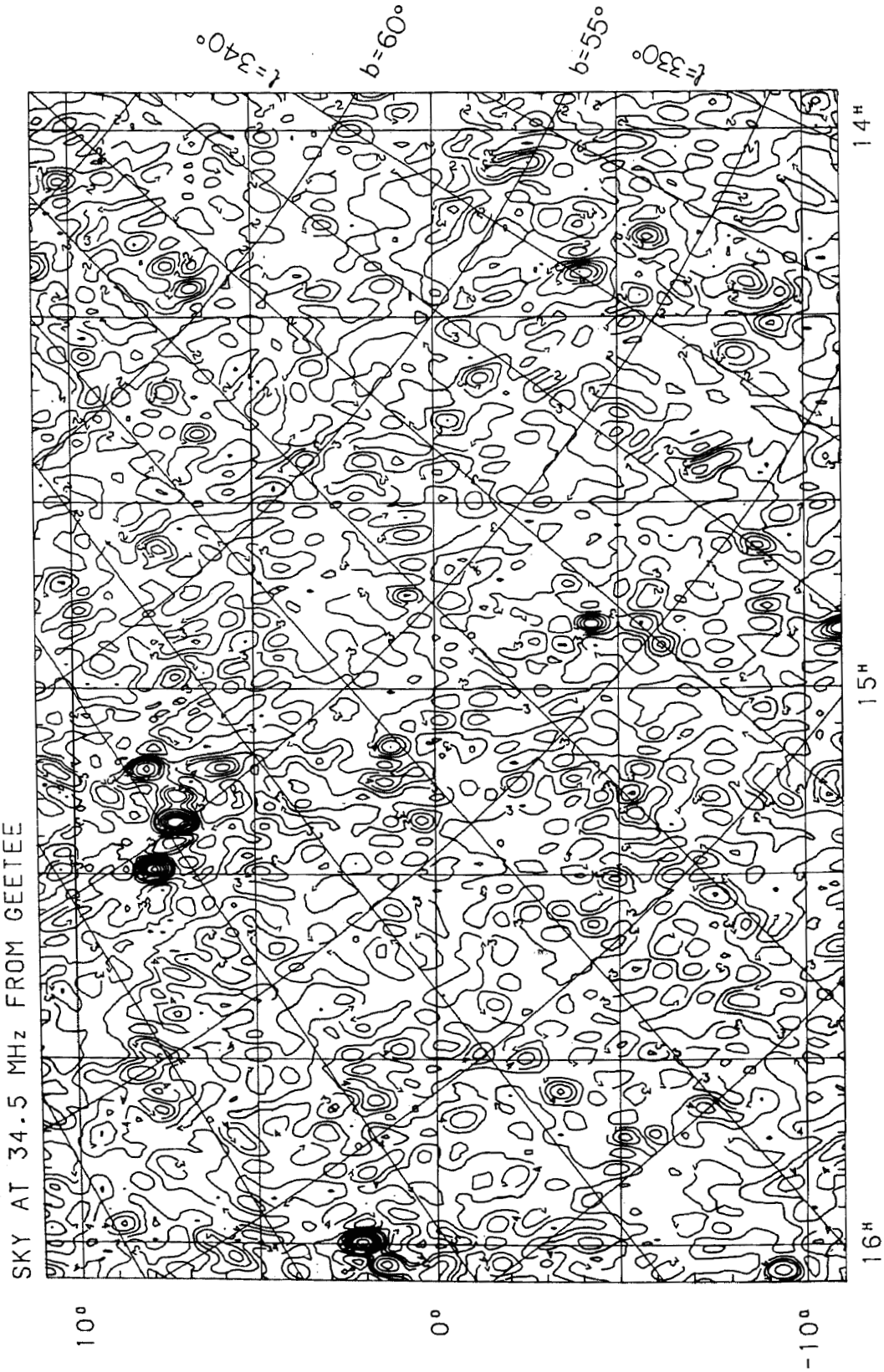
SKY AT 34.5 MHz FROM GEETEE
l=340°
b=60°
b=55°
l=330°
14H
15H
16H
10°
0°
-10°

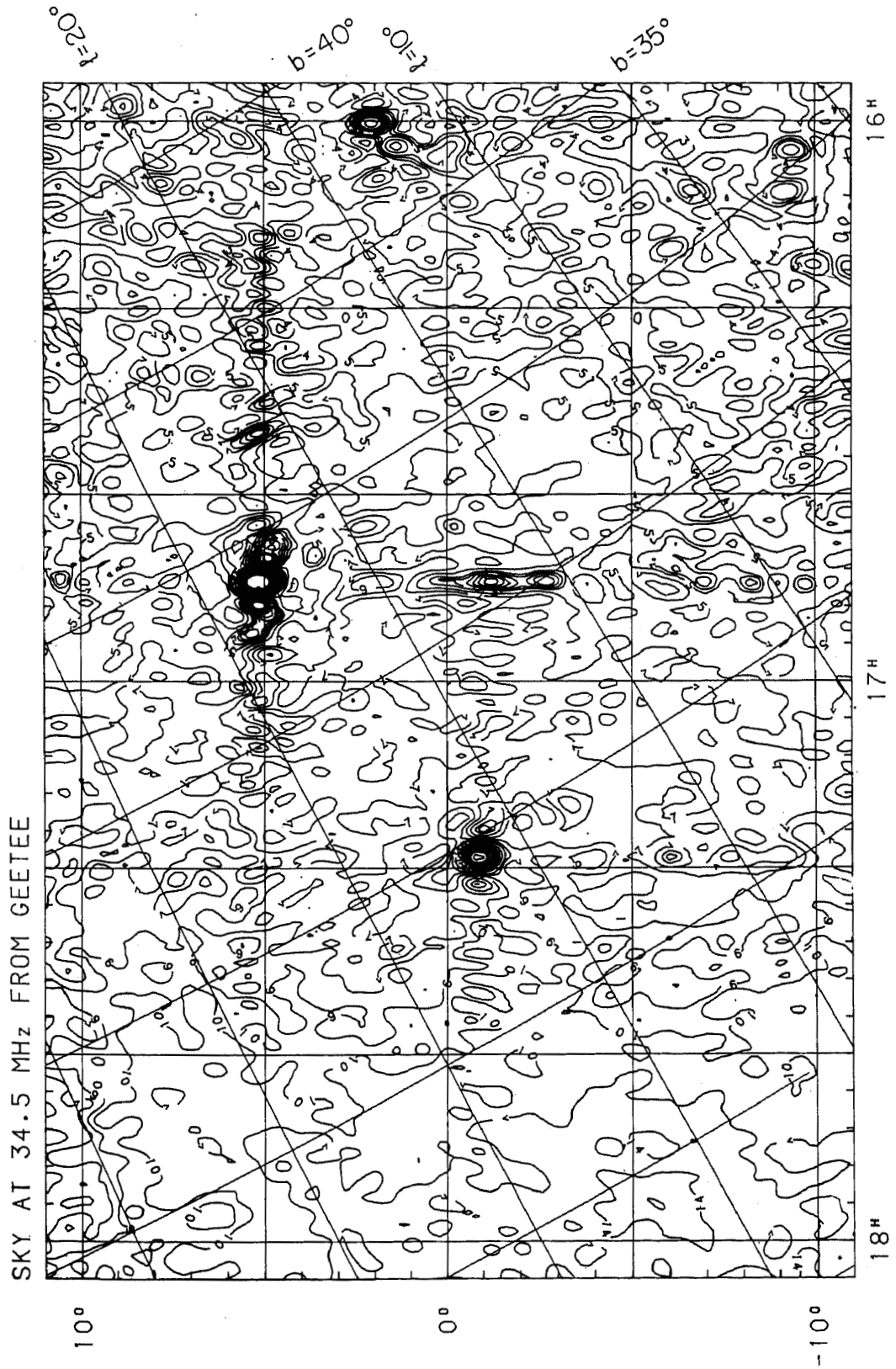
SKY AT 34.5 MHz FROM GEETEE
l=20°
b=40°
l=10°
b=35°
16H
17H
18H
10°
0°
-10°

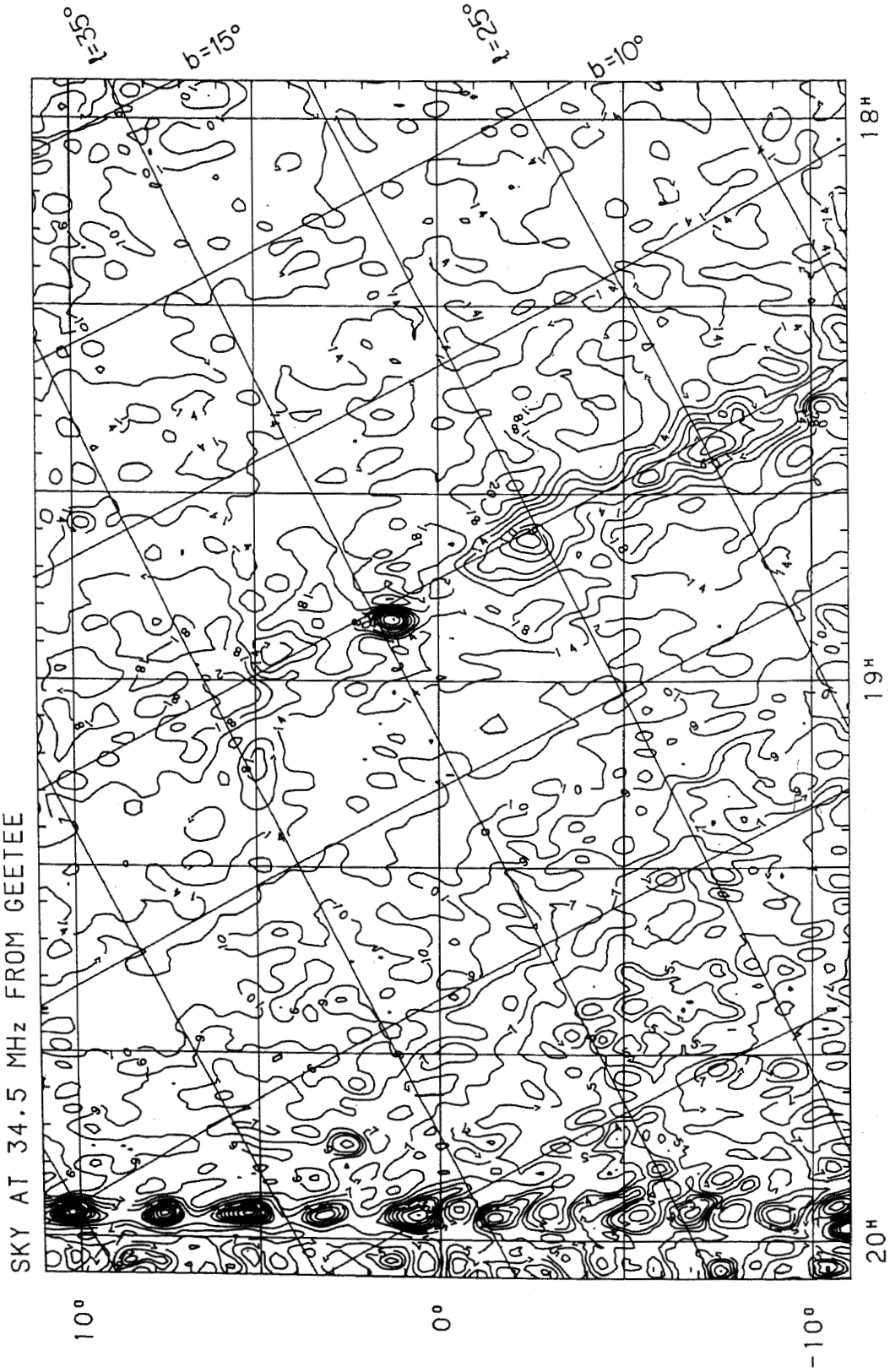
SKY AT 34.5 MHz FROM GEETEE
l=35°
b=15°
l=25°
b=10°
18H
19H
20H
10°
0°
-10°

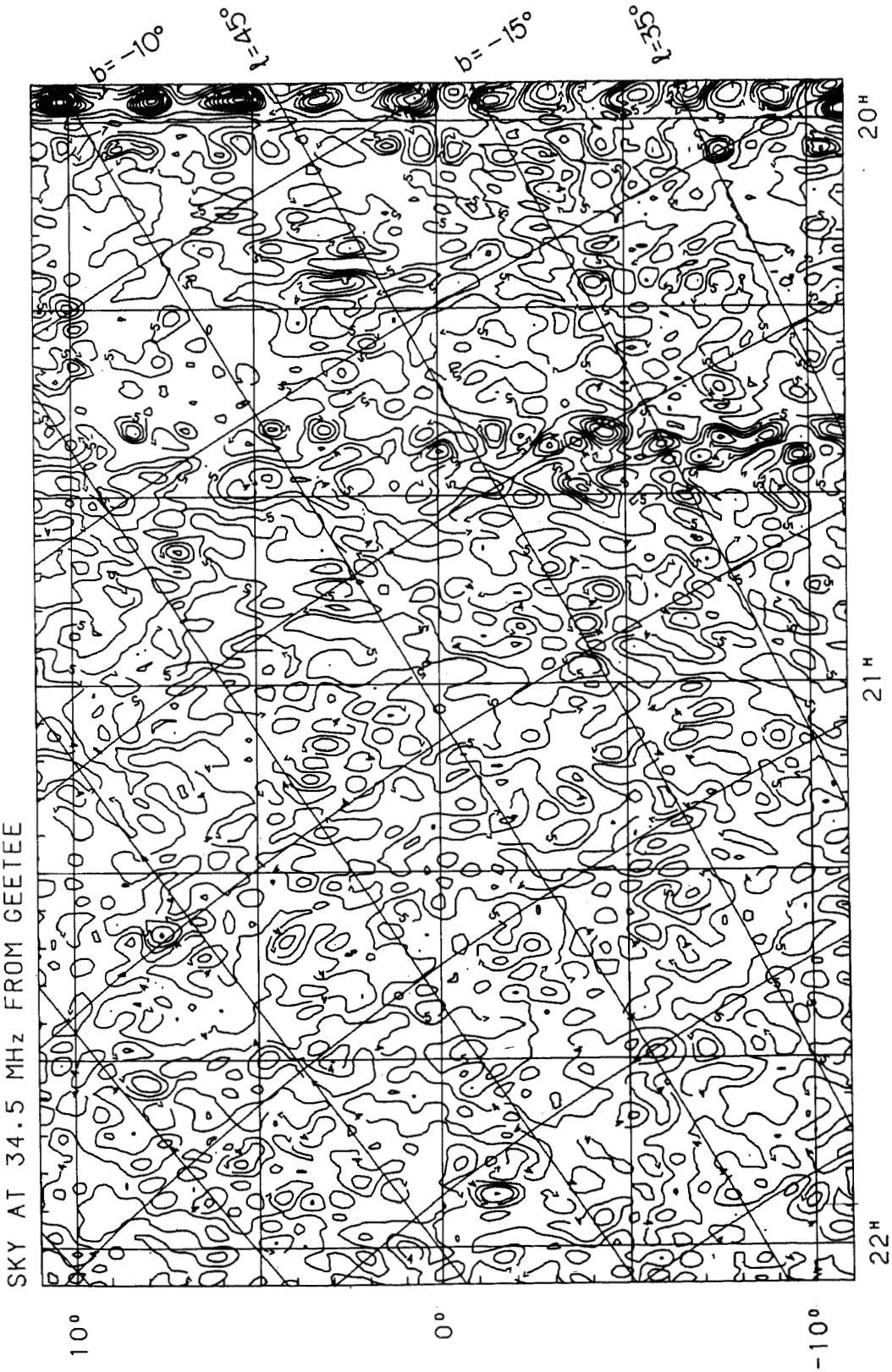
SKY AT 34.5 MHz FROM GEETEE
b=-10°
l=45°
b=-15°
l=35°
20H
21H
22H
10°
0°
-10°

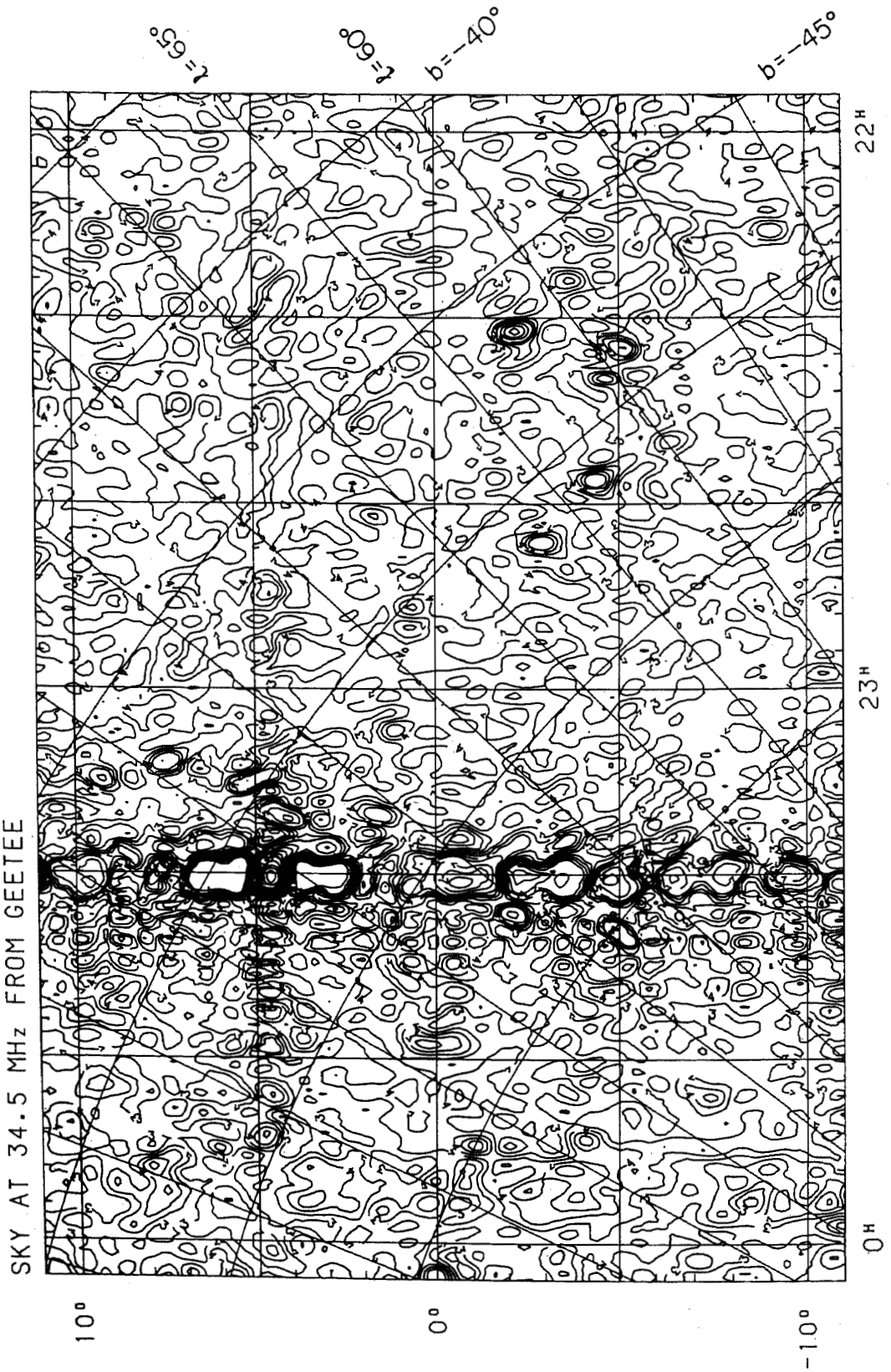
SKY AT 34.5 MHz FROM GEETEE
l=65°
l=60°
b=-40°
b=-45°
22H
23H
0H
10°
0°
-10°

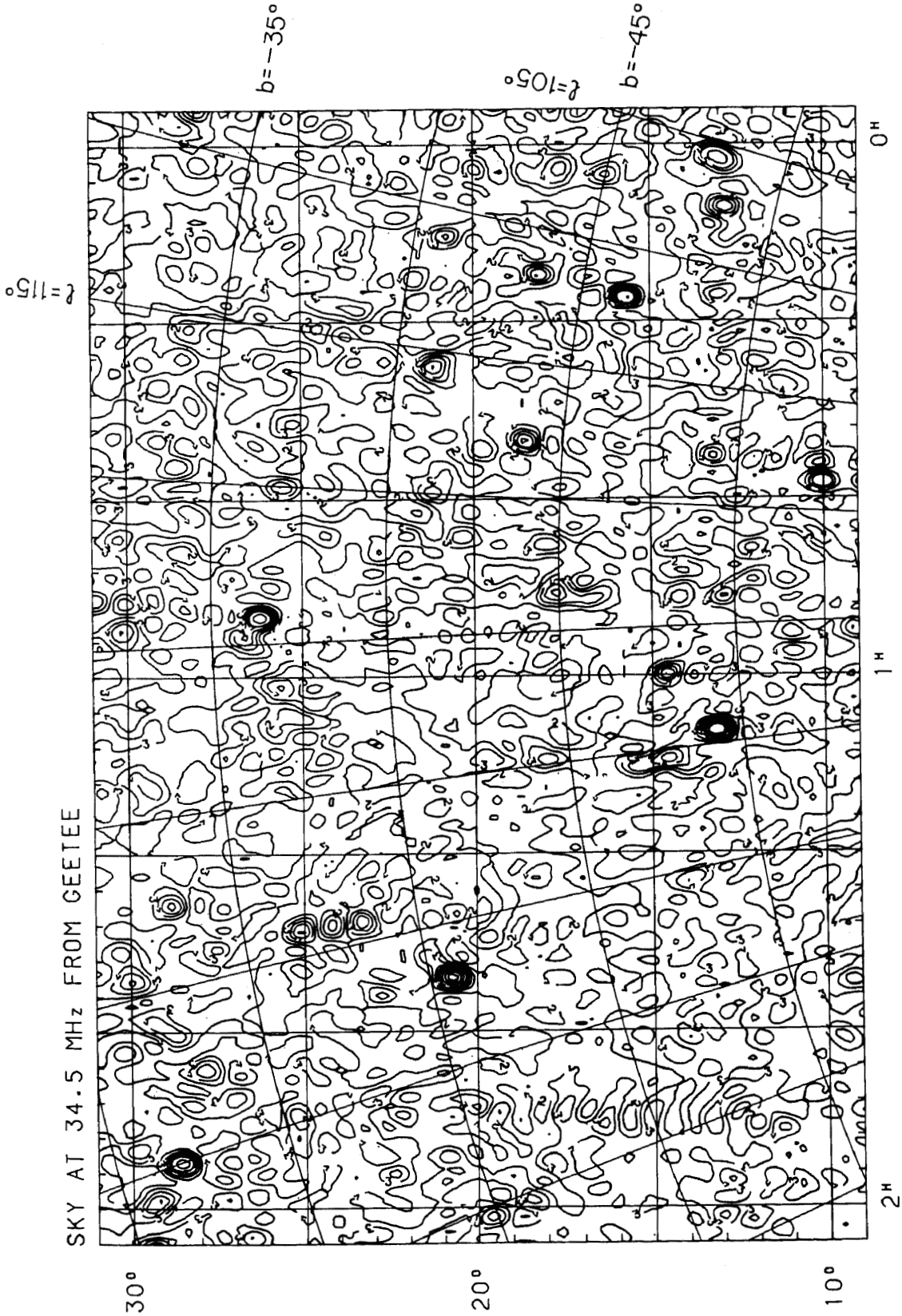
SKY AT 34.5 MHz FROM GEETEE
b=−35°
ℓ=105°
b=−45°
ℓ=115°
0H
1H
2H
30°
20°
10°

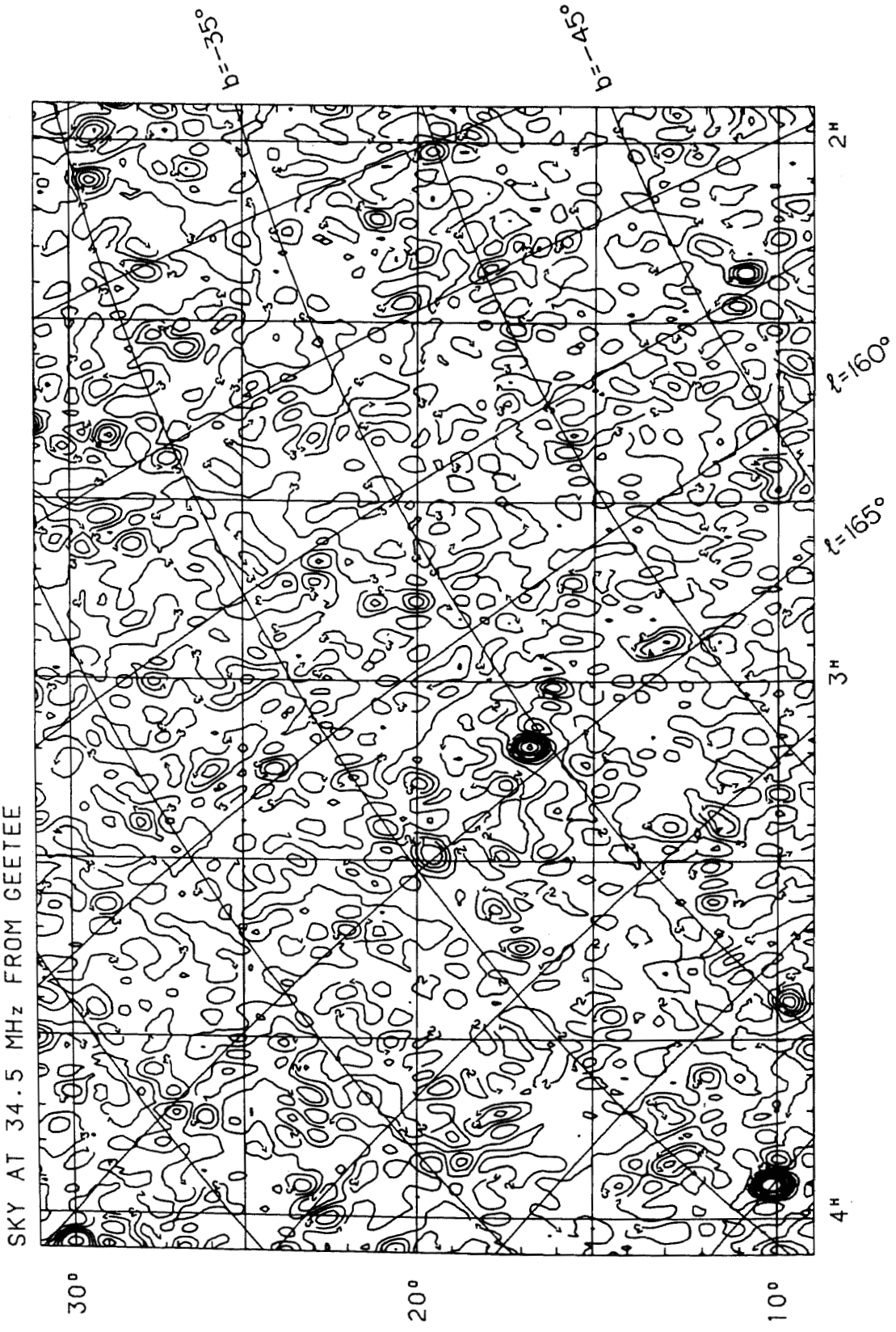
SKY AT 34.5 MHz FROM GEETEE
b=-35°
b=-45°
l=160°
l=165°
2H
3H
4H
30°
20°
10°

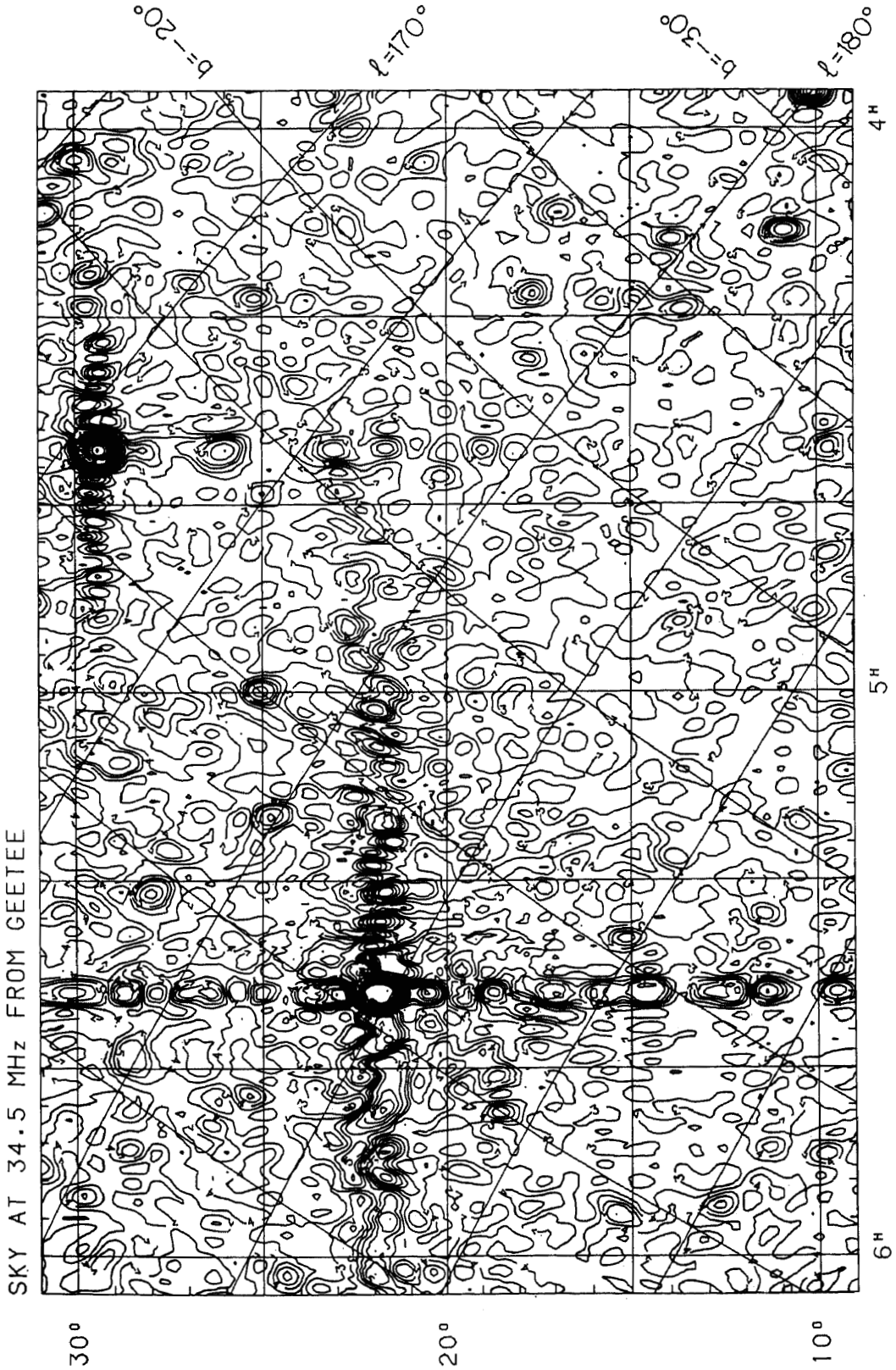
b=-20°
ℓ=170°
b=-30°
ℓ=180°
4H
5H
6H
30°
20°
10°
SKY AT 34.5 MHz FROM GEETEE

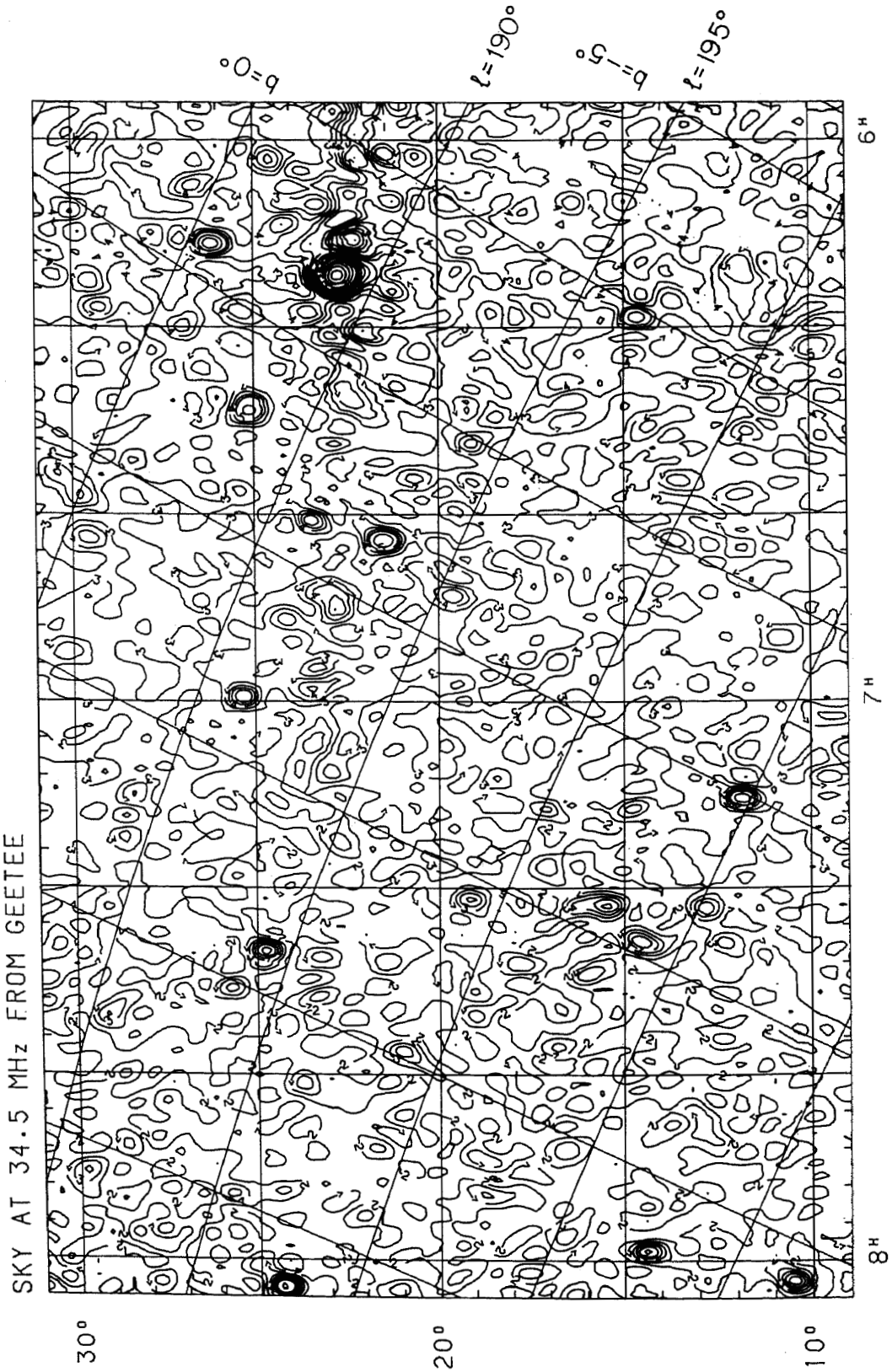
b=0°
l=190°
b=-5°
l=195°
6H
7H
8H
SKY AT 34.5 MHz FROM GEETEE
30°
20°
10°

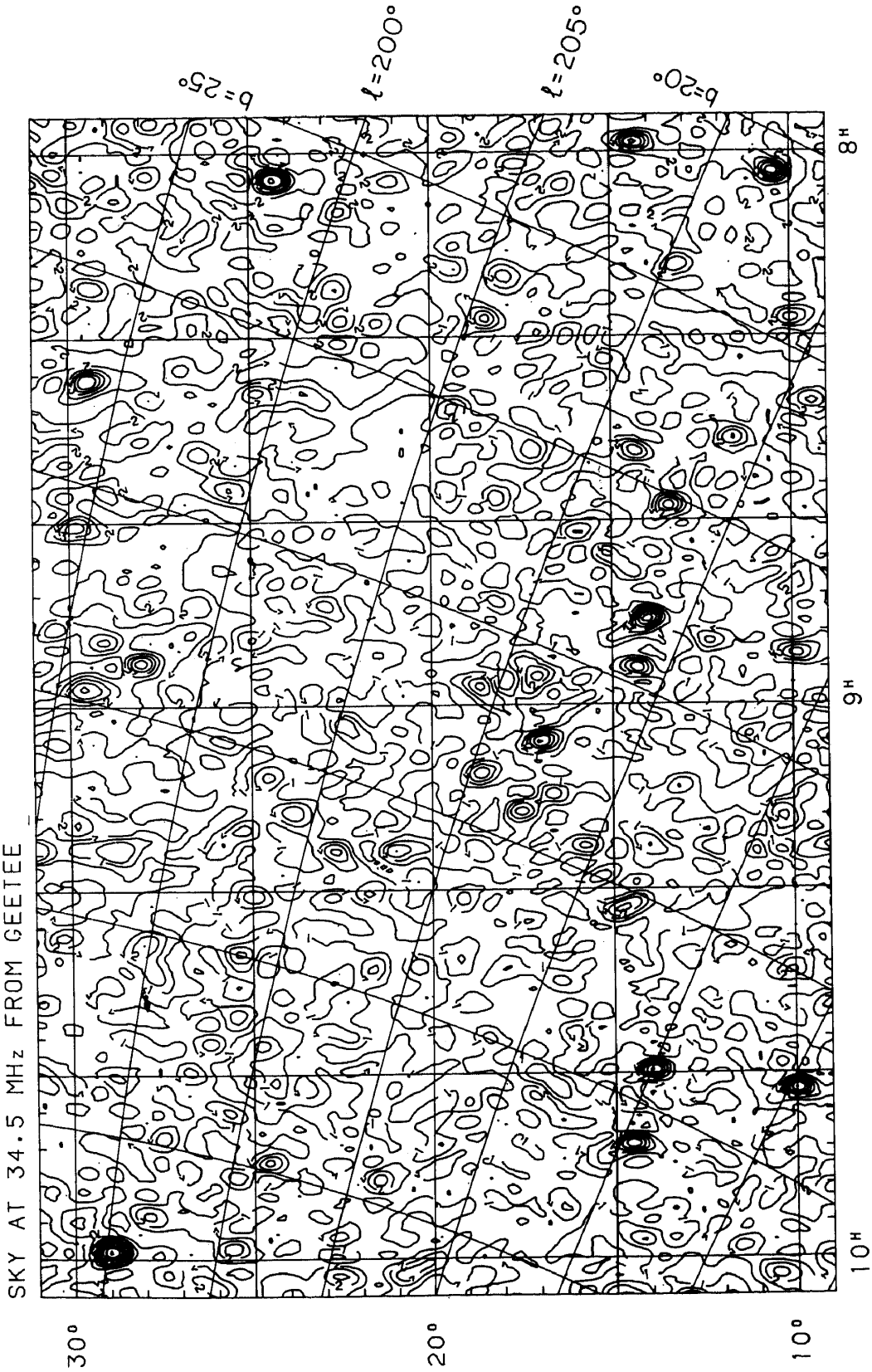
SKY AT 34.5 MHz FROM GEETEE
b=25°
l=200°
l=205°
b=20°
8H
9H
10H
30°
20°
10°

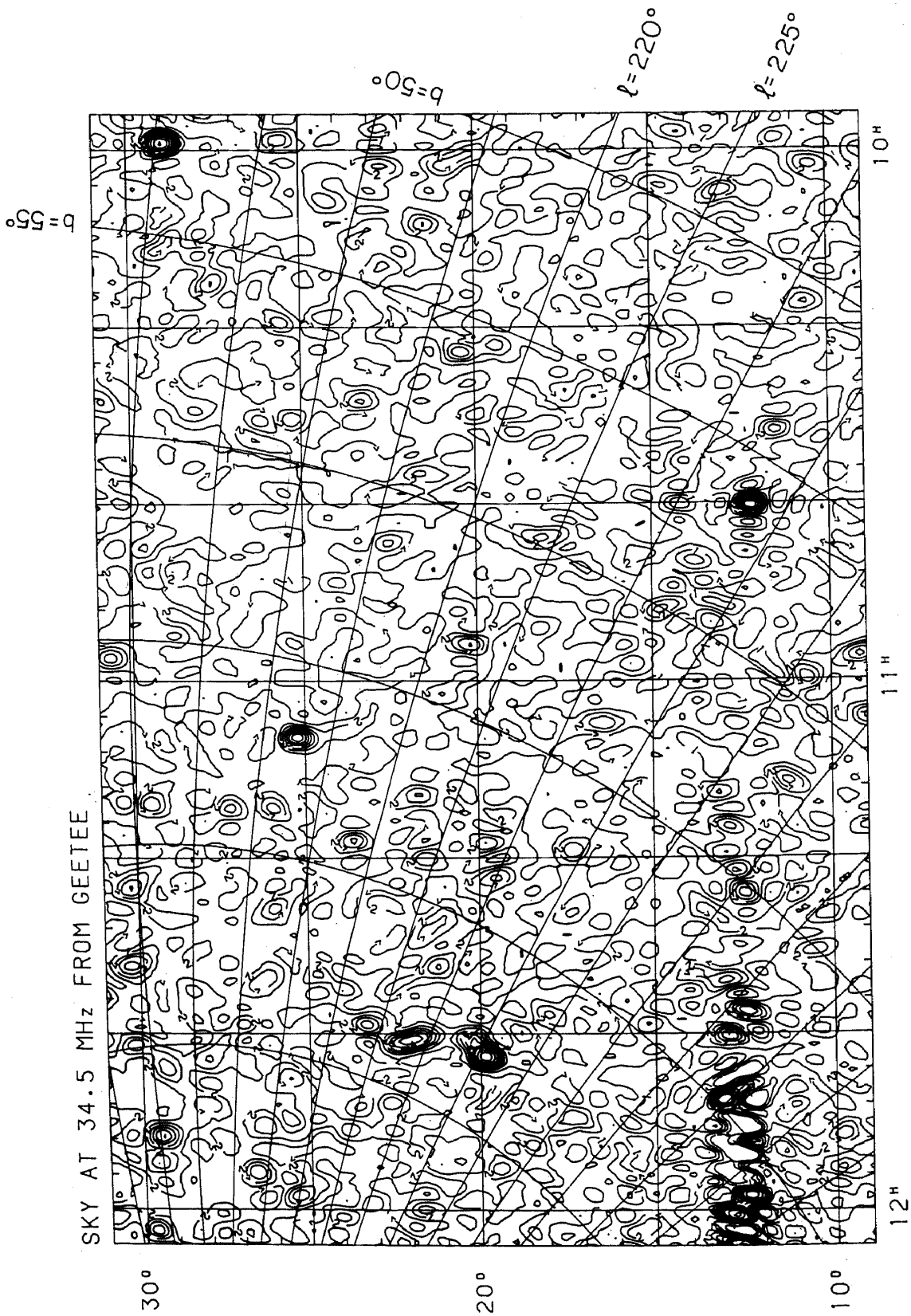
SKY AT 34.5 MHz FROM GEETEE
b=55°
b=50°
ℓ=220°
ℓ=225°
10H
11H
12H
30°
20°
10°

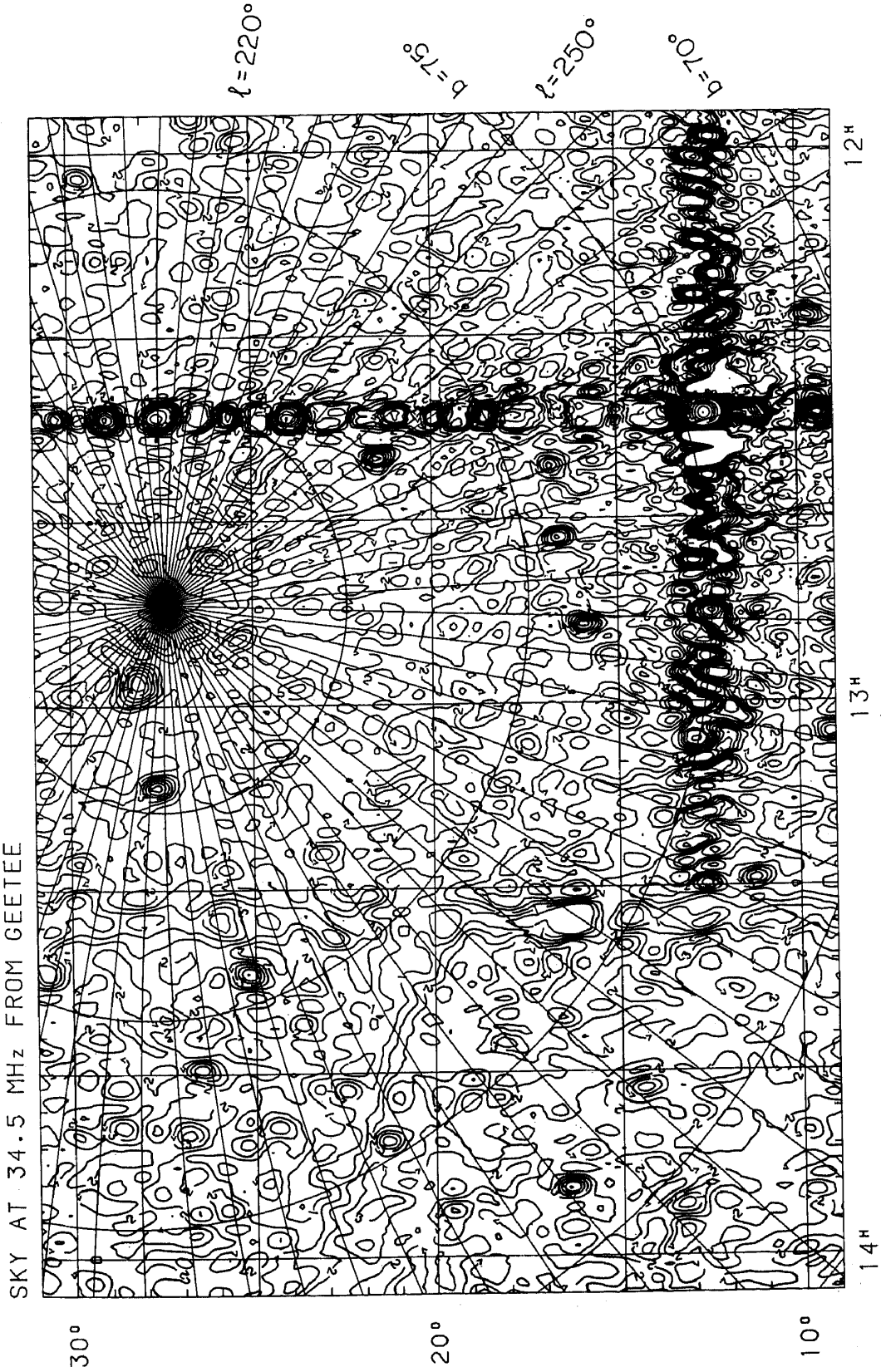
SKY AT 34.5 MHz FROM GEETEE
ℓ=220°
b=75°
ℓ=250°
b=70°
12ᴴ
13ᴴ
14ᴴ
30°
20°
10°

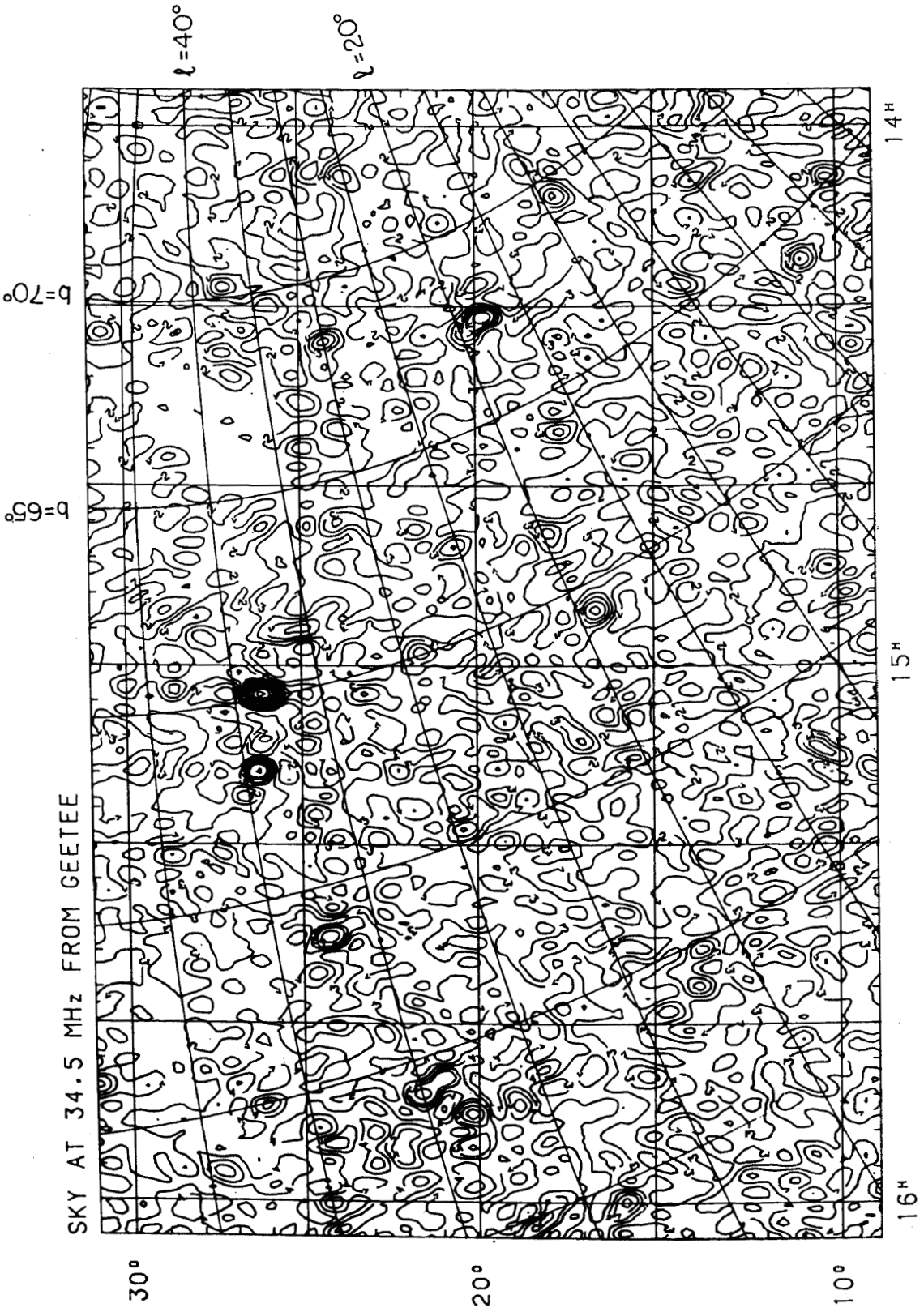
SKY AT 34.5 MHz FROM GEETEE
l=40°
l=20°
b=70°
b=65°
14ᴴ
15ᴴ
16ᴴ
30°
20°
10°

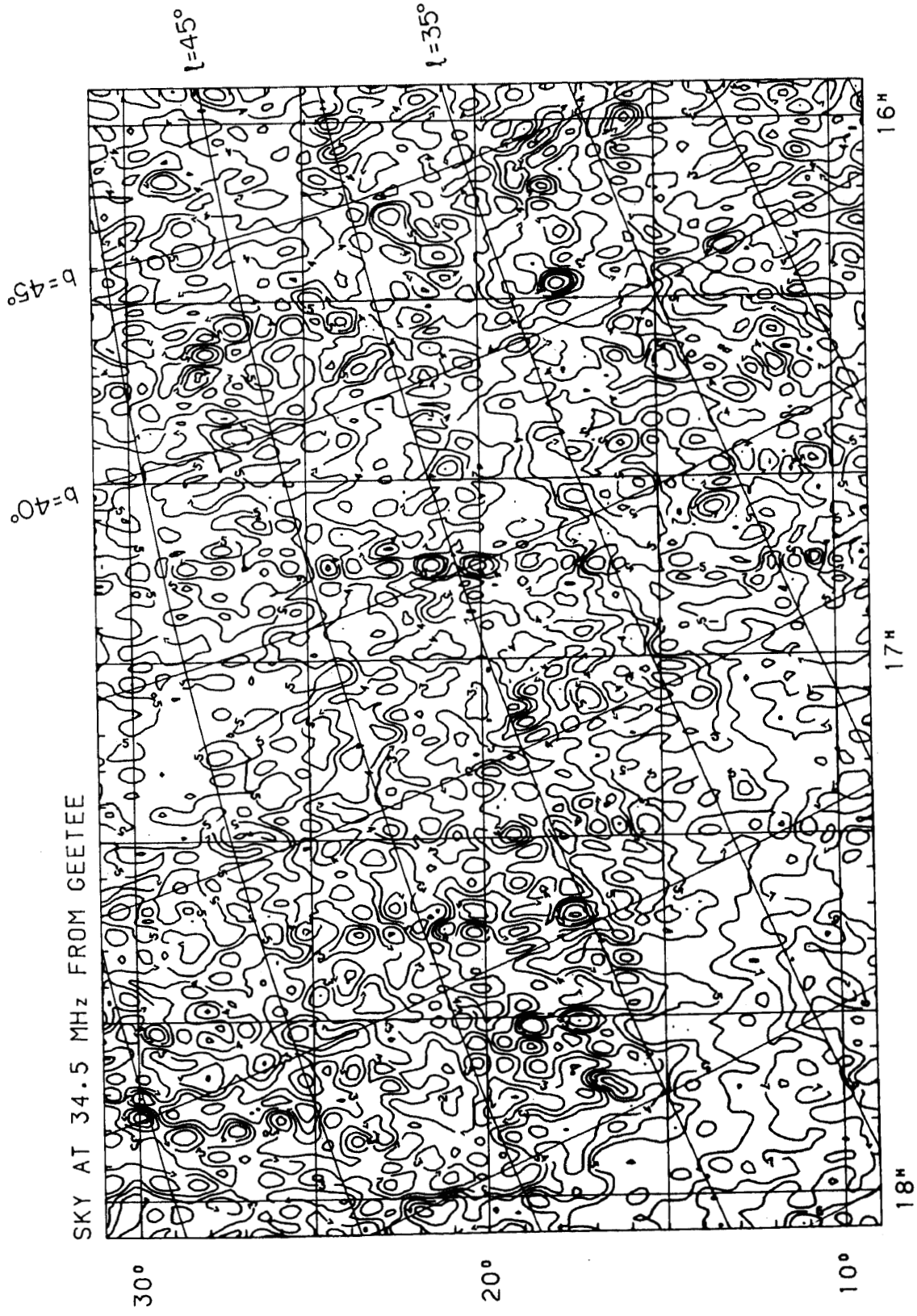
l=45°
l=35°
16ᴴ
17ᴴ
18ᴴ
b=45°
b=40°
30°
20°
10°
SKY AT 34.5 MHz FROM GEETEE

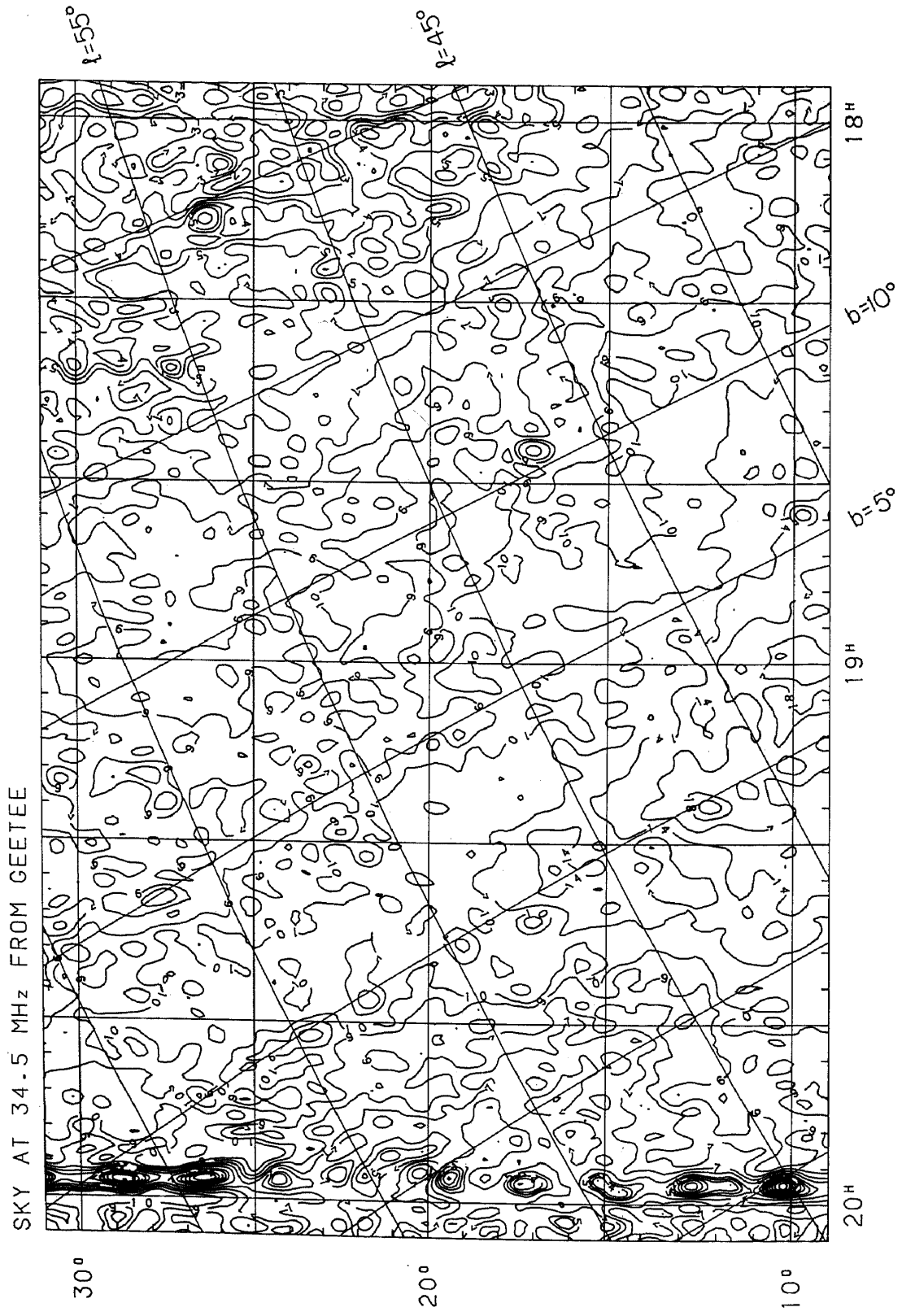
SKY AT 34.5 MHz FROM GEETEE
l=55°
l=45°
18H
19H
20H
b=10°
b=5°
30°
20°
10°

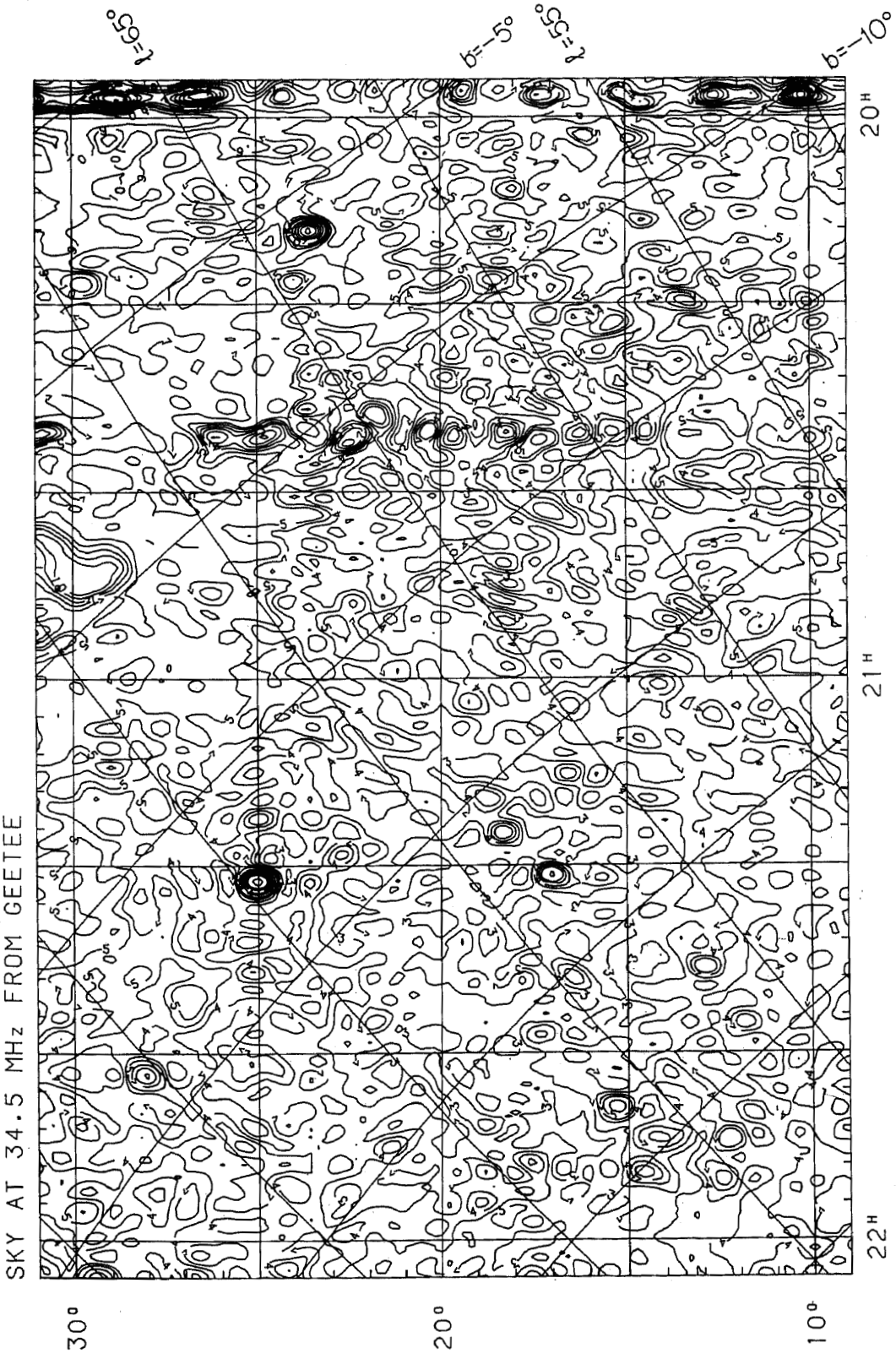
l=65°
b=−5°
l=55°
b=−10°
20ᴴ
21ᴴ
22ᴴ
30°
20°
10°
SKY AT 34.5 MHz FROM GEETEE

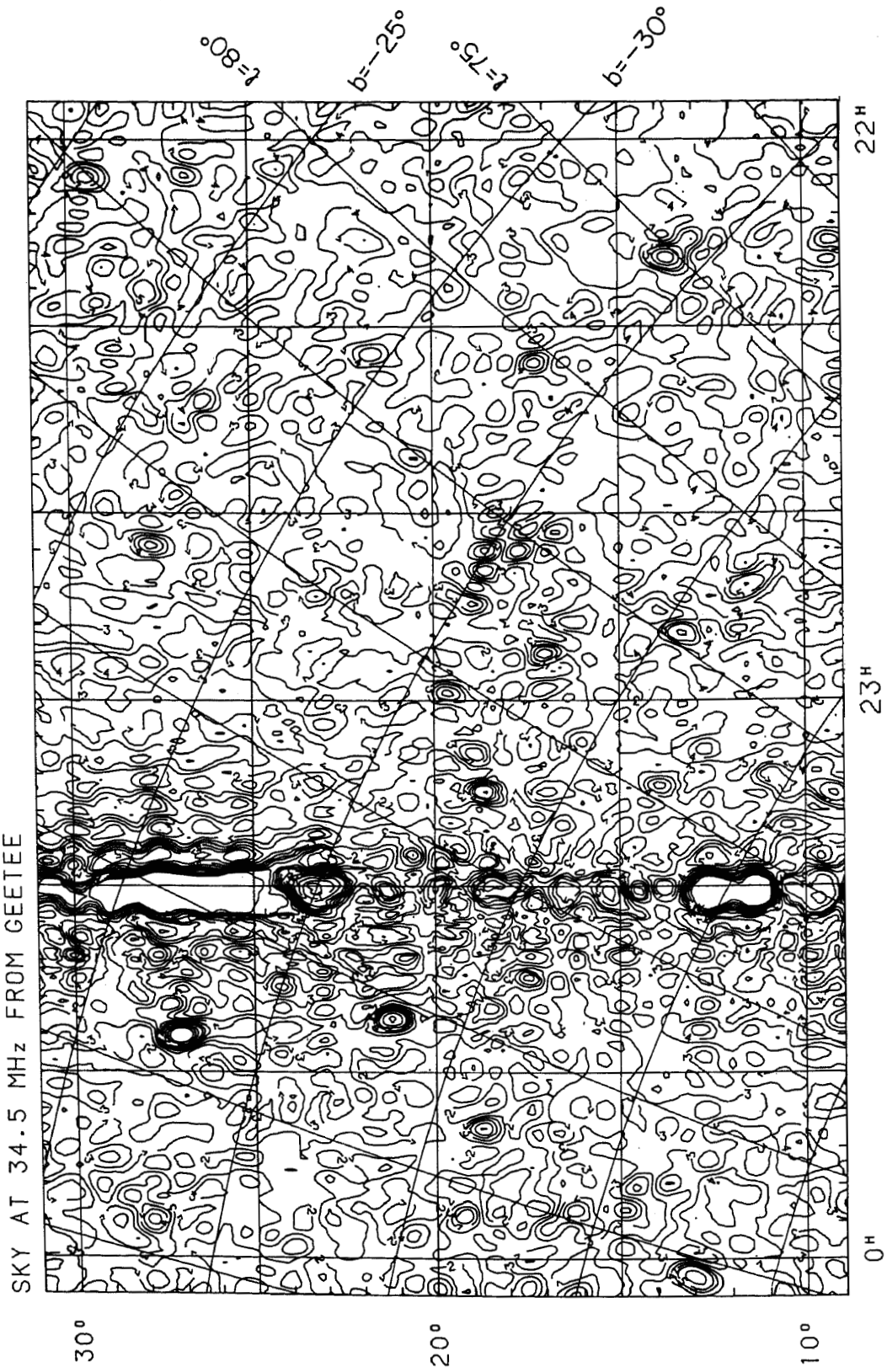
SKY AT 34.5 MHz FROM GEETEE
l=80°
b=−25°
l=75°
b=−30°
22H
23H
0H
30°
20°
10°

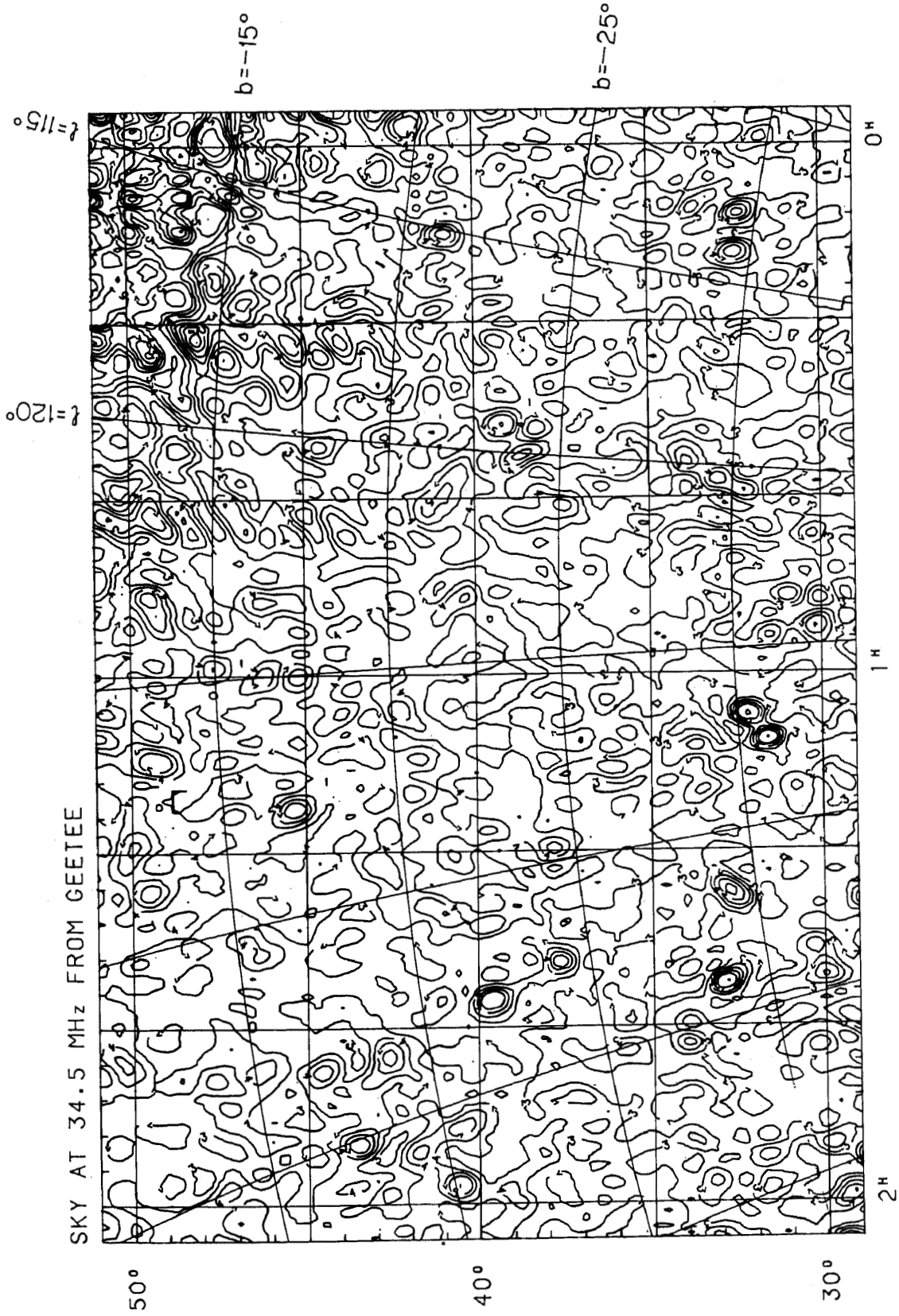
b=−15°
b=−25°
ℓ=115°
ℓ=120°
0H
1H
2H
50°
40°
30°
SKY AT 34.5 MHz FROM GEETEE

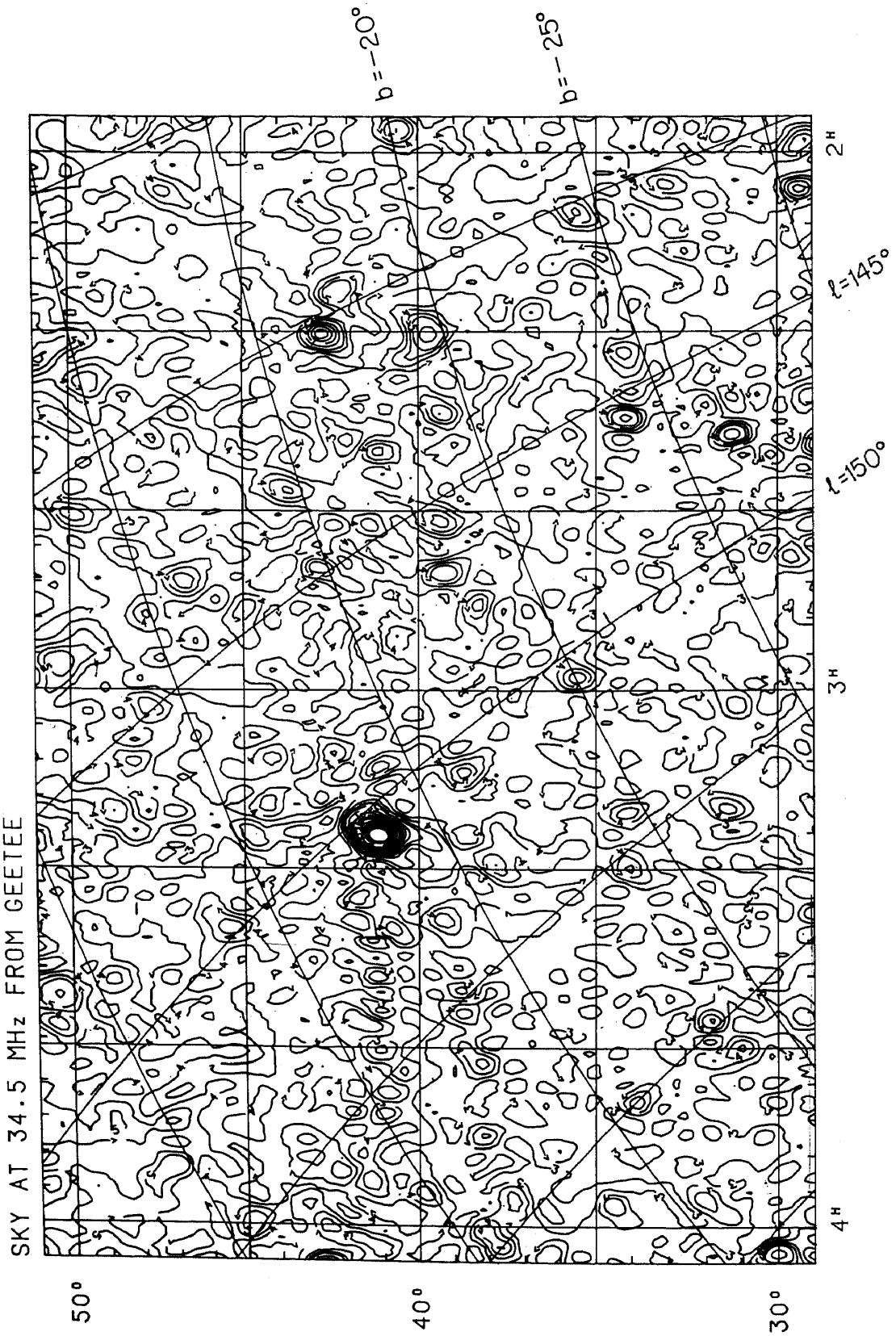
b=−20°
b=−25°
2H
3H
4H
l=145°
l=150°
50°
40°
30°
SKY AT 34.5 MHz FROM GEETEE

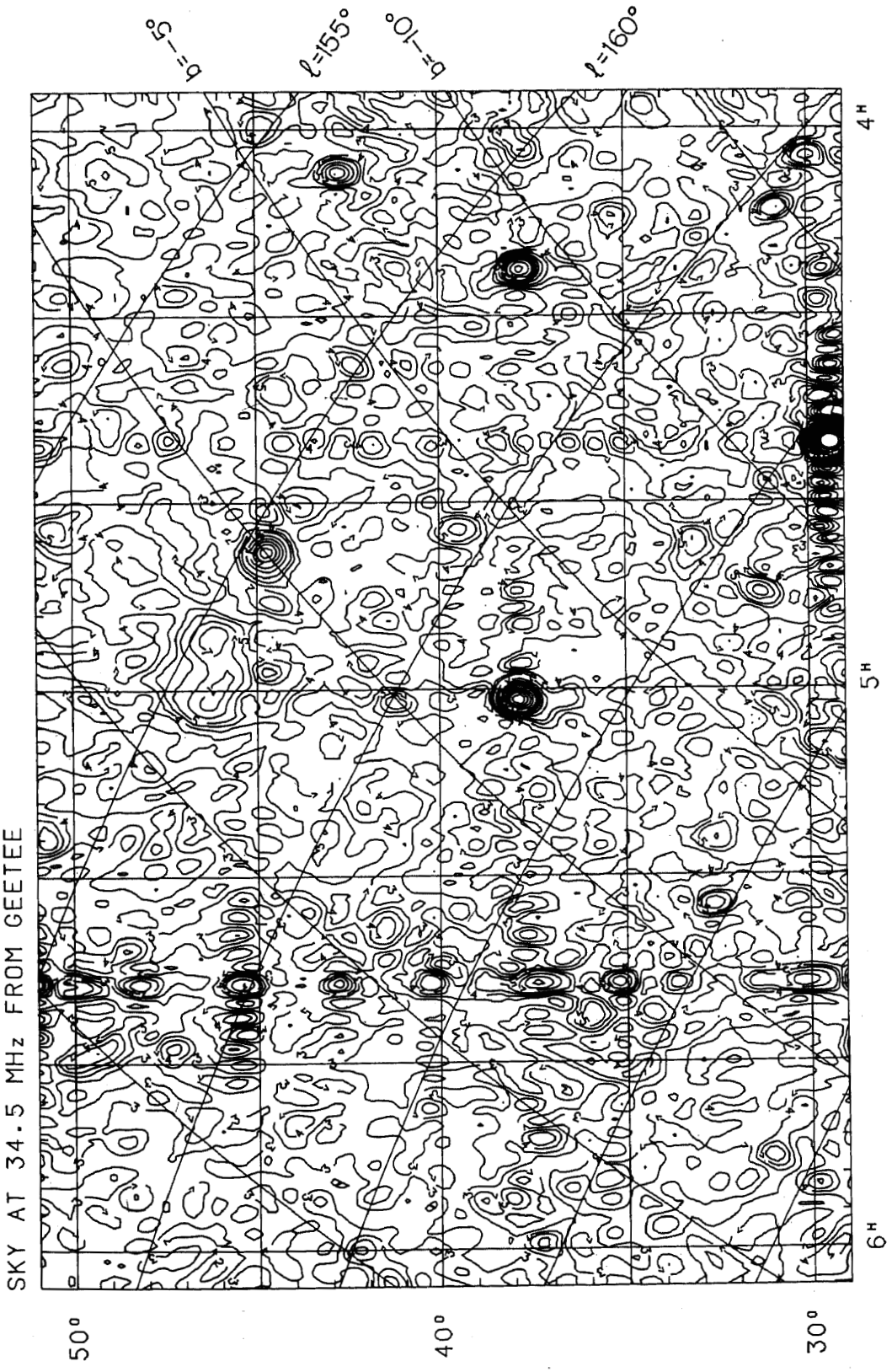
SKY AT 34.5 MHz FROM GEETEE
b=-5°
ℓ=155°
b=-10°
ℓ=160°
4H
5H
6H
50°
40°
30°

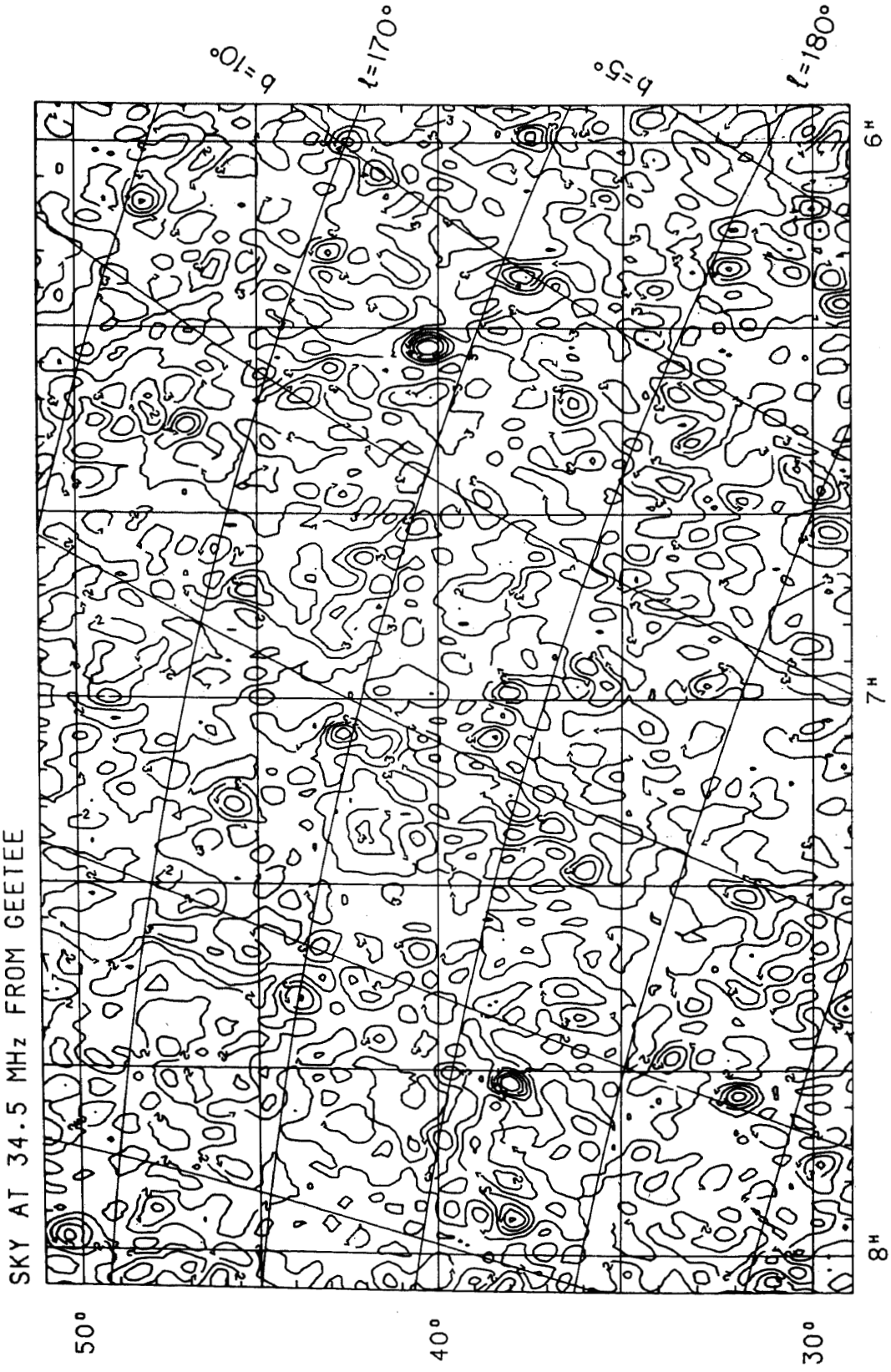
SKY AT 34.5 MHz FROM GEETEE
b=10°
l=170°
b=5°
l=180°
9H
7H
8H
50°
40°
30°

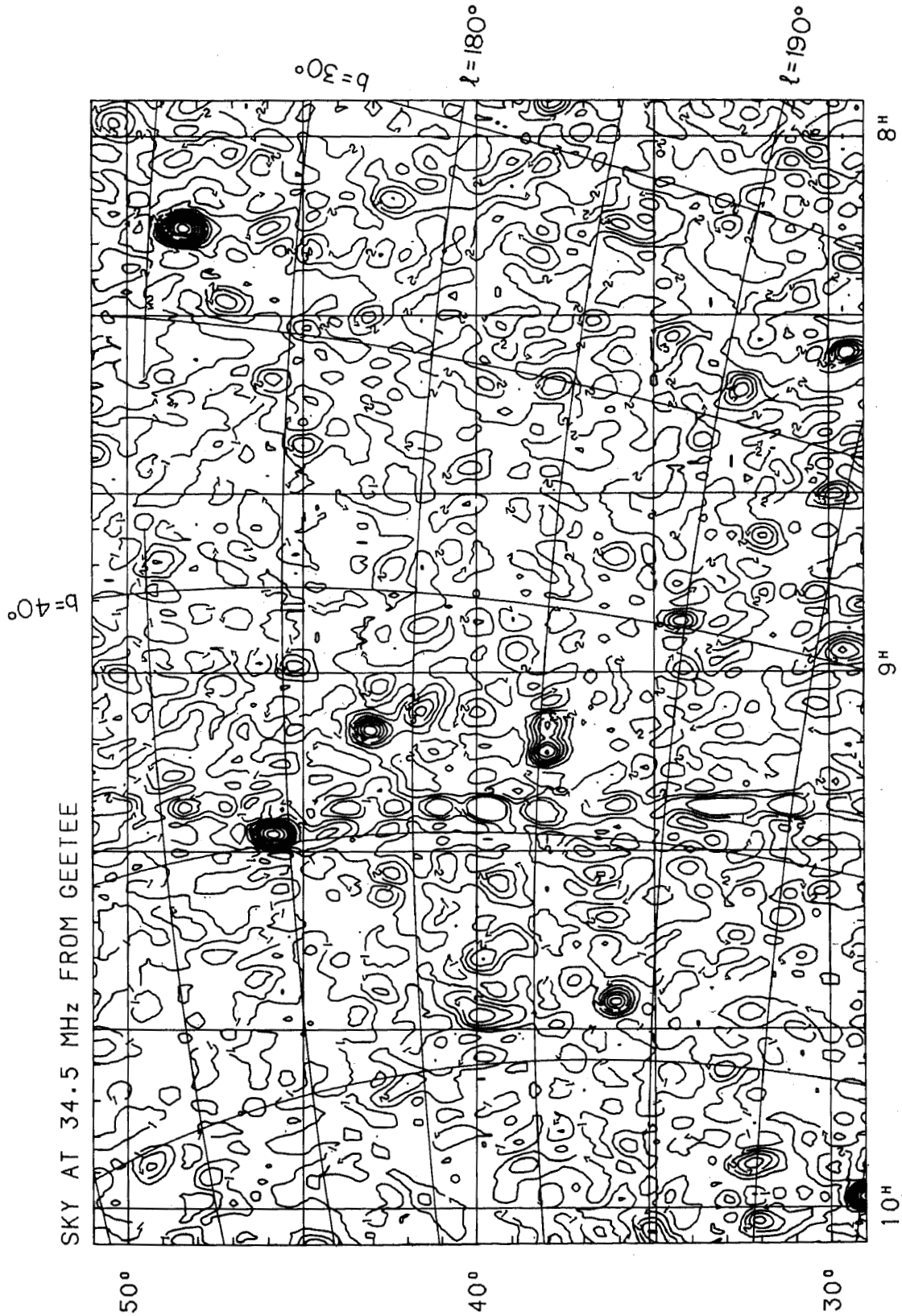
SKY AT 34.5 MHz FROM GEETEE
b=40°
b=30°
ℓ=180°
ℓ=190°
8H
9H
10H
50°
40°
30°

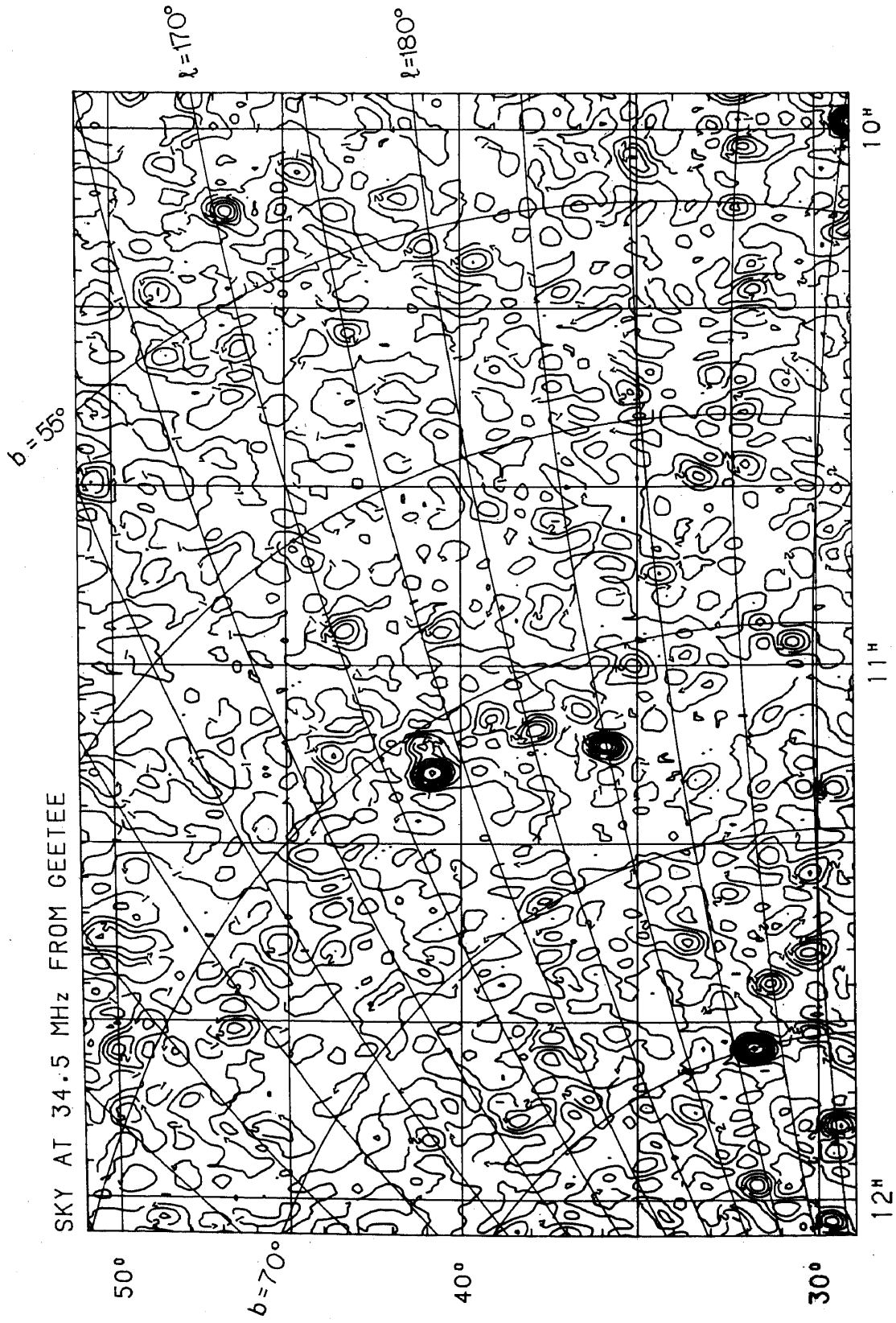
SKY AT 34.5 MHz FROM GEETEE
ℓ=170°
ℓ=180°
b=55°
b=70°
10ʰ
11ʰ
12ʰ
50°
40°
30°

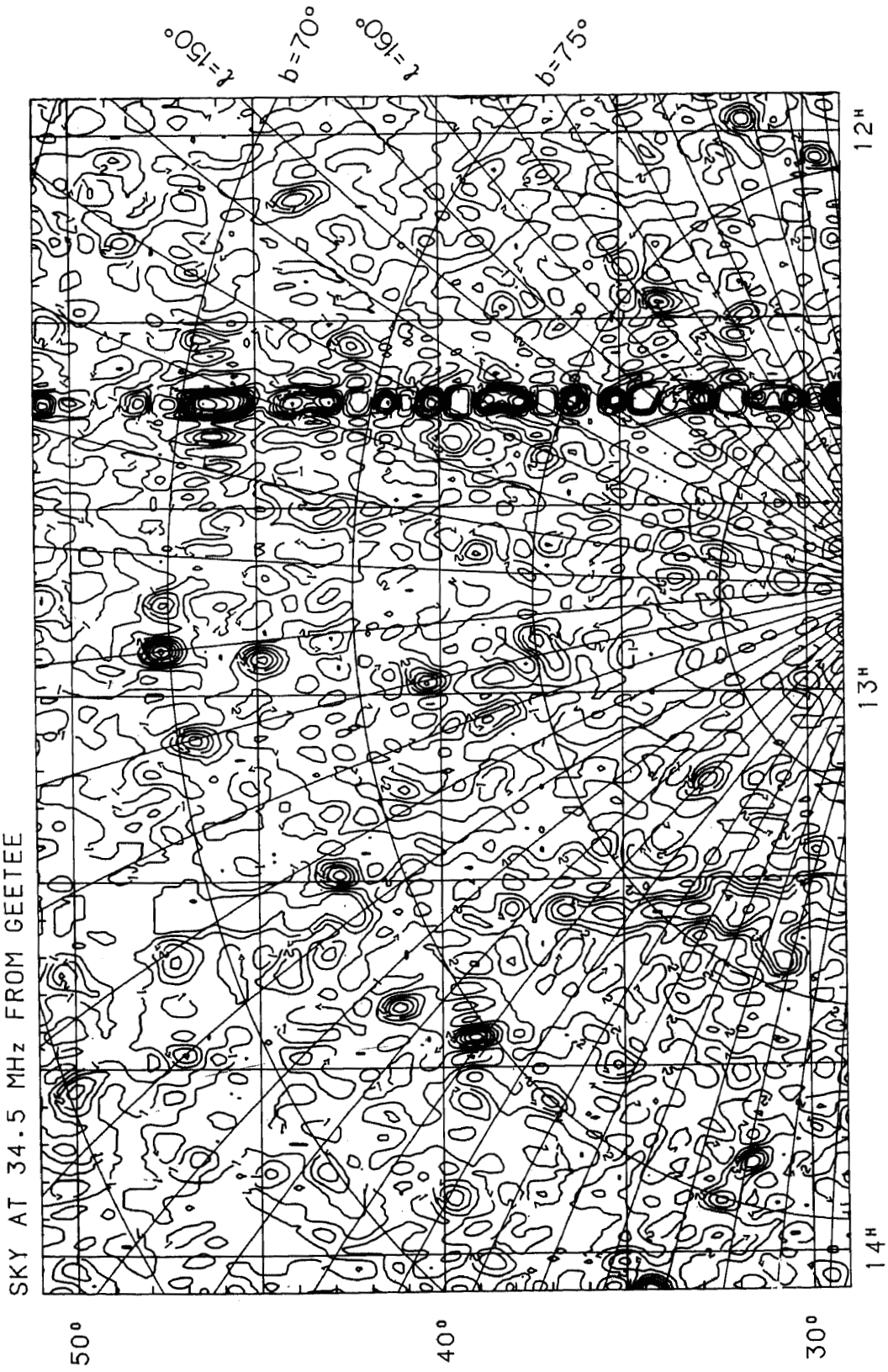
SKY AT 34.5 MHz FROM GEETEE
l=150°
b=70°
l=160°
b=75°
12H
13H
14H
50°
40°
30°

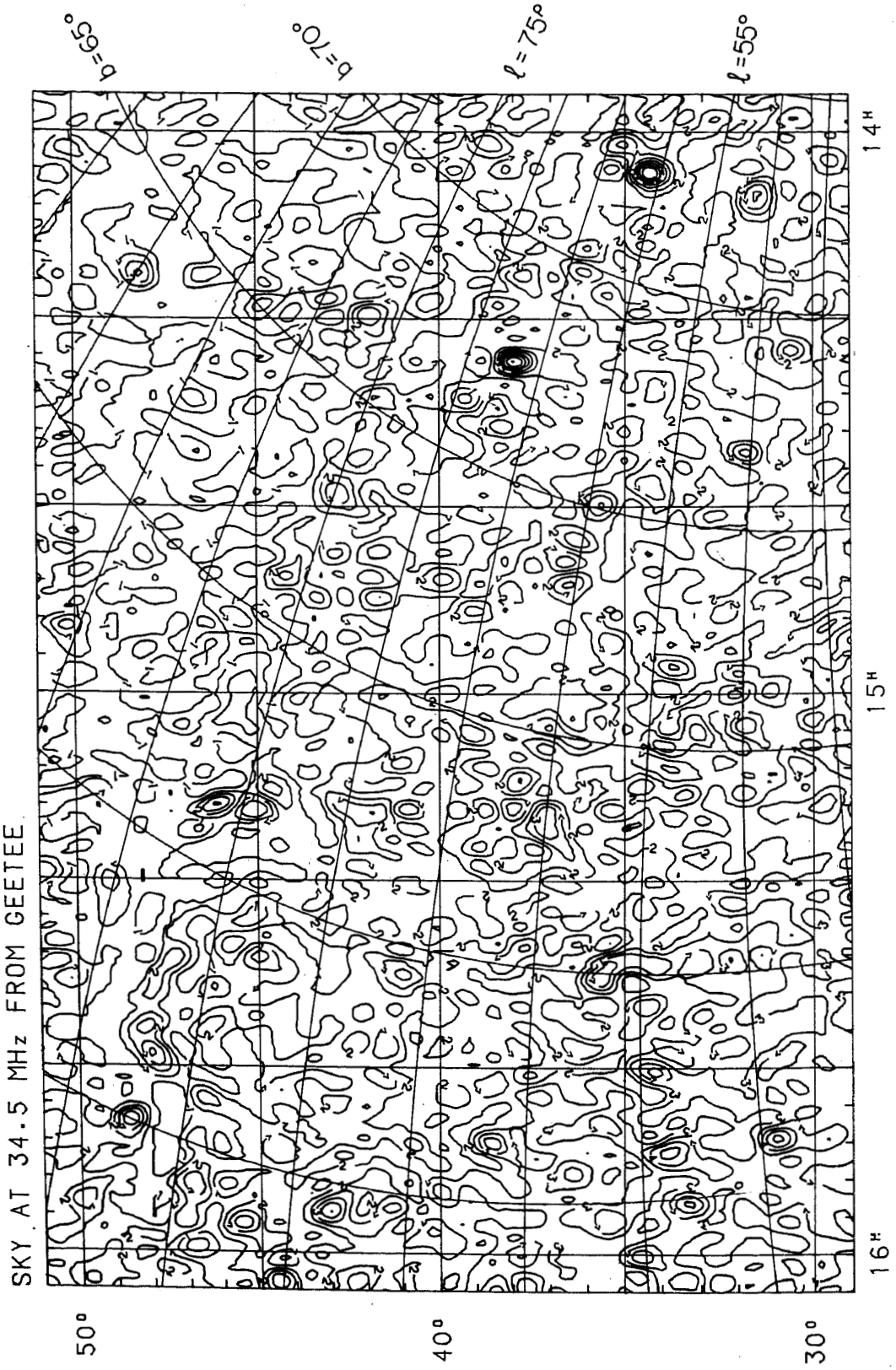
b=65°
b=70°
ℓ=75°
ℓ=55°
14ᴴ
15ᴴ
16ᴴ
50°
40°
30°
SKY AT 34.5 MHz FROM GEETEE

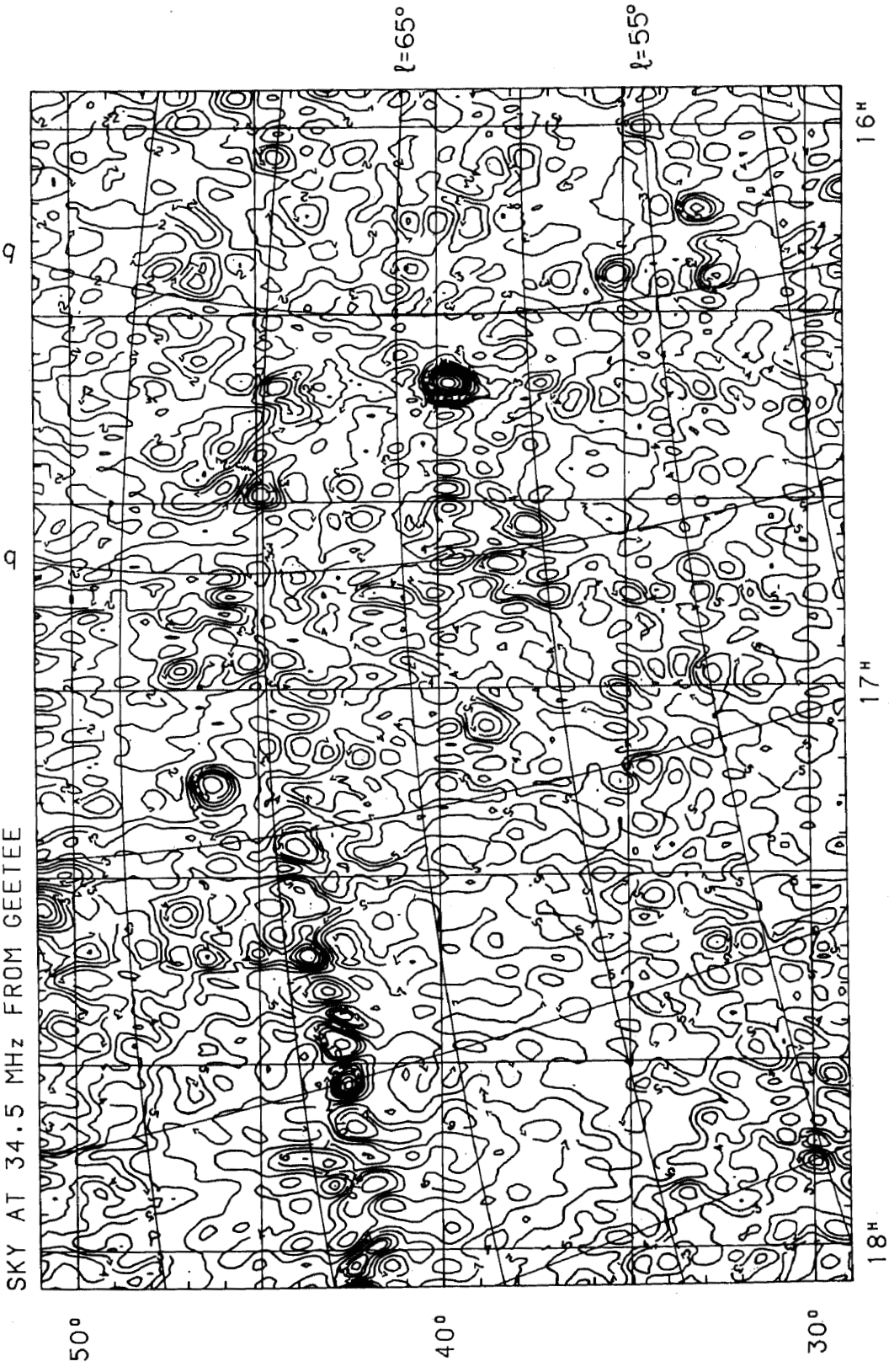
SKY AT 34.5 MHz FROM GEETEE
l=65°
l=55°
16H
17H
18H
b=45°
b=40°
50°
40°
30°

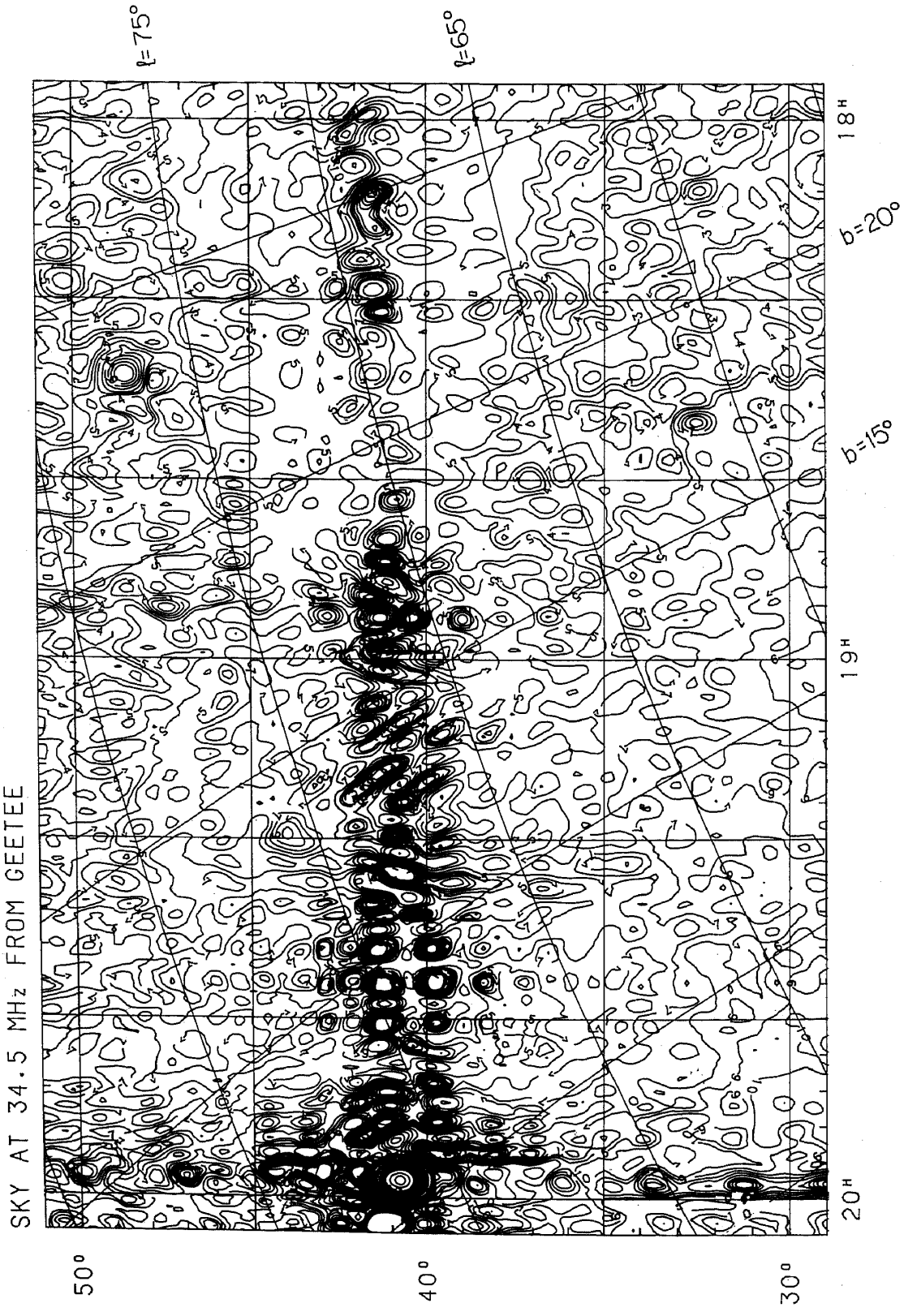
SKY AT 34.5 MHz FROM GEETEE
ℓ=75°
ℓ=65°
18ʰ
19ʰ
20ʰ
b=20°
b=15°
50°
40°
30°

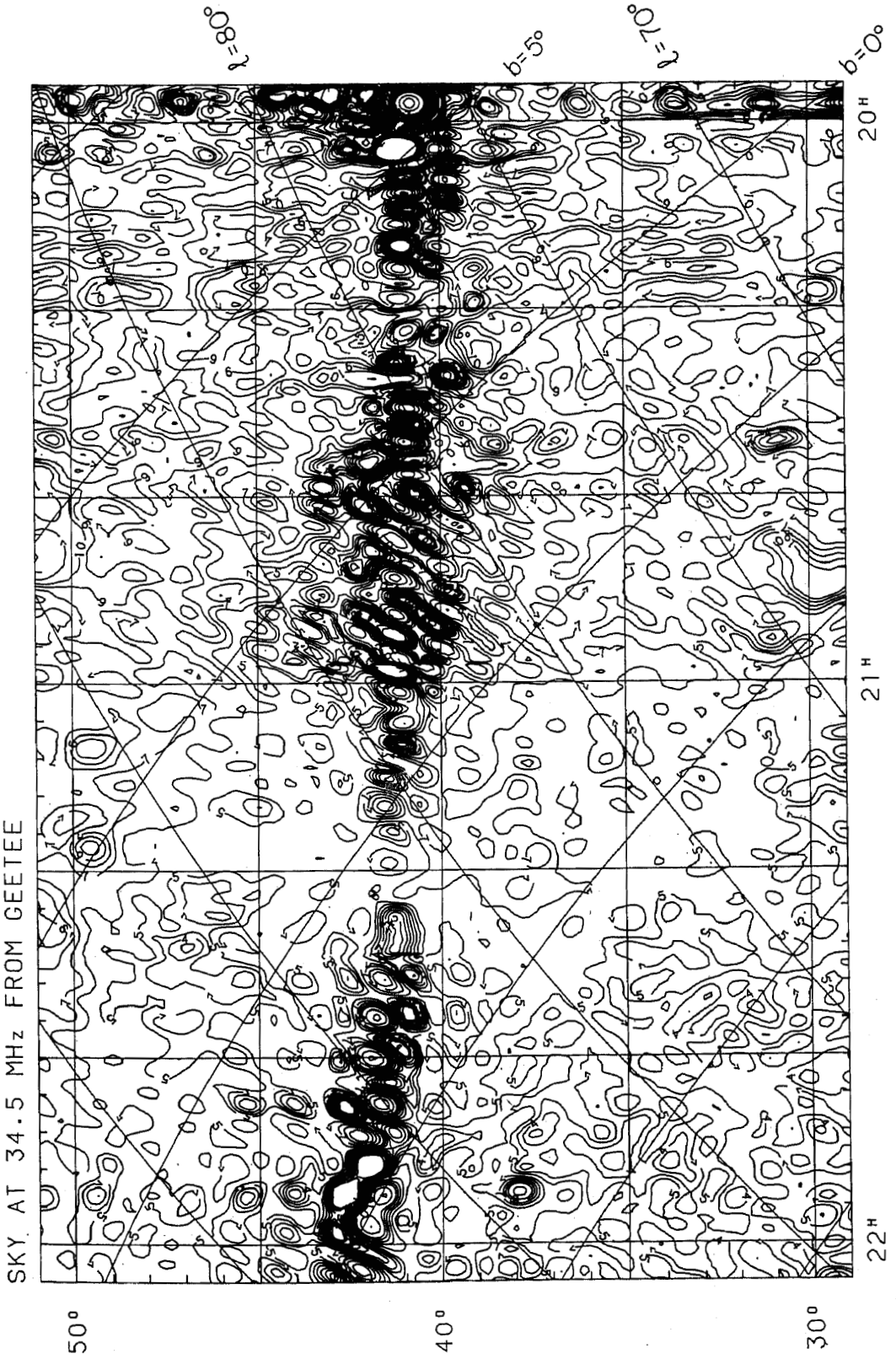
SKY AT 34.5 MHz FROM GEETEE
l=80°
b=5°
l=70°
b=0°
20ʰ
21ʰ
22ʰ
50°
40°
30°

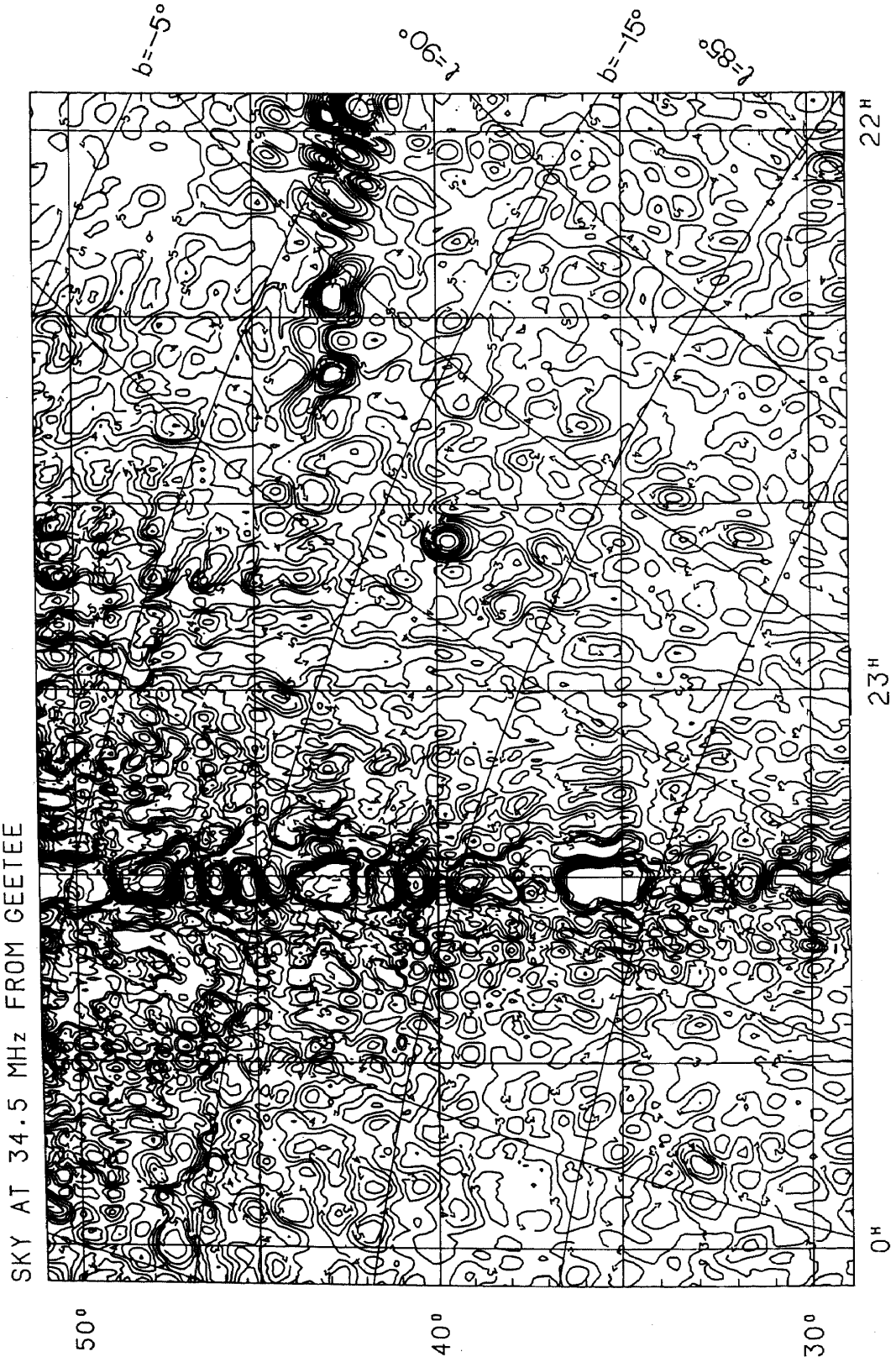
SKY AT 34.5 MHz FROM GEETEE
b=-5°
l=90°
b=-15°
l=85°
22H
23H
0H
50°
40°
30°

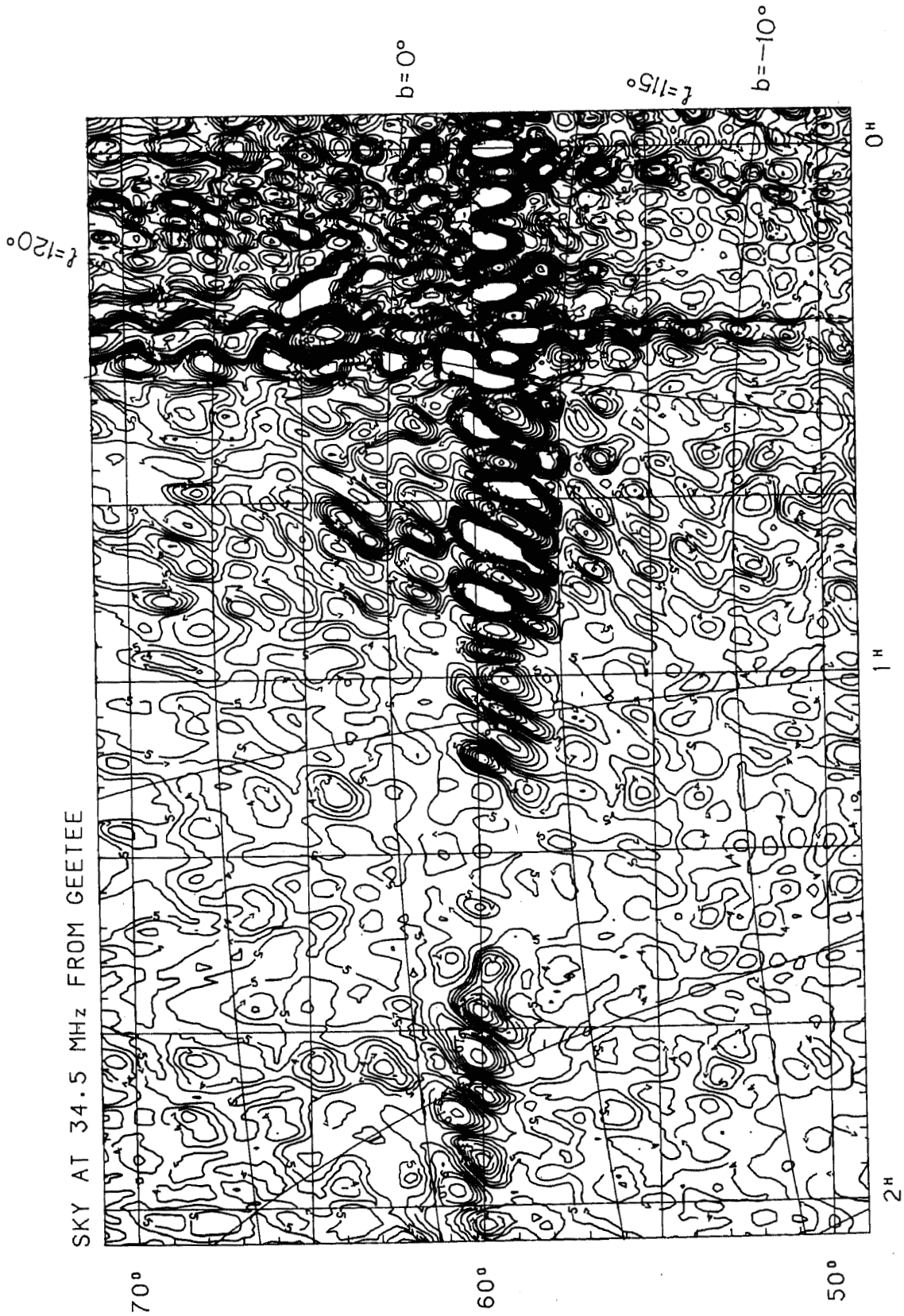
SKY AT 34.5 MHz FROM GEETEE
b=−10°
b=0°
ℓ=115°
ℓ=120°
0H
1H
2H
70°
60°
50°

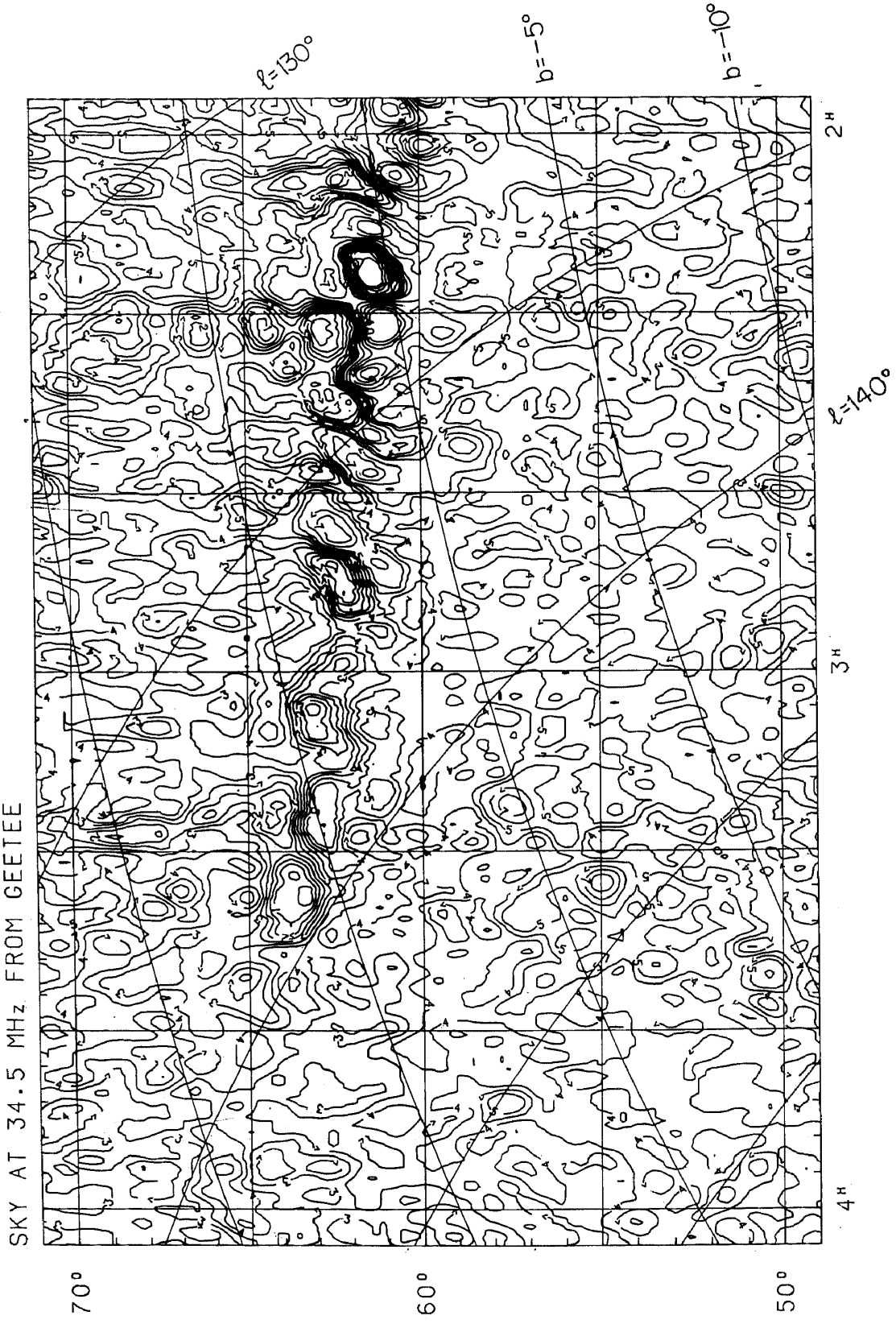
SKY AT 34.5 MHz FROM GEETEE
ℓ=130°
b=-5°
b=-10°
ℓ=140°
2H
3H
4H
70°
60°
50°

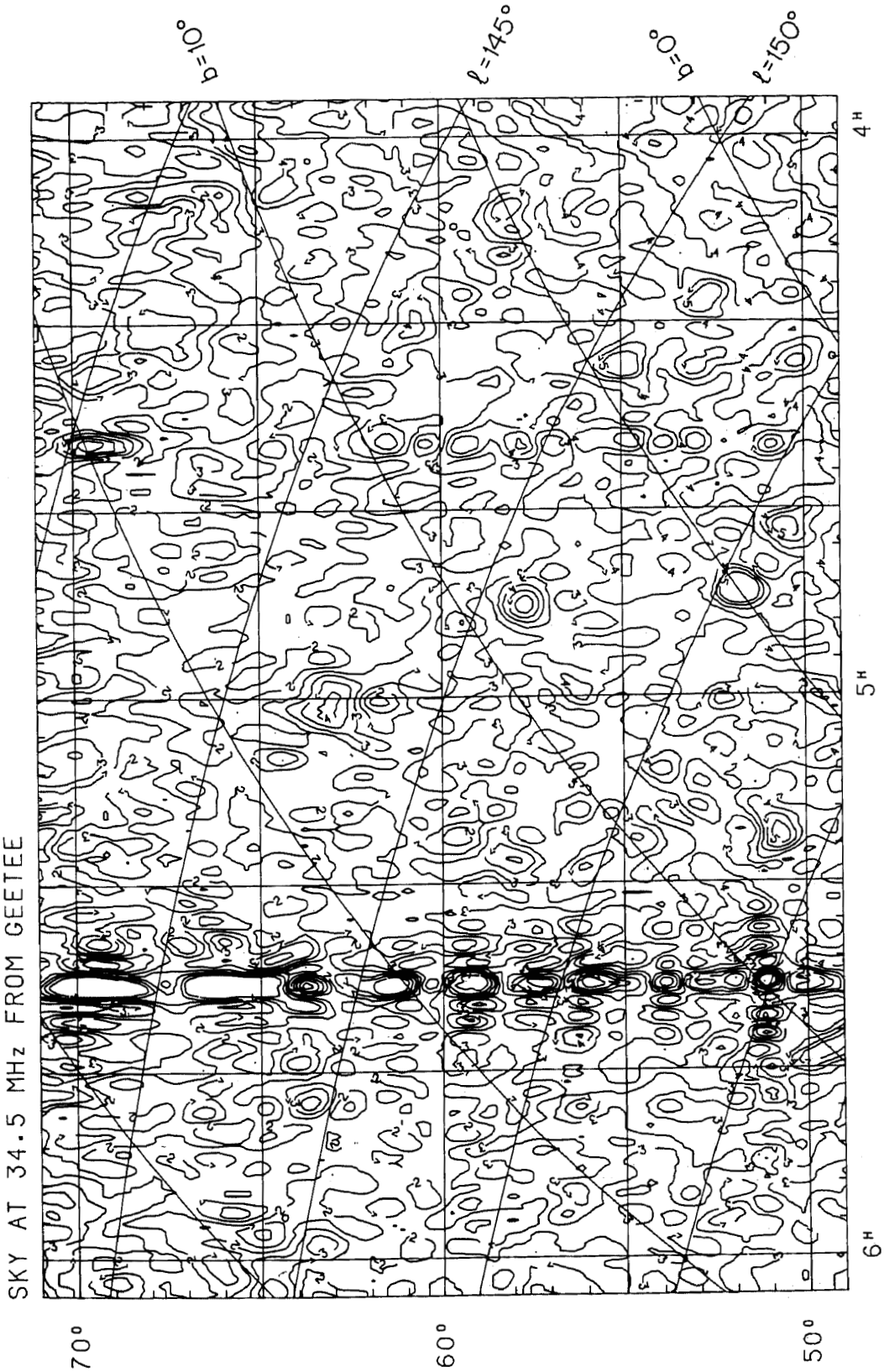
SKY AT 34.5 MHz FROM GEETEE
b=10°
ℓ=145°
b=0°
ℓ=150°
4H
5H
6H
70°
60°
50°

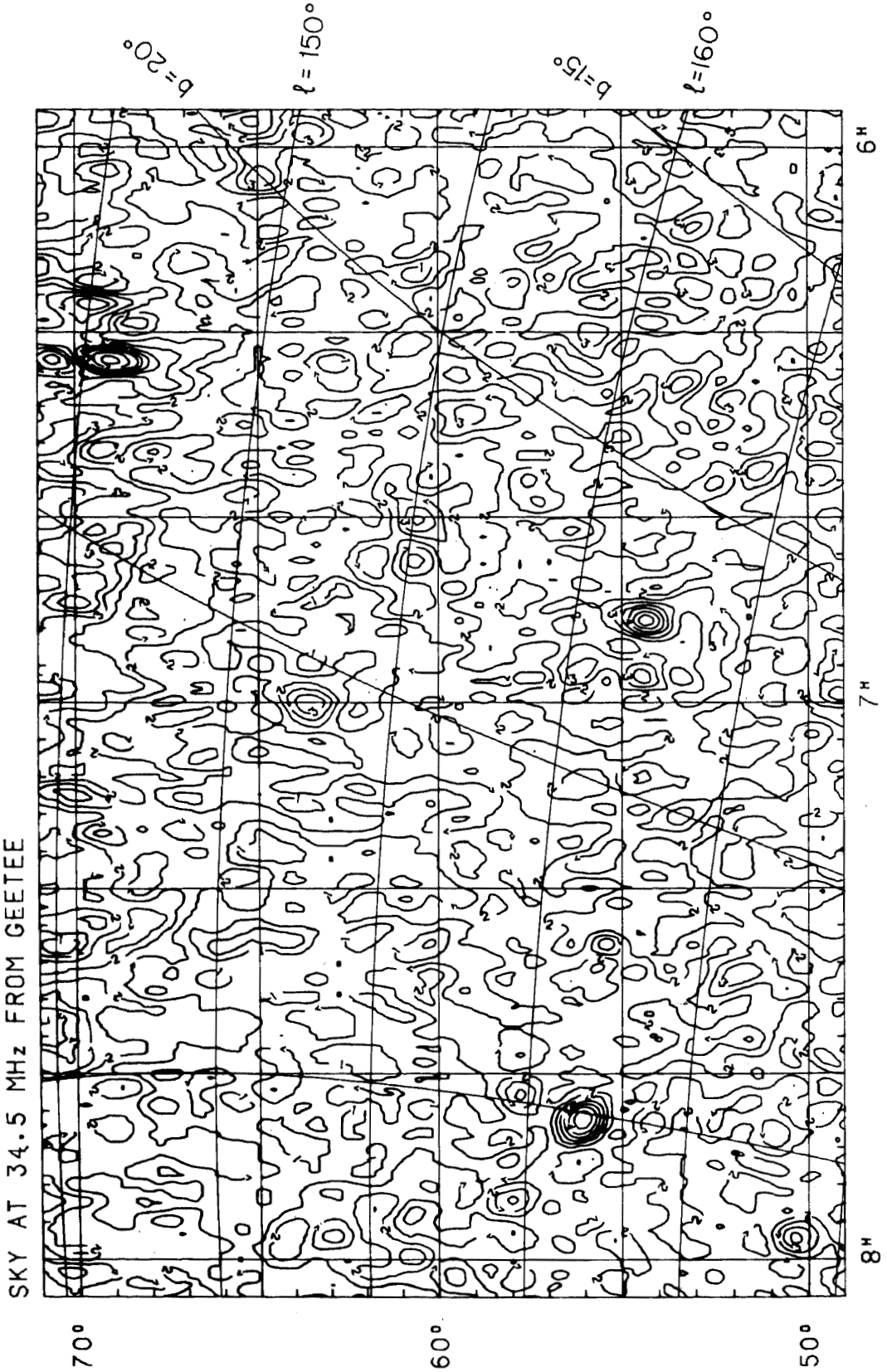
SKY AT 34.5 MHz FROM GEETEE
b=20°
ℓ = 150°
b=15°
ℓ=160°
6H
7H
8H
70°
60°
50°

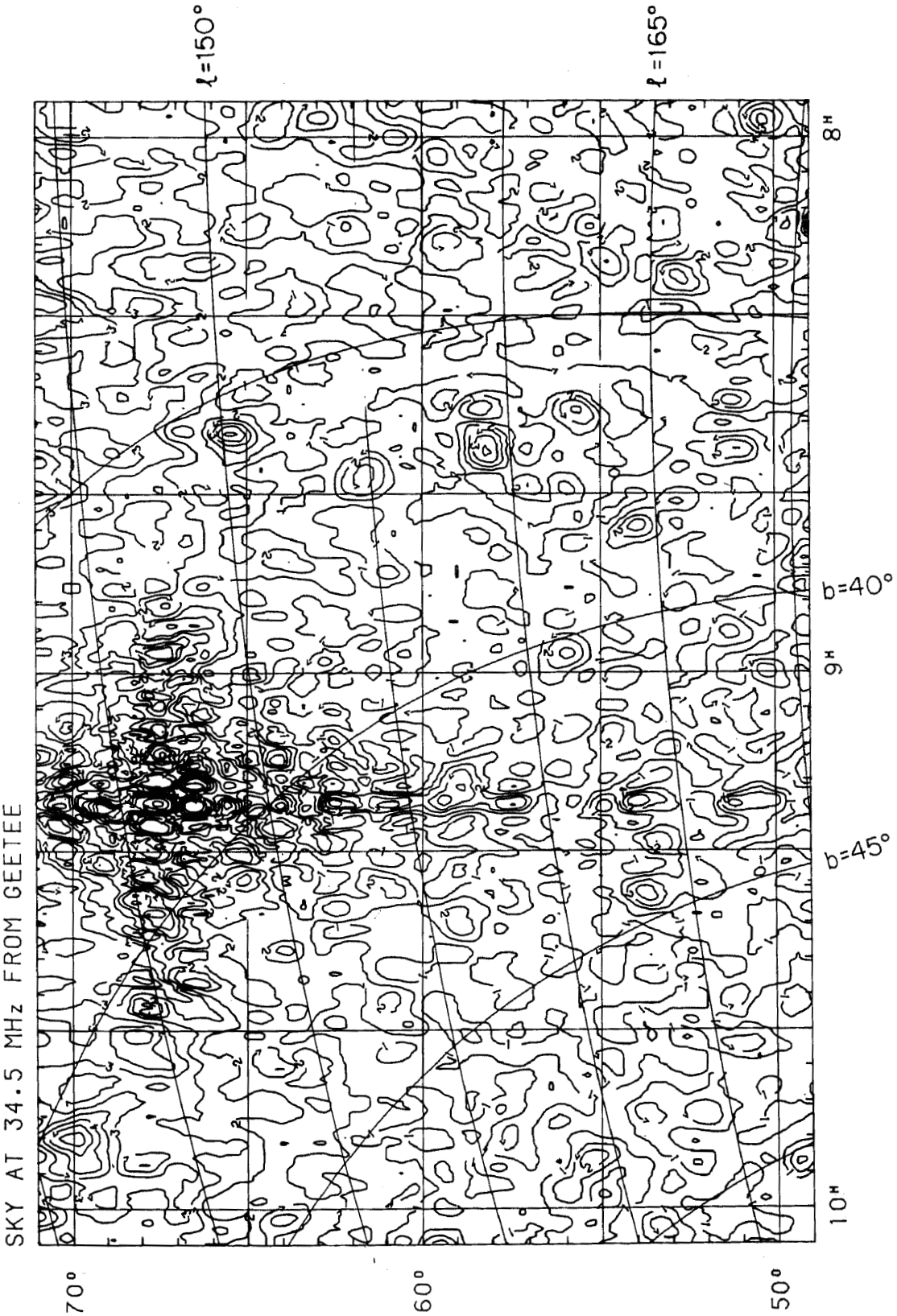
SKY AT 34.5 MHz FROM GEETEE
l=150°
l=165°
8H
6H
10H
b=40°
b=45°
70°
60°
50°

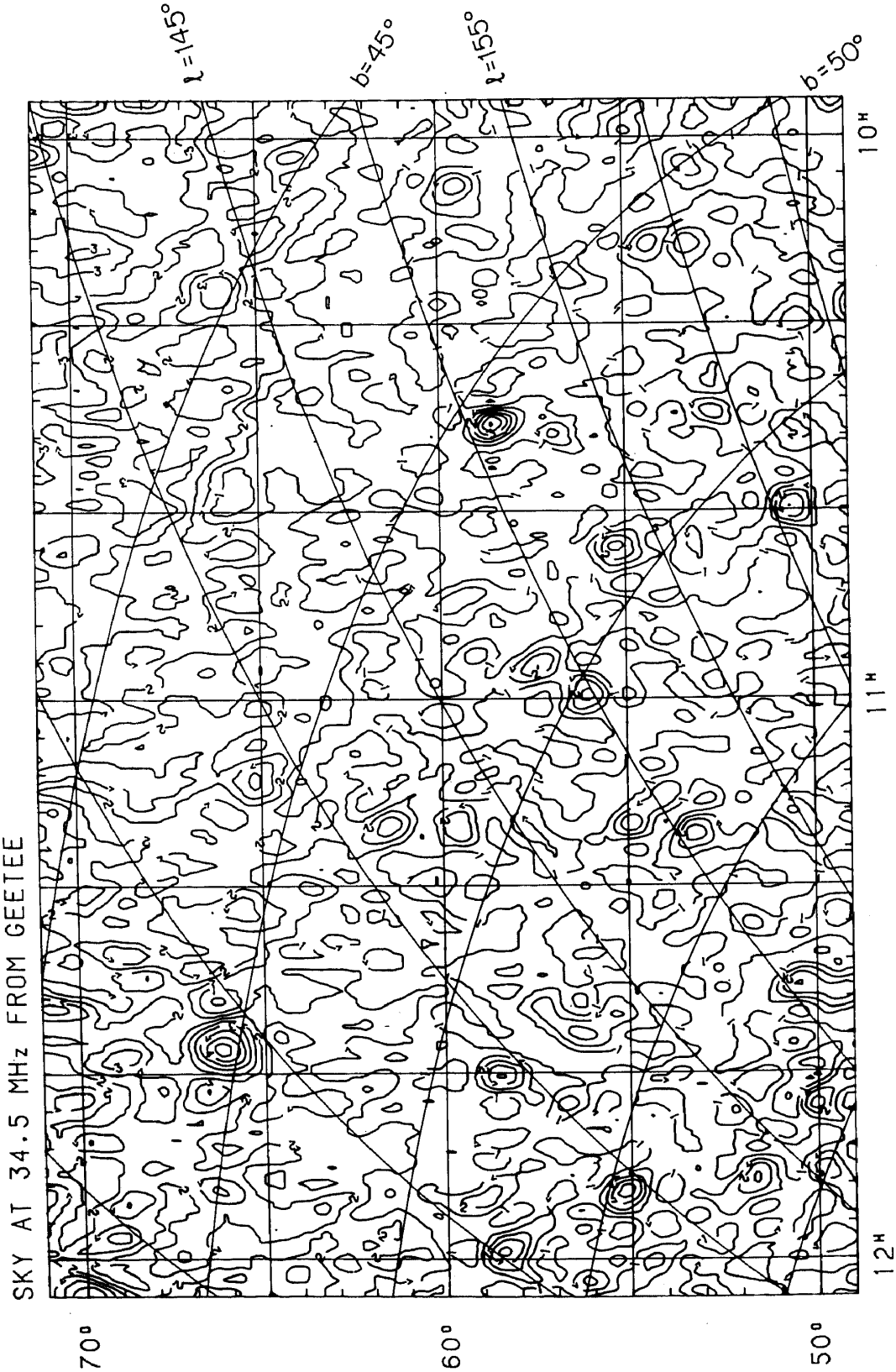
l=145°
b=45°
l=155°
b=50°
10H
11H
12H
70°
60°
50°
SKY AT 34.5 MHz FROM GEETEE

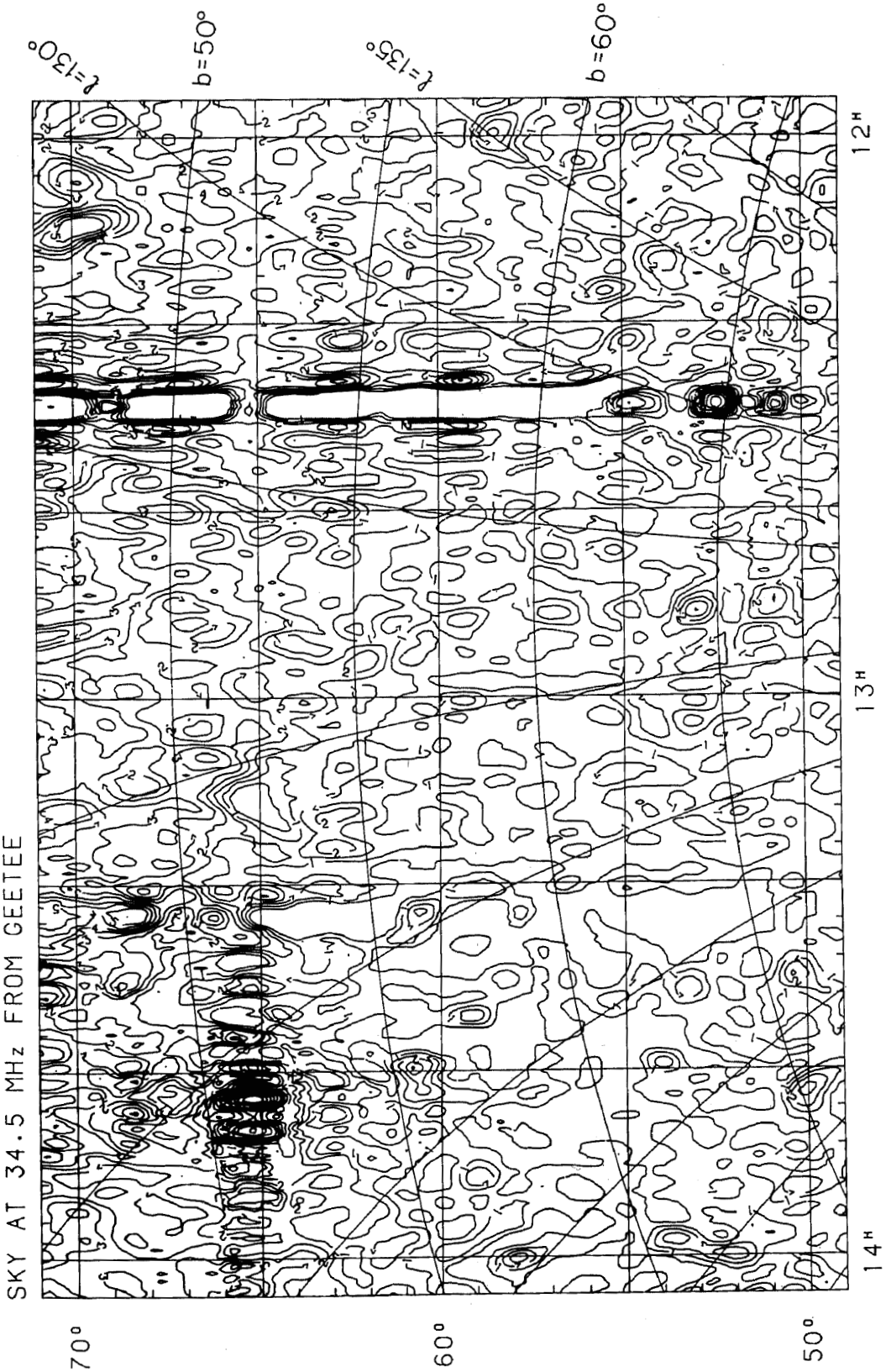
SKY AT 34.5 MHz FROM GEETEE
ℓ=130°
b=50°
ℓ=135°
b=60°
12ᴴ
13ᴴ
14ᴴ
70°
60°
50°

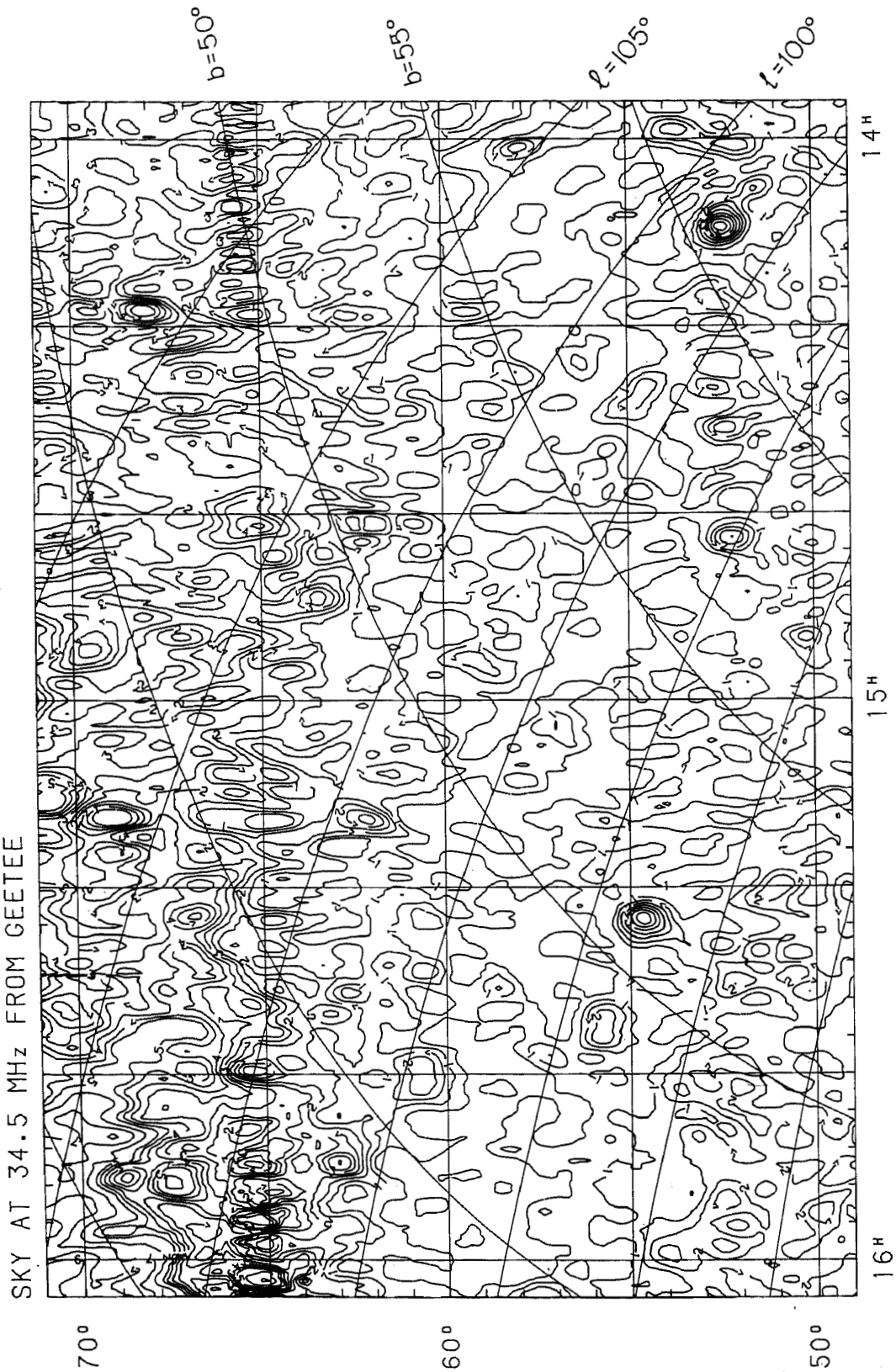
SKY AT 34.5 MHz FROM GEETEE
b=50°
b=55°
ℓ=105°
ℓ=100°
14H
15H
16H
70°
60°
50°

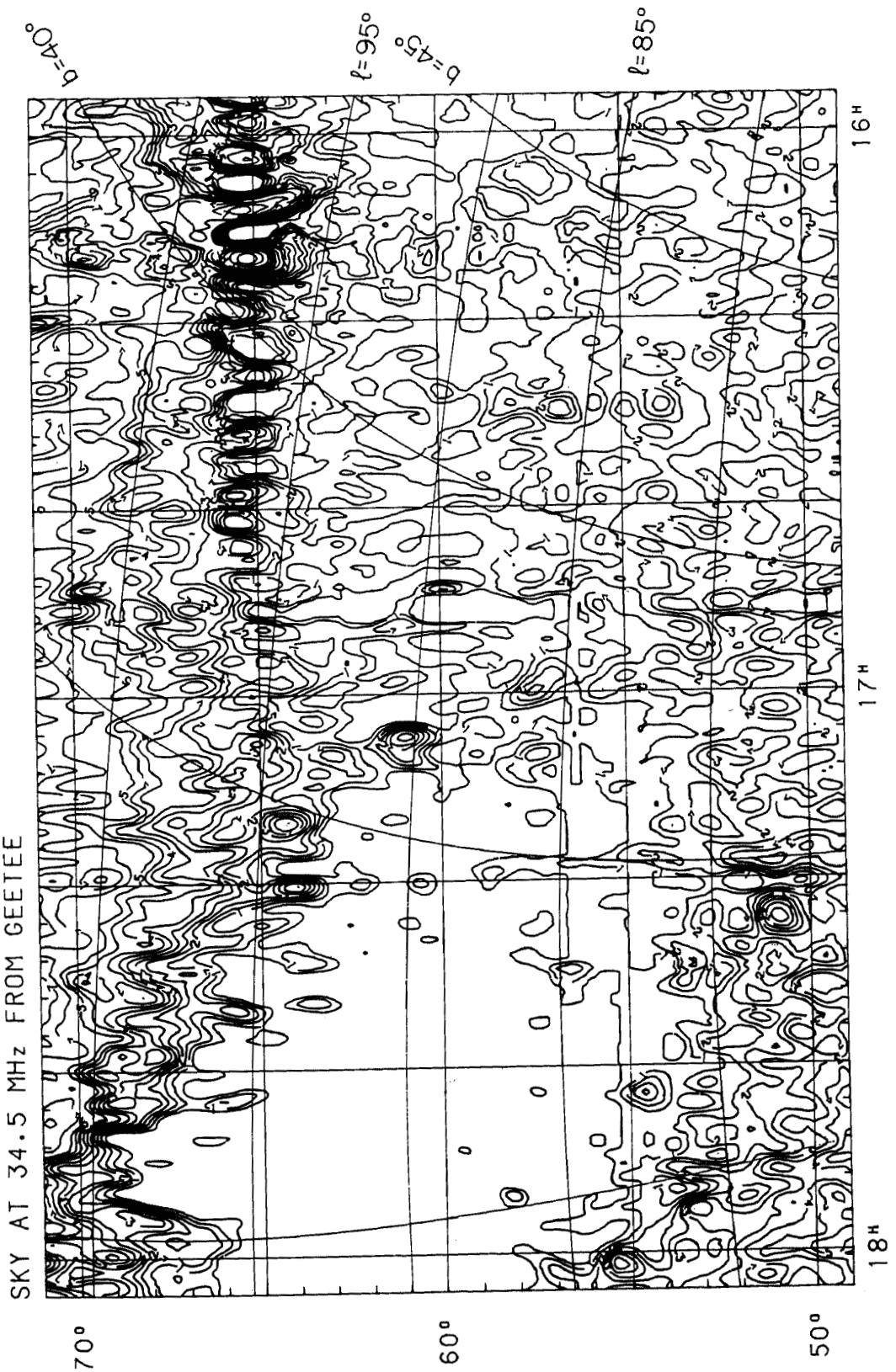
SKY AT 34.5 MHz FROM GEETEE
b=40°
ℓ=95°
b=45°
ℓ=85°
16ᴴ
17ᴴ
18ᴴ
70°
60°
50°

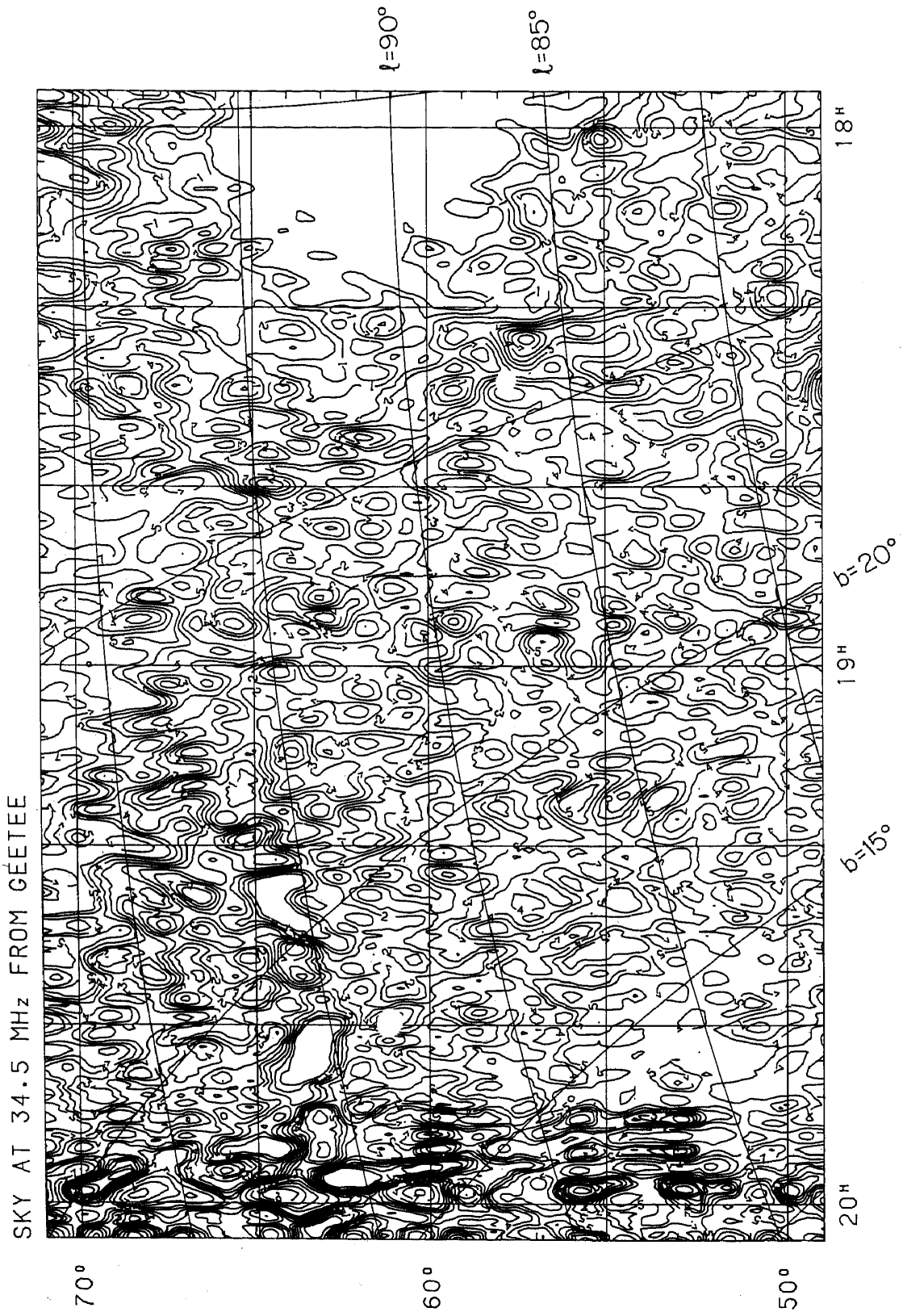
SKY AT 34.5 MHz FROM GEETEE
l=90°
l=85°
18ʰ
19ʰ
20ʰ
b=20°
b=15°
70°
60°
50°

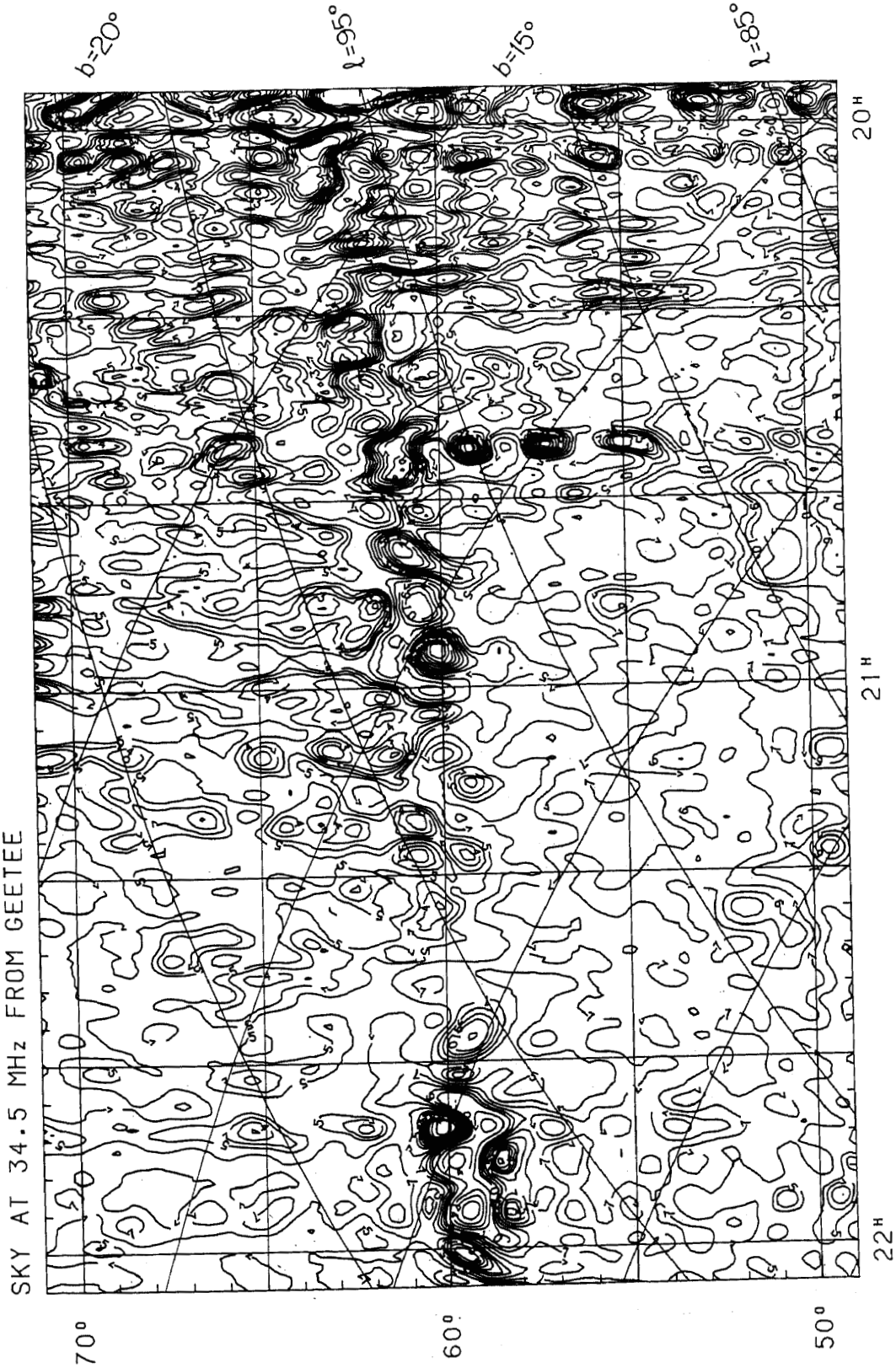
SKY AT 34.5 MHz FROM GEETEE
b=20°
l=65°
b=15°
l=85°
20H
21H
22H
70°
60°
50°

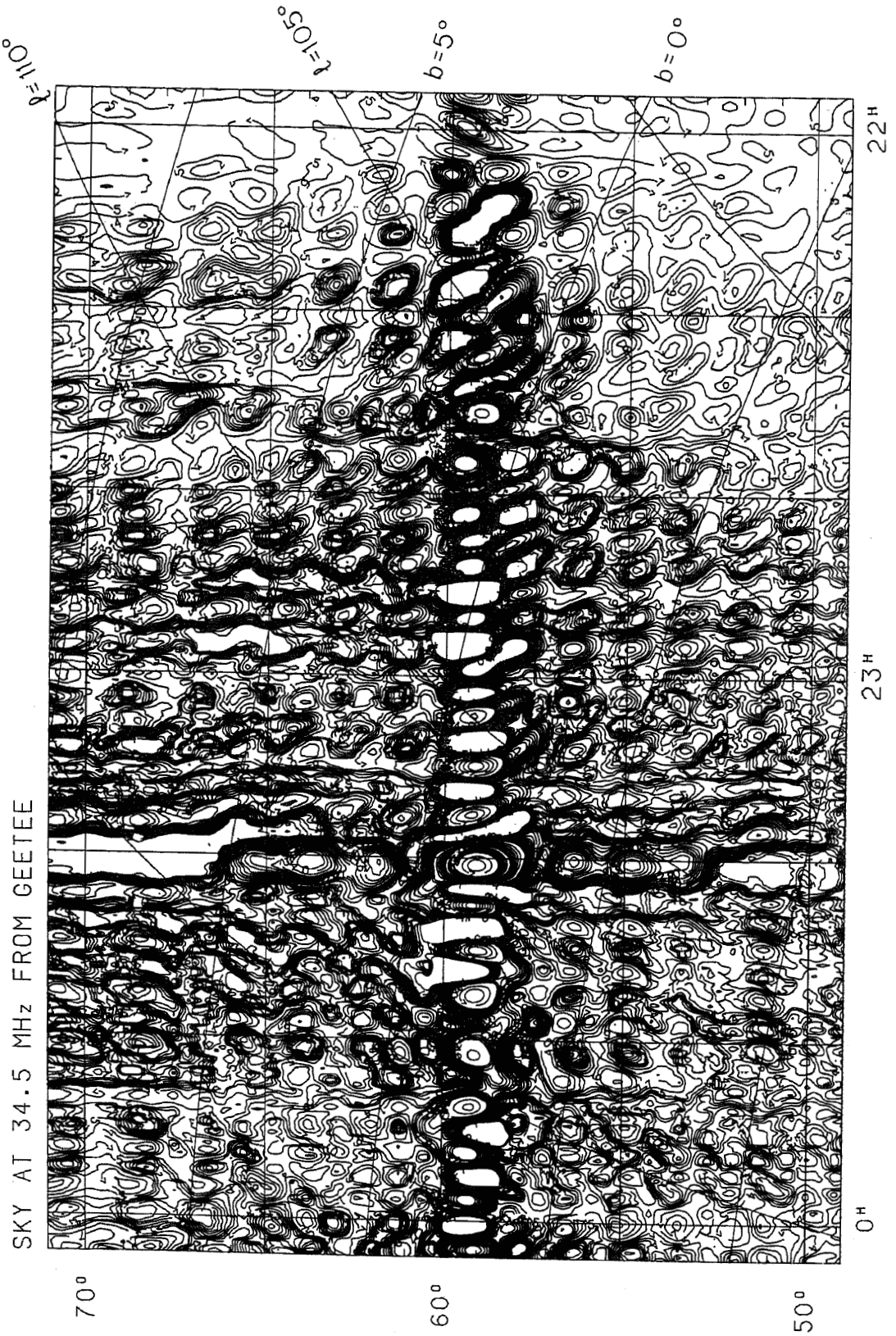
SKY AT 34.5 MHz FROM GEETEE
l=110°
l=105°
b=5°
b=0°
22H
23H
0H
70°
60°
50°